## POSSIBLE DECAY MODES IN THE HEAVY TO SUPERHEAVY ISLAND OF RANGE 98 $\leq$ Z $\leq$ 120 WITHIN THE RELATIVISTIC MEAN-FIELD APPROACH

THEEB Y. T. ALSULTAN

FACULTY OF SCIENCE UNIVERSITI MALAYA KUALA LUMPUR

2024

### POSSIBLE DECAY MODES IN THE HEAVY TO SUPERHEAVY ISLAND OF RANGE 98 $\leq$ Z $\leq$ 120 WITHIN THE RELATIVISTIC MEAN-FIELD APPROACH

#### THEEB Y. T. ALSULTAN

### THESIS SUBMITTED IN FULFILMENT OF THE REQUIREMENTS FOR THE DEGREE OF DOCTOR OF PHILOSOPHY

DEPARTMENT OF PHYSICS FACULTY OF SCIENCE UNIVERSITI MALAYA KUALA LUMPUR

#### UNIVERSITI MALAYA

#### ORIGINAL LITERARY WORK DECLARATION

Name of Candidate: Theeb Y. T. Alsultan

Registration/Matric No.: S2133277/1

Name of Degree: Doctor Of Philosophy

Title of Project Paper/Research Report/Dissertation/Thesis ("this Work"): POSSIBLE

#### DECAY MODES IN THE HEAVY TO SUPERHEAVY ISLAND OF RANGE 98 ≤ Z

#### ≤ 120 WITHIN THE RELATIVISTIC MEAN-FIELD APPROACH

Field of Study: Physical Science (Physics)

I do solemnly and sincerely declare that:

- (1) I am the sole author/writer of this Work;
- (2) This work is original;
- (3) Any use of any work in which copyright exists was done by way of fair dealing and for permitted purposes and any excerpt or extract from, or reference to or reproduction of any copyright work has been disclosed expressly and sufficiently and the title of the Work and its authorship have been acknowledged in this Work;
- (4) I do not have any actual knowledge nor do I ought reasonably to know that the making of this work constitutes an infringement of any copyright work;
- (5) I hereby assign all and every rights in the copyright to this Work to Universiti Malaya ("UM"), who henceforth shall be owner of the copyright in this Work and that any reproduction or use in any form or by any means whatsoever is prohibited without the written consent of UM having been first had and obtained;
- (6) I am fully aware that if in the course of making this Work I have infringed any copyright whether intentionally or otherwise, I may be subject to legal action or any other action as may be determined by UM.

Candidate's Signature Date: Aug 09, 2024

Subscribed and solemnly declared before,

Witness's Signature\_ Date: Aug 09, 2024

# POSSIBLE DECAY MODES IN THE HEAVY TO SUPERHEAVY ISLAND OF RANGE 98 $\leq$ Z $\leq$ 120 WITHIN THE RELATIVISTIC MEAN-FIELD APPROACH ABSTRACT

This thesis aims to explore alpha radioactivity in superheavy nuclei using semi-empirical and microscopic approaches. The primary objectives include: firstly, examining the influence of nuclear rotation on the decay half-lives of superheavy nuclei within the range  $98 \le Z \le 120$  using the axially deformed relativistic Hartree-Bogoliubov theory in the continuum (DRHBc), which incorporates recent semi-empirical formulae to provide a systematic understanding of alpha-radioactivity. The findings suggest that the predictions made by all semi-empirical formulae align more closely with the available experimental data when considering the rotation effect. However, it has been demonstrated that the impact of nuclear rotation gradually diminishes as the atomic nucleus becomes heavier. Secondly, the in-medium effects are incorporated into the R3Y NN potential through density-dependent nucleon-meson coupling within the relativistic Hartree-Bogoliubov (RHB) framework. This relativistic medium-dependent R3Y, called DD-R3Y NN potentials, are for the first time used to obtain the nucleus-nucleus potential as input into the Preformed cluster-decay model (PCM). The penetration probability is calculated using the WKB approximation, and the preformation probability  $(P_{\alpha})$  is estimated using a recently derived formula, which is based on parameters well known to influence the radioactivity of the  $\alpha$  -particles. A close correlation is observed between the  $\alpha$ -preformation factor and the crucial role of the pairing correlation in the  $\alpha$ -decay process. Furthermore, the  $P_{\alpha}$  values for the even-even nuclei are generally found to be of higher magnitude than those for the odd-A nuclei. The results further affirm the odd-even staggering effect on the  $Q_{\alpha}$  values and its accompanying effects on other observables such as the charge

radii and the decay half-lives, which can be largely attributed to the pairing correlation and Pauli blocking of the unpaired valence nucleons. Thus, correlations are established between bulk properties and decay properties in the ground state of <sup>207,208</sup>Th isotopic chains.

**Keywords**: Heavy and Superheavy Nuclei, Alpha Radioactivity, Relativistic Mean-Field Approach, Nuclear Shape, Rotational Energy Correction, Semi-Empirical Formulas, Decay Energy and Half-Lives, Relativistic Hartree-Bogoliubov, Cluster Preformation, Alpha Particle, Cluster Decay Mode, Odd-Even Staggering.

#### MOD PEREPUTAN YANG BERKEMUNGKINAN DI PULAU SANGAT-BERAT

#### DALAM JULAT $98 \le Z \le 120$ DALAM PENDEKATAN MEDAN

#### MIN RELATIVISTIK

#### **ABSTRAK**

Tesis ini bertujuan untuk meneroka radioaktiviti Alfa dalam nukleus sangat-berat dengan menggunakan pendekatan separa empirik dan mikroskopik. Objektif utama termasuk: pertama, mengkaji pengaruh putaran nuklear pada separuh hayat pereputan untuk nukleus sangat-berat dalam julat  $98 \le Z \le 120$  dengan menggunakan teori Hartree-Bogoliubov relativistik terubah berbentuk secara paksi dalam kontinum (DRHBc), yang menggabungkan formula separa empirikal terkini untuk memberikan pemahaman sistematik tentang radioaktiviti Alfa. Penemuan ini menunjukkan bahawa ramalan yang dibuat oleh kesemua formula separa empirikal lebih rapat dengan data eksperimen yang tersedia ada dengan mempertimbangkan kesan putaran. Walau bagaimanapun, ia telah menunjukkan bahawa kesan putaran nuklear secara beransur-ansur berkurangan apabila nukleus atom menjadi lebih berat. Kedua, kesan dalam sederhana dimasukkan ke dalam potensi R3Y NN melalui gandingan nukleon-meson yang bergantung kepada ketumpatan dalam rangka kerja Hartree-Bogoliubov (RHB) relativistik. R3Y yang bergantung pada sederhana relativistik ini, yang dipanggil potensi DD-R3Y NN, buat pertama kalinya digunakan untuk mendapatkan potensi nukleus-nukleus sebagai kemasukan ke dalam model pereputan kelompok (PCM) terdahulu. Kebarangkalian penembusan dikira menggunakan anggaran WKB, dan kebarangkalian prabentuk  $(P_{\alpha})$  dianggarkan dengan menggunakan formula terbitan baru-baru ini, yang berdasarkan parameter yang terkenal untuk mempengaruhi radioaktiviti zarah  $\alpha$ -. Kolerasi rapat diperhatikan antara faktor  $\alpha$ -prabentuk dan peranan penting korelasi berpasangan dalam proses pereputan  $\alpha$ . Tambahan pula, nilai  $P_{\alpha}$  untuk

nukleus genap umumnya didapati mempunyai magnitud yang lebih tinggi daripada nukleus ganjil-A. Keputusan selanjutnya mengesahkan bahawa kesan ganjil genap pada nilai  $Q_{\alpha}$  dan kesan yang disertakan pada benda boleh diperhatikan lain seperti jejari cas dan separuh hayat pereputan, yang sebahagian besarnya boleh dikaitkan dengan korelasi berpasangan dan penyekatan Pauli bagi nukleon valens yang tidak berpasangan. Oleh itu, korelasi antara sifat pukal dan sifat pereputan dalam keadaan dasar rantai isotop  $^{207,208}$ Th diwujudkan.

**Kata kunci**: Nukleus Heavy dan Superheavy, Pereputan Alpha, Pendekatan Medan Min Relativistik, Bentuk Nuklear, Tenaga Pembetulan Putaran, Formula Separuh Empirikal, Tenaga Pereputan dan Separuh Nyawa, Relativistik Hartree-Bogoliubov, Praformasi, Zarah Alpha, Mod Pereputan Kelompok, Ganjil-Genap Mengejutkan.

#### **ACKNOWLEDGEMENTS**

First and foremost, I offer my sincere gratitude to Allah (SBW) for helping me carry out my PhD study successfully at the University of Malaya (UM), Kuala Lumpur, Malaysia. My overwhelming thanks go to my supervisors, Associate Prof.Dr.Mrutunjaya Bhuyan and Prof.Dr.Goh Boon Tong, for their enthusiasm, inspiration, and great efforts in explaining things clearly and simply. Throughout the writing of my thesis, they provided me with encouragement, sound advice, effective teaching, and numerous valuable ideas. I also wish to express my gratitude to Associate Prof.Dr.Raj Kumar and Dr.Joshua Majekodunmi for their joint cooperation, excellent guidance, and helpful suggestions. Additionally, I am very thankful to all members of the Physics Department, University of Malaya (UM), Kuala Lumpur, Malaysia, including examiners, chairpersons, lecturers, and professors, for providing me with the resources to learn and understand.

Finally, I am forever indebted to my beloved parents, my wife (Salsabeel), my daughters (Tala and Doaa) and my siblings for their understanding, endless patience and encouragement when it was most needed to complete my PhD studies in theoretical physics at the University of Malaya(UM). I cannot conclude without thanking my colleagues and friends for their support and encouragement, which will always inspire me. I hope to continue in my own small way. Simply put, this thesis would not have been possible without their moral support.

Dr. Theeb Alsultan

#### TABLE OF CONTENTS

Abst	ract	ii
Abst	rak	١
Ackı	nowledgements	vi
Tabl	e of Contents	vii
List	of Figures	X
List	of Tables	xii
List	of Symbols and Abbreviations	xiv
List	of Appendices	XV:
СНА	APTER 1: INTRODUCTION	1
1.1	Research Background	]
1.2	Statement of Problem	
1.3	Objective of the Study	5
1.4	Limitation of the study	6
1.5	Significance of Study	7
1.6	Outline of study	8
СНА	APTER 2: LITERATURE REVIEW	10
2.1	Introduction	10
2.2	Nuclear Drip-line	10
2.3	Superheavy Nuclei	11
	2.3.1 Synthesis of Superheavy Nuclei	13
2.4	Alpha Decay of SHN	15
2.5	Preformation Probability of $\alpha$ -Decay	16

2.6	Hindra	nce Factor	17
2.7	Nuclea	r Rotation	17
CHA	APTER	3: THEORETICAL FORMALISM	19
3.1	Introdu	action	19
3.2	Semi-Empirical Formulae		
3.3	3.3 Microscopic Approaches		
	3.3.1	Deformed Relativistic-Hartree- Bogoliubov theory in continuum (DRHBc)	23
	3.3.2	Relativistic-Hartree-Bogoliubov (RHB) Formalism	26
		3.3.2.1 Medium-dependent Relativistic <i>NN</i> potential	27
3.4	The Do	ouble Folding Technique	30
3.5	The W	KB Penetration Probability	31
3.6	The Pr	eformed Cluster-Decay Model	32
	3.6.1	A New Preformation Probability	33
3.7	Pairing	g Correlation	34
CH	APTER	4: RESULTS AND DISCUSSION	36
4.1	Introdu	action	36
4.2	Nuclea	ar Rotation Corrections on $\alpha$ -decay Half-lives of SHN	36
	4.2.1	Bulk Properties of SHN within $98 \le Z \le 120$	37
	4.2.2	Alpha Decay Half-lives of Superheavy Nuclei within $98 \le Z \le 120$ using different Semi-Empirical Formulae	42
	4.2.3	Systematic Study of Rotational effect on even-even <sup>254,256</sup> Rf isotopes	46
4.3	-	icle clustering of the newly discovered <sup>207,208</sup> Th decay chains within Approach	50
	4.3.1	Structural Properties of <sup>207,208</sup> Th Isotopic Chains	50

CHAPTER 5: SUMMARY AND CONCLUSION  References	
List of Publications and Papers Presented	••••
Appendices	

#### LIST OF FIGURES

Figure 2.1:	Three-dimensional representation of the theoretical island of stability in nuclear physics. Adopted from (W. Greiner, 2012)	14
Figure 4.1:	The profile of the DRHBc (PC-PK1) estimated (a) binding energies without (open shape) and with rotation correction (half-open shape) for an illustrative case of $Z = 98 - 112$ isotopic chains. The results are compared with the available experimental data (solid shape) (Kondev et al., 2021). (b) Quadrupole deformation $\beta_2$ of $Z = 98 - 104$ . A similar profile is observed for all the considered systems (with slightly different magnitudes), but only a few are shown here for the sake of clarity.	37
Figure 4.2:	The calculated $Q_{\alpha}$ for SHN with $Z=98$ -120 as a function of the neutron number of the daughter nuclei $(N_d)$ for DRHBc (solid line with blue circle) and DRHBc+ $\theta$ (solid line with magenta star) using the PC-PK1 parameter set in comparison with those calculated from the WS4 (N. Wang et al., 2014) (solid line with red rectangles) and the experimental data (Kondev et al., 2021) (solid black sphere), wherever available.	38
Figure 4.3:	Variation of the decay energy $(Q_{\alpha})$ as a function of neutron number of the daughter nuclei $(N_d)$ using DRHBc (PC-PK1) and the relativistic mean-field based (NL3 and DD-ME2) parameters sets for a representative case of $Z=108$ . The results are compared with the $Q_{\alpha}$ values estimated from the WS4 and the available experimental data (Kondev et al., 2021)	38
Figure 4.4:	The estimated half-lives (in logarithmic scale) of SHN for $Z=98$ - 120 using DRHBc (solid line and shape) and DRHBc+ $\theta$ (dashed line and open shape ) for PC-PK1 parameter set as a function of neutron number of the daughter nuclei (N <sub>d</sub> ) for six semi-empirical formulae. The results are compared with experimental results(Kondev et al., 2021) (solid black sphere) and the WS4 (N. Wang et al., 2014) (dotted line and half-open shape)	40
Figure 4.5:	The estimated half-lives (in logarithmic scale) of SHN for $Z = 98$ - 116 for DRHBc (solid line and shape) and DRHBc+ $\theta$ (dashed line and open shape) using the PC-PK1 parameter set for the nuclei with experimental data (Kondev et al., 2021) (solid black sphere) along with the WS4 (N. Wang et al., 2014) (dotted line and half-open shape) for six different empirical formula	41

Figure 4.6:	The calculated decay energy ( $Q_{\alpha}$ -values) for the decay chains (a) $^{254}\mathrm{Rf} \rightarrow ^{250}\mathrm{No} \rightarrow ^{246}\mathrm{Fm} \rightarrow ^{242}\mathrm{Cf} \rightarrow ^{238}\mathrm{Cm}$ and (b) $^{256}\mathrm{Rf} \rightarrow ^{252}\mathrm{No} \rightarrow ^{248}\mathrm{Fm} \rightarrow ^{244}\mathrm{Cf} \rightarrow ^{240}\mathrm{Cm}$ for DRHBc and DRHBc+rot using the PC-PK1 parameter set in comparison with the experimental data (Kondev et al., 2021).	48
Figure 4.7:	The predicted logarithm of half-lives against mass number by the six models compared with experimental results (Kondev et al., 2021) for(a) $^{254}$ Rf $\rightarrow$ $^{250}$ No $\rightarrow$ $^{246}$ Fm $\rightarrow$ $^{242}$ Cf $\rightarrow$ $^{238}$ Cm and (b) $^{256}$ Rf $\rightarrow$ $^{252}$ No $\rightarrow$ $^{248}$ Fm $\rightarrow$ $^{244}$ Cf $\rightarrow$ $^{240}$ Cm for DRHBc and DRHBc+rot. using the PC-PK1 parameter set in comparison with the experimental data (Kondev et al., 2021). The legends are split into both figures for the sake of visibility.	49
Figure 4.8:	The radial distribution of the total density ( $\rho_T = \rho_P + \rho_N$ ) obtained from the RHB (DD-ME2) parameter set for <sup>207</sup> Th (solid red line) and <sup>208</sup> Th (blue dashes) decay chains. The density of the $\alpha$ -particle ( <sup>4</sup> He) in green dash-dotted lines is deduced from experimental data	
	(De Vries et al., 1987)	51
Figure 4.9:	A profile of the pairing energies (upper panels a and b) and the quadrupole deformation parameter $\beta_2$ (lower panel c and d) along the $^{207,208}$ Th decay chains	52
Figure 4.10:	The estimated DD-ME2 binding energy per nucleon for each participating nuclei within the <sup>207,208</sup> Th decay chains. The open black- and closed black- squares denotes the <sup>207</sup> Th and <sup>208</sup> Th decay chain respectively. For comparison, the experimental binding energies (blue circles) are taken from ref. (M. Wang et al., 2021)	53
	A schematic representation of the total interaction potential of $^{207}$ Th $\rightarrow$ $^{203}$ Ra + $\alpha$ as a function of the mass-center distance between the decaying fragments (R). Prior to the decay process, $\alpha$ -particle (purple circle) is assumed to pre-exist within the $^{207}$ Th -parent nuclei (red circle). The orange circle represents the daughter nucleus ( $^{203}$ Ra).	54
Figure 4.12:	The estimated $\alpha$ -preformation probabilities ( $P_{\alpha}$ ) versus the parent nuclei for the <sup>207,208</sup> Th decay chains.	55
Figure 4.13:	$\log_{10} T_{1/2}$ values for the $^{207,208}$ Th decay chains. The experimental half-lives are obtained from ref. (Kondev et al., 2021; Yang et al., 2022) and given in Table 4.4.	56

#### LIST OF TABLES

Table 3.1:	The point coupling constant and the pairing strengths of PC-PK1 parameter set.	24
Table 3.2:	Density Dependent meson-nucleon exchange coupling DD-ME2 parameter set. All masses are given in MeV	27
Table 4.1:	The calculated standard deviation ( $\sigma$ ) of the logarithmic half-lives (with and without nuclear rotation effect) of 98 $\leq$ Z $\leq$ 118 using VSS, mB1, SemFIS2, R, Wang and MYQZR formulae.	43
Table 4.2:	Comparison of the logarithm of half-lives of the even-even chains (a) $^{254}\mathrm{Rf} \rightarrow ^{250}\mathrm{No} \rightarrow ^{246}\mathrm{Fm} \rightarrow ^{242}\mathrm{Cf} \rightarrow ^{238}\mathrm{Cm}$ and (b) $^{256}\mathrm{Rf} \rightarrow ^{252}\mathrm{No} \rightarrow ^{248}\mathrm{Fm} \rightarrow ^{244}\mathrm{Cf} \rightarrow ^{240}\mathrm{Cm}$ using six different semi-empirical formulae. The predictive accuracy of each of these formulae is evaluated by comparing them to the experimental data (Kondev et al., 2021). The $\alpha$ -decay energies ( $Q_{\alpha}$ ) for the above decay chains are calculated from the DRHBc formalism. See details in the text	47
Table 4.3:	The predicted DD-ME2 values for pairing energy $(E_{pair})$ , center of mass energy $E_{cm}$ ), binding energy (B.E), binding energy per nucleon (B.E/A), charge radii $(r_c)$ , proton radii $(r_p)$ and neutron radii $(r_n)$ , root-mean-square radii $(r_{rms})$ and the quadrupole deformation $(\beta_2)$ . The energies are expressed in MeV and radii in fm.	52
Table 4.4:	The calculated $\alpha$ -preformation probabilities ( $P_{\alpha}$ ) and the half-lives of $^{207,208}$ Th decay chains. The experimental half-lives are deduced from the latest evaluated nuclear properties table (Kondev et al., 2021) and the recent experimental measurements (Yang et al., 2022). The experimental decay energies ( $Q_{\alpha}^{exp}$ ) in MeV are taken from refs. (Uusitalo et al., 2005; Yang et al., 2022)	57
Table A.1:	Comparison of the logarithm of half-lives of the even-even with atomic numbers island from $98 \le Z \le 120$ using six different semi-empirical formulae. The predictive accuracy of each of these formulae is evaluated by comparing them to the experimental data(Kondev et al., 2021). The $\alpha$ -decay energies ( $Q_{\alpha}$ ) are calculated from the DRHBc formalism with PC-PK1 Parmerter set and formula for global mass (WS4) (N. Wang et al., 2014). The $Q_{\alpha}$ and $T_{1/2}$ are in units of MeV and s, respectively.	86

#### LIST OF SYMBOLS AND ABBREVIATIONS

 $A_{\mu}$  : Four-vector potentials.  $E_{cm}$  : Center of mass energy.

 $E_{pair}$ : Pairing energy.

 $F_{\mu\nu}$  : Field strength tensor of the photon field.

*I* : Moment of inertia.

N : Neutron number of the parent nucleus (A-Z).  $N_d$  : Neutron number of the daughter nucleus.

P : Penetration probability.  $P_{\alpha}$  : Preformation Probability.

 $Q_{\alpha}$  : Decay energy.

 $R_0$ : Radius of the parent nucleus.

T : Isovector terms.  $T_{1/2}$  : Decay half-life.

Z : Atomic number of the parent nucleus.

 $\alpha_S$ ,  $\alpha_V$ ,  $\alpha_{TS}$  and  $\alpha_{TV}$ : Coupling constants.

 $\beta_2$  : Quadrupole deformation.

 $eta_S, \gamma_S ext{ and } \gamma_V$  : Medium effects.  $\delta_S, \delta_V, \delta_{TS} ext{ and } \delta_{TV}$  : Gradient terms.  $\eta_A$  : Mass asymmetries.  $\eta_Z$  : Charge asymmetries.  $\lambda$  : Decay constant.

 $\begin{array}{ccc}
\nu_0 & : & \text{Assault frequency.} \\
\omega & : & \text{isoscalar vector.} \\
\rho & : & \text{isovector vector.}
\end{array}$ 

: Total density  $(\rho_T = \rho_P + \rho_N)$ .

 $\rho_{\alpha}$  : Density of  $\alpha$ -particle.

 $\rho_d$  : Density of the daughter nucleus.

 $\sigma$  : Standard Deviation.  $\sigma$  : isoscalar scalar.

 $\tau_{3i}$ : The third component of the isospin.

 $g_{\sigma}, g_{\omega}$  and  $g_{\rho}$  : coupling constants of the participating mesons.

 $m_{\sigma}$ ,  $m_{\omega}$  and  $m_{\rho}$  : Mesons masses.

 $r_B$ : Relative separation between the centers of frag-

ments.

 $r_c$  : Charge radii.  $r_n$  : Neutron radii.  $r_p$  : Proton radii.

 $r_{rms}$ : Root-mean-square radii.

B.E : Binding energy.

B.E/A : Binding energy per nucleon.BCS : Bardeen–Cooper–Schrieffer.

DD-ME2 : Density-Dependent Meson Couplings.

DD-R3Y : Density Dependent Relativistic (Mean-Field)-3-

Yukawa.

DRHBc : Deformed Relativistic Hartree-Bogoliubov the-

ory in the continuum.

DRHBc +  $\theta$  : Deformed Relativistic Hartree-Bogoliubov the-

ory in the continuum with rotation.

Expt. : Experimental data.

mB1 : Modified Brown Formula.MYQZR : Modified YQZR formula.

NN : Nucleon-Nucleon.
OES : Odd-Even Staggering.

OPEP : One-Pion Exchange Potential.

PC-PK1 : Relativistic Point-Coupling Density Functional.

PCM : Preformed Cluster Model.
QHD : Quantum Hadrodynamic.

R : Royer formula.

R3Y : Relativistic (Mean-Field)-3-Yukawa. RHB : Relativistic Hartree-Bogoliubov.

RMF : Relativistic Mean-Field. SCMF : Self-Consistent Mean Field.

SemFIS2 : Semi-Empirical Relationship Based on Fission

Theory.

SHN : Superheavy Nuclei.
Theo. : Theoretical data.

VSS : Viola-Seaborg Formula.

Wang : Wang formula.

WKB : Wentzel-Kramers-Brillouin.

WS4 : Weizsäcker-Skyrme Nuclear Mass Tables.

### LIST OF APPENDICES

Appendix A:	Appendices	82

#### **CHAPTER 1: INTRODUCTION**

#### 1.1 Research Background

The evolution of nuclear physics has been a journey marked by groundbreaking discoveries and theoretical advancements that span more than a century. Beginning with the pioneering work of J.J. Thomson in 1897, the discovery of the electron shattered the notion of the atom as indivisible and set the stage for further exploration into the subatomic realm (Thomson, 1897). Ernest Rutherford's gold foil experiment in 1909 unveiled the atomic nucleus, revolutionizing our understanding of atomic structure and proposing the planetary model of the atom, which depicted electrons orbiting a central nucleus (Rutherford & Geiger, 1908). This experiment not only confirmed the existence of the nucleus but also revealed its concentrated mass, housing most of the mass of atoms within a tiny, positively charged core.

Subsequent developments in nuclear physics led to the identification of various types of radiation such as alpha, beta, and gamma—through experiments involving radioactive decay. These discoveries, coupled with Albert Einstein's famous equation  $E = mc^2$  in 1905 (Einstein, 1905), which demonstrated the equivalence of mass and energy, laid the groundwork for understanding nuclear processes and the immense energy released in nuclear reactions. The experiment carried out by James Chadwick in 1932 led to the identification of the neutron emitted by Beryllium nuclei when bombarded with  $\alpha$  particles from a radioactive source (Chadwick, 1932). Following this discovery, neutron-proton theory gained prominence. This theory posits that the nucleus consists of neutrons and protons, collectively known as nucleons, with electrons occupying the extranuclear space, thereby rendering the nuclei electrically neutral. The neutron-proton theory has been instrumental in elucidating various aspects of nuclei, including the explanation of different

nuclear isotopes, which include their spin, nuclear magnetic moments,  $\beta$  decay and  $\alpha$  decay processes, as well as nuclear stability. Hideki Yukawa proposed the first successful theory of nucleon-nucleon interaction through meson exchange. He suggested that neutrons and protons are surrounded by meson composite clouds, and the exchange of mesons is responsible for binding the nucleons. This theory gained support from free neutron and proton magnetic moments. The Yukawa theory generalized the relation between particles and forces, implying the existence of a new particle, later identified as the  $\pi$  meson. The modern theory of interactions through particle exchanges is based on quantum field theory, where interactions are assumed to be instantaneous at low energies, allowing the derivation of interaction potentials (Yukawa, 1935). During that period, the precise characteristics of nuclear forces was unknown. This led to the development of theoretical models aimed at studying the nuclear properties of nuclei.

The macroscopic description of nuclei emerged as a critical aspect of nuclear physics, with various models such as the Yukawa potential, optical model, liquid-drop model, and shell model shaping our understanding of nuclear behavior. The liquid-drop model, proposed by George Gamow and others, treated the nucleus as a drop of incompressible fluid, elucidating nuclear stability and reaction properties. Concurrently, the shell model, developed by Maria Goeppert Mayer and J. Hans D. Jensen, provided a framework for understanding the arrangement of protons and neutrons within atomic nuclei in terms of energy levels or shells (Mayer & Jensen, 1961). These theoretical frameworks were pivotal in advancing our comprehension of nuclear phenomena and guiding experimental research. The current nuclear physics research revolves around investigating nuclei under extreme

The current nuclear physics research revolves around investigating nuclei under extreme conditions, such as high excitation energies and spin. Additionally, researchers are actively engaged in synthesizing superheavy elements to expand the boundaries of the periodic table. This concerted effort aims to push the limits of our understanding of nuclear structure

and behavior, opening new frontiers in scientific exploration (Smits et al., 2024, 2023).

The  $\alpha$ -decay is one of the most dominant decay modes of unstable (radioactive) nuclei in the transactinides and/or superheavy region ( $Z \ge 104$ ) and plays a crucial role in nuclear physics and astrophysics (especially in stellar nucleosynthesis) (Clark & Rudolph, 2023; Velasquez et al., 2023). The study of superheavy nuclei (SHN) represents an active area of research in nuclear physics that has attracted the attention of theorists and experiments (Giuliani et al., 2019; Ismail et al., 2022; Jain et al., 2022; Koyuncu & Soylu, 2020; J.-H. Liu et al., 2017; Lopez-Martens et al., 2022; Y. T. Oganessian et al., 2022; Sridhar et al., 2019). In terrestrial laboratories, SHNs are produced by the fusion of light nuclei, using particle accelerators (S. Hofmann & Münzenberg, 2000a; Münzenberg & Morita, 2015; Y. T. Oganessian et al., 2006, 2004, 1999; Ts et al., 2000). This effort has hitherto yielded remarkable success in the synthesis of nuclei with  $Z \le 118$  while those with Z > 118 await experimental synthesis. The decay characteristics of SHN reveal a clear possibility of enhanced stability (shell closure property) at Z = 114, 120, or 126, N = 184.Thus, a number of theoretical studies have been directed towards the prediction of  $\alpha$ -decay half-lives of SHN with Z > 118 (H.-M. Liu et al., 2019; Manjunatha, 2016; Seyyedi, 2021). Although most of these studies aim to explore the limit of the existence of SHNs as well as their structural properties, the precision of the conventional theoretical models used has been greatly challenged due to the variability of the nuclear proximity potential and the introduction of various other physical effects that may possibly explain the uncertainties in the superheavy region (Ghodsi & Amiri, 2021). Besides, the shape of SHN is an important factor in understanding their properties and behaviour (Ćwiok et al., 2005; Heenen et al., 2015).

#### 1.2 Statement of Problem

With the exception of double-magic nuclei, most nuclei on the nuclear chart deviate from the spherical shape. Furthermore, there is considerable evidence that suggests that SHNs can exist in both ground and intrinsic excited states as well as different deformed (or superdeformed and hyperdeformed) isomeric states (Bhuyan, Patra, & Gupta, 2011; Marinov et al., 2007, 2009; Patra et al., 2009, 2007). Thus, it is assumed that the participating nuclei are deformed. The deformed relativistic Hartree-Bogoliubov theory with continuum (DRHBc) (Li et al., 2012; Zhou et al., 2010) is well known to give a suitable description of deformed exotic nuclei. In this study, the binding energies are calculated using the DRHBc formalism, which is adept at incorporating the deformation and continuum effects simultaneously. The inclusion of the continuum effect is highly crucial for the drip-line region which comprises about 9035 nuclei within the range  $98 \le Z \le 120$  which is predicted to be bound and thus, extends the existing nuclear territory. Within the mean-field approximation, it is plausible to consider the many-body correlations with symmetry breaking such as loss of translational invariance and rotational invariance (Ring & Schuck, 1980). In order to restore broken symmetry, it is essential to include the rotational correction energy (P.-W. Zhao et al., 2010).

On the other hand, recent experiments and theoretical explorations have demonstrated that  $\alpha$ -decay studies provide a viable means to investigate the nuclear structure of nuclei with shell closure by proton number Z > 82 (Andreyev et al., 2000, 1819; Uusitalo et al., 2005). More interestingly, this region is enriched with the existence of a multiphoton-multihole intruder state and the possibility of shape-coexistence. A new thorium isotope  $^{207}$ Th has been recently discovered (Yang et al., 2022). The authors reported that the  $\alpha$ -decay energies ( $Q_{\alpha}$ ) of the nuclei that have Z > 82 and N < 126 follow a step-wise pattern as the number of neutrons decreases along the isotopic chain. This conjecture is

contrary to the common notion where a smooth upward trend is expected (Z. Zhang et al., 2021). To resolve this discrepancy and gain further insight, it is crucial to theoretically probe the structural and decay properties of the nuclei in this region. In addition, several quantities that are used in exploring the nuclear properties (such as the binding energy (Heisenberg, 1932), single nucleon separation energy (Fu et al., 2016; Jiang et al., 2012) and the charge radius (Angeli et al., 2009; De Groote et al., 2020; Marsh et al., 2018)) manifest odd-even staggering as the proton or neutron number changes. There is an ample evidence that odd-even staggering (OES) has a considerable effect on alpha preformation probabilities and their decay half-lives  $(T_{1/2})$  as a result of the pairing effect and blocking of certain orbitals by unpaired nucleons (Deng & Zhang, 2021; Seif, 2015; Xu & Ren, 2005). Since the penetration process gives no distinction between the odd and even nuclei, the OES effect in  $T_{1/2}$  is traceable to the alpha preformation probabilities (Sun et al., 2017). On the contrary, the conventional Bethe-Weizsäcker semi-empirical mass formula (Bethe & Bacher, 1936; Weizsäcker, 1935) gives the impression that the OES is somewhat negligible in  $Q_{\alpha}$  since both the parent nucleus and its daughter are odd-A (odevity) and, therefore, the pairing terms in their binding energies cancel out (J. Dong et al., 2011; T. Dong & Ren, 2010; Jia et al., 2021). This strengthens the motivation to undertake a detailed investigation in this region using the preformed cluster-decay model (PCM).

#### 1.3 Objective of the Study

The present study is aimed at investigating the instability of exotic nuclei using both semi-empirical formulae (which assist in circumventing computational complexities and allow for straightforward extrapolation) and the microscopic approaches (which incorporate relativistic and continuum effects arising from the emission of alpha particles from unbound states, which are not adequately described by traditional models). Specifically, the aim of this doctoral thesis includes a few emerging problems in  $\alpha$ -radioactivity are:

- i. To investigate the influence of nuclear rotation on the decay half-lives of superheavy nuclei within the range  $98 \le Z \le 120$  is investigated using the axially deformed relativistic Hartree-Bogoliubov theory in the continuum (DRHBc). The various recent empirical formulae will be included in the analysis, which provides systematic anatomy of the  $\alpha$ -radioactivity.
- ii. To incorporate the medium effects in the R3Y NN potential through the density-dependent nucleon-meson coupling within the relativistic Hartree-Bogoliubov (RHB) approach. The relativistic medium-dependent R3Y, the so-called DD-R3Y NN potentials are used to obtain the nuclear potential as input into the Preformed cluster-decay model (PCM). The improved model is applied in the investigation of the structure and decay properties of the recently discovered  $\alpha$ -emitting  $^{207}$ Th isotope and the known  $^{208}$ Th decay chains. For the first time, the newly derived preformation probability formula which incorporates the influential factors of  $\alpha$ -decay is adopted.
- iii. To establish the correlations between the bulk properties and decay properties in the ground state of  $^{207,208}$ Th isotopic chains.

#### 1.4 Limitation of the study

This study only considers alpha decay processes involving ground state-to-ground state transitions. This limitation excludes the exploration of other decay modes or excited state transitions in the decay mechanisms of heavy and superheavy nuclei which have been studied in previous works. Furthermore, all nuclei in the study are assumed to be spherical. This assumption does not incorporate the potential influence of nuclear deformation on alpha decay properties since studies on the degree of shape freedom have been previously investigated, and undue repetition is avoided here. It is noteworthy that the study incorporates nuclear rotational correction as a new degree of freedom. The study relies on semi-empirical formulas and microscopic models to predict alpha decay

properties. These frameworks provide valuable insights and offer a good compromise between accuracy and computational cost.

#### 1.5 Significance of Study

Exploring  $\alpha$ -radioactivity in superheavy nuclei using semi-empirical and microscopic approaches addresses some key challenges in nuclear physics, ranging from understanding the structure and stability of exotic nuclei to refining theoretical models for predicting nuclear decay properties. The significance of this study lies in its comprehensive investigation of exotic nuclei, particularly focusing on the decay properties of superheavy nuclei and the recently discovered  $\alpha$ -emitting isotopes. Specifically, the significance is as follows:

- i. **Understanding Exotic Nuclei:** Exotic nuclei, especially those in the superheavy region, present intriguing challenges due to their extreme conditions. Investigating their decay properties provides valuable insights into nuclear structure and stability, which are fundamental in understanding the behavior of matter at the nuclear level.
- ii. **Role of Nuclear Rotation:** The study aims to explore how nuclear rotation affects the decay half-lives of superheavy nuclei. This investigation contributes to our understanding of the dynamics of nuclear processes under rotational influences, providing essential information for theoretical models and experimental interpretations.
- iii. **Incorporating Medium Effects:** By incorporating medium effects through density-dependent nucleon-meson coupling within the relativistic Hartree-Bogoliubov approach, the study enhances the accuracy of models used to describe nuclear interactions. This incorporation of medium effects is crucial for more realistic predictions of nuclear properties, especially in exotic systems.
- iv. **Correlation Studies:** Establishing correlations between bulk properties and decay properties in specific isotopic chains, such as <sup>207,208</sup>Th, enhances our understanding

of the interplay between various nuclear properties. These correlations provide valuable constraints for theoretical models and offer insights into the underlying physics governing nuclear phenomena.

#### 1.6 Outline of study

Chapter 1 of this thesis serves as the gateway into the present research endeavor, encompassing several critical elements essential for establishing context and laying the groundwork for subsequent chapters. It commences with a concise historical narrative delving into  $\alpha$ -radioactivity and superheavy nuclei, tracing their evolutionary trajectory from early discoveries to contemporary theoretical frameworks. The problem statement reflecting the gaps and challenges existing within the current understanding of these phenomena is also explained in detail. Following this, the chapter elucidates the precise objectives and the limitations of the present study.

Chapter 2 is devoted to different approaches employed in investigating  $\alpha$ -radioactivity within the superheavy region. Specifically, this chapter delves into two primary approaches: the semi-empirical formulae and microscopic methods such as the relativistic Hartree-Bogoliubov (RHB) formalism. Furthermore, the concept of preformation probability of  $\alpha$ -Decay is thoroughly examined within this context. By scrutinizing existing literature, this chapter identifies pertinent gaps that underscore the significance and necessity of the present study.

Chapter 3 is dedicated to a comprehensive examination of the methodologies employed within this study. Firstly, it outlines in detail the six semi-empirical formulae used, elucidating their individual components. Following this, the chapter delves into the microscopic approach known as the relativistic Hartree-Bogoliubov (RHB) formalism. Additionally, it explores the integration of medium effects into the R3Y NN potential through density-dependent nucleon-meson couplings, providing insights into the theoretical

underpinnings of this incorporation. Moreover, the chapter elucidates the double folding technique with the densities of both daughter nuclei and alpha particles. Finally, a succinct overview of the preformed cluster model (PCM) is presented.

Chapter 4 constitutes an in-depth analysis of the findings stemming from the current investigation. It offers a meticulous examination of the impact of nuclear rotation corrections on the  $\alpha$ -decay half-lives of superheavy nuclei (SHN) and the manifestation of  $\alpha$ -particle clustering within the newly discovered  $^{207,208}$ Th decay chains using the RHB approach. Furthermore, the study endeavors to establish correlations between the bulk properties and decay properties of the ground state within the mentioned isotopic chain.

In **Chapter 5**, a comprehensive summary and conclusive insights derived from the present study on SHN are provided. Additionally, this chapter outlines avenues for future research and suggests potential directions for further studies.

#### **CHAPTER 2: LITERATURE REVIEW**

#### 2.1 Introduction

This chapter offers a concise review of previous research, underlying assumptions, and key factors that underpin the present study. It delves into the advances in both experimental investigations and theoretical endeavors within the superheavy region, while also acknowledging their respective constraints. Additionally, it provides justification for the novel inclusion of nuclear rotation corrections. Furthermore, it articulates the necessity of pursuing this theoretical investigation through two distinct approaches: semi-empirical and microscopic. The rationale behind the advance of theory and its application to the preformed cluster decay model for  $\alpha$  clustering systems is also explored.

#### 2.2 Nuclear Drip-line

The investigation into the limits of nuclear stability is a fascinating topic in contemporary nuclear physics. This entails studying the emission of nucleons from the ground state of both spherical and deformed nuclei, which allows for an evaluation of the proton and neutron drip lines. Drip line nuclei behave differently than stable nuclei because of the isospin dependency of the nuclear force. When moving away from the valley of stability, a critical juncture is reached at which the valence nucleons are no longer sufficiently confined by the nuclear force, resulting in their emission. These extremes define the boundaries of the nuclear landscape, with the proton drip line extending to prototactinium (Z = 91) on one side and the neutron drip line extending up to oxygen (Z = 8) on the other. Furthermore, the occurrence of high neutron-to-proton (N/Z) ratios in these nuclei results in a variety of abnormal phenomena, including halo nuclei, shape coexistence, neutron skins, and shell quenching. These phenomena can be largely attributed to the coupling of bound states to the particle continuum, the loosely bound nature of the outermost nucleon, and significant

alterations in the shell structure.

#### 2.3 Superheavy Nuclei

Superheavy nuclei are atomic nuclei containing a very large number of protons and neutrons, typically significantly beyond the range of naturally occurring isotopes. These nuclei lie at the extreme end of the periodic table, with atomic numbers (the number of protons) well beyond those found in stable elements. The search for superheavy nuclei is driven by scientific curiosity about the limits of nuclear stability and the desire to explore the properties of matter under extreme conditions (Smits et al., 2023).

The quest for superheavy elements, commenced with Transactinide Z=104 in 1961 in Dubna, has been a focal point. This effort has been greatly aided by the advancements in accelerator technology and computational capabilities over the years. The seminal advancement in theoretical investigation came with the prediction of Z=126 nuclei, with particular attention to the prospect of an 'island of stability' around Z=114 and N=184 (Malov et al., 2021; Okunev, 2018). It was previously speculated that this island was surrounded by a 'sea of instability,' suggesting the potential existence of symmetric spherical close-shell nuclei as shown in Fig. 2.1. However, this perception was altered by the discovery of Z=108 nuclei, in which the spherical symmetric close shell nuclei to deformed shell stabilized nuclei and predicts a neutron shell closure at N=162 (Smolańczuk, 1997; Stone et al., 2019). Thus, this conjecture improves the stability against fission and predicts the existence of double magic nuclei in the instability sea, notably around <sup>270</sup><sub>108</sub>Hs (S. Hofmann, 2015; Y. T. Oganessian et al., 2017). A number of theoretical studies have predicted the discovery of Z=120, 126, and nuclei with even greater shell stability than Z=114 (Armbruster, 2000; Rydin, 2011; Yadav et al., 2023). There have been no consistent definition for the SHN. Some explain that the SHN commences from Z=104, while others align it with the emergence of transactinide elements. Basically, the stability of these nuclei is dependent on the shell effect, and their decay half-life should not fall below  $10^{14}$  seconds.

For the past two decades, one of the notable goals in nuclear physics is in the study, identification, and synthesis of superheavy nuclei (SHN) as well as the measurement of their decay lifetime. The interest in SHN has been recently rejuvenated on the successful grounds of hot and cold fusion reactions (Eichler et al., 2007; S. Hofmann & Münzenberg, 2000b; Y. Oganessian, 2007; Y. T. Oganessian et al., 2012, 2011, 2004; Ts et al., 2000). As a result of fission, the production rate of SHN reduces drastically with the atomic number Z of the fused system, and thus, the analysis of their spectroscopy is usually tedious. Besides, the Coulomb repulsion between the proton becomes enhanced when approaching the proton dripline. Until now, with the advent of sophisticated radioactive ion beam facilities, SHN within the range Z = 110 - 118 has been successfully synthesized in the laboratory (Eichler et al., 2007; S. Hofmann & Münzenberg, 2000b; Y. Oganessian, 2007; Y. T. Oganessian et al., 2012, 2011, 2004; Ts, 2001). This necessitates a detailed study of possible decay modes and stability of synthesis nuclei. Moreover, the identification of nuclei in the experimentally unknown territory of the SHN is of central interest to contemporary physicists around the world. The experimental signature for observing the decay properties of superheavy elements is mainly by  $\alpha$ -emissions and accompanied by spontaneous fission, which is currently a domain of intense research. Thus, the discovery of superheavy elements have become a potential testing tool for various theoretical formalisms. The literature is replete with various theoretical studies used for the prediction of  $\alpha$  decay half-lives (Akrawy et al., 2018; Cai et al., 2020; Hassanzad & Ghodsi, 2021; Manjunatha et al., 2021). The theoretical framework based on the nuclear mean-field approach is categorized into two: the first is the microscopic-macroscopic (mic-mac) model (Adamian et al., 2018; Bhagwat et al., 2012; Jachimowicz et al., 2018; Mirea et al., 2011) which

combines the macroscopic bulk properties of the liquid drop model with the microscopic quantum mechanical Strutinsky shell correction. The second includes the microscopic Hartree/ Hartree-Fock calculations in which the Skyrme and relativistic mean-field (RMF) models are solved in a self-consistent manner for both ground and intrinsic excited states (Ahmad et al., 2012; Jain et al., 2022; Joshua et al., 2022; Pei et al., 2007; Typel & Brown, 2003; Ward et al., 2013, 2015; Yahya & Falaye, 2021). In particular, Using various parameter sets, the Skyrme-Hartree-Fock and RMF models have been employed in the exploration of nuclei with Z = 120 in which N = 182 and/or 184 are predicted as the most probable spherical shell closure in the superheavy region (Bender et al., 2001; Bhuyan & Patra, 2012; Kruppa et al., 2000; Reinhard et al., 2000; W. Zhang et al., 2005).

#### 2.3.1 Synthesis of Superheavy Nuclei

To understand the island of stability, theoretical predictions have spurred efforts to synthesize the heaviest or superheavy nuclei. The synthesis of nuclei within the island of stability can be very complex because the available nuclei used as targets and projectiles do not possess the required number of neutrons. Additionally, the experimental challenge begins with increasing atomic number, as the production cross-section decreases exponentially with increasing atomic number. In the literature, it is known that the heaviest nuclei have been synthesized in heavy-ion fusion reactions. In this process, a compound nucleus is formed with some excitation energy. Based on the excitation energy of the compound nucleus and its survival probability in the neutron emission process, this reaction has been classified into two categories:

(i) **Cold fusion reaction**: In this category of reaction, when the heavy target nuclei  $^{208}$ Pb or  $^{209}$ Bi fuse with massive projectile nuclei (A = 50 - 70), a compound nucleus is formed with an excitation energy of 20-11 MeV, and evaporation products are obtained with Z = 104 - 112 (S. Hofmann & Münzenberg, 2000b; Morita et al., 2004; Y. T. Oganessian,

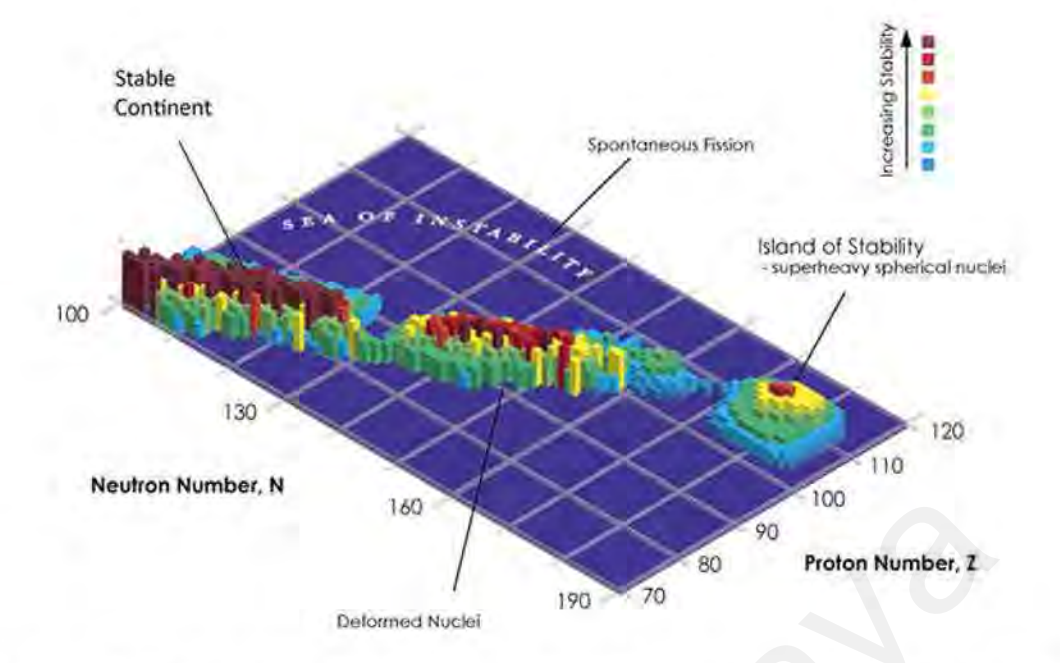


Figure 2.1: Three-dimensional representation of the theoretical island of stability in nuclear physics. Adopted from (W. Greiner, 2012)

1988). The main advantage of this reaction is that the transition of this nucleus to the ground state occurs through the emission of only one neutron and gamma rays. As the mass of the projectile ion increases, the cross-section for the formation of the evaporation product decreases sharply due to limitations on fusion that emerge in the entrance channel of the reaction. Using the cold fusion reaction for the first time, elements with atomic numbers Z = 107 - 112 were synthesized and their radioactive decay was investigated.

(ii) Hot Fusion Reaction with  $^{48}$ Ca Ions: In contrast, hot fusion reactions involve heavy actinides as targets and  $^{48}$ Ca as projectiles. These reactions yield compound nuclei with excitation energies ranging from 30-40 MeV, commonly referred to as hot fusion reactions. However, the formation of the compound nucleus competes with strongly asymmetric fission in this scenario. The transition to the ground state involves the emission of three or four neutrons and gamma rays. This reaction exhibits a low survival probability due to fission events, which interrupt the cooling process through sequential neutron emission. In particular, the choice of neutron-rich isotopes, such as  $^{48}$ Ca as the projectile and  $^{244}$ Pu, and  $^{248}$ Cm as targets, aims to produce compound nuclei near closed-shell values of Z = 114

and N = 184. This reaction has been used for the synthesis of heavy nuclei with  $Z \ge 112$ , where the cold fusion reaction is at the limit of the experimental possibilities.

#### 2.4 Alpha Decay of SHN

Due to the unstable nature of SHN, it is often influenced by external factors such as the injection of energy through interactions with nucleons or through spontaneous radioactive decay. This process can involve the emission of various particles or radiation, including alpha ( $\alpha$ ) and beta ( $\beta$ ) particles, gamma ( $\gamma$ ) radiation, as well as light particles or nuclei such as two-proton emissions. In this study, the primary focus is specifically on alpha decay. Alpha decay is a form of radioactive decay in which an unstable nucleus releases excess energy by spontaneously ejecting an alpha particle <sup>4</sup>He. This decay process can be represented as:

$${}_{Z}^{A}X_{N} \rightarrow {}_{Z-2}^{A-4}Y_{N-2} + \alpha,$$
 (2.1)

where the parent nucleus X yields a daughter Y by emitting an  $\alpha$ -particle. This decay process occurs as a result of the increasing Coulomb repulsion force, which is proportional to the square of the atomic number ( $Z^2$ ) compared to the nuclear binding force which is proportional to the mass number (A). Due to the stability and high binding energy (28.3 MeV) of the alpha particle, it becomes the preferred decay product for numerous nuclei to release the maximum possible kinetic energy.

The formation of a helium nucleus is feasible within nuclei containing a neutron-rich and proton-rich composition, typically characterized by  $A \le 150$ . In such heavy nuclei, nucleons are situated far away from the nuclear shell closure and held together by certain collective degrees of freedom. As earlier mentioned,  $\alpha$ -particle formation is energetically favoured over the formation of two protons. In principle, the quantum mechanical tunneling of the pre-formed alpha particle across the barrier requires a positive energy state (Q-value)

(Majekodunmi, Bhuyan, et al., 2022). This phenomenon known as the preformed cluster decay model (PCM) stems from the well-established Quantum Mechanical Fragmentation Theory (QMFT), where the Gamow theory of alpha decay was used (Fink et al., 1974; Maruhn & Greiner, 1974). The phenomenon of alpha decay, observed since 1920, is explained through two distinct approaches: cluster-like and fission-like. In the cluster-like perspective, alpha decay occurs naturally, while the fission-like approach emphasizes an asymmetric mass distribution in the parent nuclei. The identification of highly asymmetric mass fragmentation, initially observed in heavy nuclei such as <sup>238</sup>U, underscores the role of the effects of the quantum shell in the penetration of the barrier. Contemporary research endeavors, both theoretical and experimental, strive to forecast the half-life of alpha decay, driven by the pursuit of discovering the heaviest elements. Studies on alpha decay in heavy nuclei indicate it as the most probable decay mode in nuclei having neutron numbers N = 159-165 (Budaca & Silisteanu, 2011; Sridhara et al., 2021).

#### 2.5 Preformation Probability of $\alpha$ -Decay

In PCM models (or alpha-decay-like models), holds the assumption that an  $\alpha$ -particle is already formed within the parent nucleus prior to penetrating through the potential barrier with a specified Q-value. The decay fragments (daughter nucleus and emitted  $\alpha$ -particle) are formed in the ground state with a specific preformation probability  $P_{\alpha}$ . Hence,  $P_{\alpha}$  encapsulates the structural characteristics of the decaying parent nucleus. In the microscopic context, determining the precise value of  $P_{\alpha}$  can be challenging due to the intricacies inherent in the nuclear many-body problem.  $P_{\alpha}$  in alpha radioactivity may be significantly below unity, as evidenced by previous studies (Ahmed et al., 2015; Prathapan et al., 2023; Yahya et al., 2024). Consequently, to estimate the preformation probability  $P_{\alpha}$  a phenomenological scaling factor proposed by Blendowske and Walliser (Blendowske & Walliser, 1988). To overcome this limitation of the mass-dependent formula, in this

study a recently proposed universal  $\alpha$  cluster preformation formula established based on concepts that consider the influence of the mass and charge asymmetry ( $\eta_A$  and  $\eta_Z$ ), the  $\alpha$ -particle mass  $A_{\alpha}$  and the Q value is used. The new expression  $P_{\alpha}$ , as well as its effect and advantages, will be discussed in subsequent chapters of this thesis.

#### 2.6 Hindrance Factor

In the context of alpha decay, the hindrance factor refers to a measure of suppression or reduction (a phenomenon in which the decays of odd-A nuclei are hindered) in the decay rate of a particular nuclear transition, leading to a slower decay rate compared to what is predicted by simple one-body theories. Factors that impact the rate of decay include:

- 1. the presence of unpaired nucleons which influences  $\alpha$ -particle preformation.
- 2. a non-zero angular momentum (i.e.  $\ell \neq 0$ ) which results in higher barrier
- 3. change in spin which impedes alpha decay.

In other words, it provides a quantification of the deviation (resulting in a slower decay rate) observed in a specific alpha decay compared to what would be expected from systematic patterns based on ground state (g.s.) to ground state (g.s.) transition rates of neighboring even-even nuclei (Gallagher Jr & Rasmussen, 1957). Hindrances to alpha decay can also occur in even-even nuclei if a transition leads to an excited state in the daughter nucleus. In the present study, it is salient to note that only the g.s.  $\rightarrow$  g.s. transition ( $\ell = 0$ ) is considered.

#### 2.7 Nuclear Rotation

The decay properties of SHN are closely linked with the nuclear shell stability, isospin dependence of the nuclear structure, deformation, rotation and vibrational properties, single-particle energy level as well as fusion-fission dynamics (Bhuyan, 2015; Bhuyan, Patra, & Gupta, 2011; Fiset & Nix, 1972; Nilsson et al., 1969; Patra et al., 2009; Staszczak

et al., 2013). An  $\alpha$ -cluster chain can gain extra stability via the rotation of the nuclear system (Ren et al., 2022; K. Zhang et al., 2022). Within the mean-field approximation, it is pertinent to consider many-body correlations with symmetry breaking, such as the loss of translational and rotational invariance (Ring & Schuck, 1980). As a result, the deformed state gives a poor estimate of the angular-momentum quantum number, taking a semblance of an intrinsic ground state. To restore the broken symmetry, corrections to the binding energies are taken into account. In principle, the centrifugal force favours a linear chain configuration having a large moment of inertia although, a very high angular momentum leads to the fission of the linear chain. Thus far, only a little attention has been given to the rotational effect on the stability of proton-rich nuclei, especially in the highly debated superheavy region and thus, this will be one of the main focuses of the present study.

#### **CHAPTER 3: THEORETICAL FORMALISM**

#### 3.1 Introduction

In this chapter, an exploration is conducted into the theoretical formalism underlying the estimation of  $\alpha$ -decay half-lives, with a focus on six distinct semi-empirical formulae. These formulae, including the VSS formula, mB1 formula, SemFIS2 formula, R Formula, Wang Formula, and MYQZR formula, offer essential insights into the various factors influencing the  $\alpha$ -decay process, such as the number of proton and neutrons, the number of mass, the isospin asymmetry and the obstacles. Furthermore, microscopic approaches are discussed, particularly the Self-Consistent Mean Field (SCMF) framework, providing comprehensive insights into nuclear properties across different nuclei. Specifically, attention is directed towards the Deformed Relativistic Hartree-Bogoliubov theory in the continuum (DRHBc), which employs the meson-exchange density functional to elucidate nucleon interactions within many-body systems. Additionally, the Relativistic Hartree-Bogoliubov (RHB) formalism is examined, emphasizing the medium-dependent relativistic NN potential and the density-dependent meson-nucleon exchange coupling. The calculation of the nuclear interaction potential involves the utilization of the double folding technique, integrating RHB densities over the density-dependent R3Y NN potential. This total interaction potential, in combination with the Coulomb potential, forms the basis for estimating the WKB penetration probability of the emitted  $\alpha$ -particle, a crucial step in predicting  $\alpha$ -decay half-lives using the preformed cluster-decay model.

#### 3.2 Semi-Empirical Formulae

Here, six different semi-empirical formulae are used to estimate the  $\alpha$ -decay half-lives. This helps to evaluate relative constituents/ingredients such as the proton, neutron, mass number, isospin asymmetry, and hindrance factor that pose a significant influence on the

 $\alpha$ -decay process.

(a) VSS formula: The phenomenological formula of Viola and Seaborg (Viola Jr & Seaborg, 1966) is based on the well-known Gamow model. It incorporates the hindrance factor  $h_{log}$  for nuclei with unpaired nucleons and is linearly dependent on the number of protons in the parent nucleus. It is given by

$$\log_{10} T_{1/2}^{VSS} = (aZ + b)Q^{-\frac{1}{2}} + cZ + d + h_{log}.$$
 (3.1)

The constants are a = 1.66175, b = -8.5166, c = -0.20228, d = -33.9069 and  $h_{log} = 0$  for the even-even systems considered.

(b) mB1 formula: The modified Brown (mB1) formula (Sobiczewski et al., 1989) provides a similar formulation that includes an additional hindrance term  $h^{mb1}$  which depends on parity:

$$\log_{10} T_{1/2}^{mb1} = a(Z - 2)^b Q^{-\frac{1}{2}} + c + h^{mb1}, \tag{3.2}$$

where constants a = 13.0705, b = 0.5182, c = -47.8867 and  $h^{mb1} = 0$ .

(c) SemFIS2 formula: The semi-empirical formula based on fission theory (SemFIS2) was introduced by Poenaru (Akrawy et al., 2022; D. Poenaru & Ivascu, 1984; D. Poenaru et al., 1980; D. N. Poenaru et al., 2006) for  $\alpha$ -decay takes the expression

$$\log_{10} T_{1/2}^{SemFIS2} = 0.43429 \chi(x, y) K - 20.446 + H^f, \tag{3.3}$$

where

$$K = 2.52956Z_d [A_d/AQ]^{\frac{1}{2}} [\cos^{-1} \sqrt{r} - \sqrt{r(1-r)}]$$
(3.4)

and  $r = 0.423Q(1.5874 + A_d^{1/3})/Z_d$ . The numerical coefficient  $\chi$ , close to unity, is a  $2^{nd}$ -order polynomial:

$$\chi(x,y) = B1 + x(B2 + xB4) + y(B3 + yB6) + xyB5, \tag{3.5}$$

where the parameter values deduced for trans-uranium nuclei are B1 = 0.985415, B2 = 0.102199, B3 = -0.024863, B4 = -0.832081, B5 = 1.50572 and B6 = -0.681221. The hindrance factor  $H^f = 0$  for even-even nuclei. The reduced variables x and y are given as

$$x = (N - N_i)/(N_{i+1} - N_i), N_i < N \le N_{i+1}$$
(3.6)

$$y = (Z - Z_i)/(Z_{i+1} - Z_i), Z_i < Z \le Z_{i+1}$$
(3.7)

with the distance from the nearest magic-plus-one neutron and proton numbers  $N_i = ..., 51, 83, 127, 185, 229, ..., Z_i = ..., 29, 51, 83, 127, ...;$  Thus, for nuclei in the superheavy region

$$y = (N - 127)/(185 - 127), x = (Z - 83)/(127 - 83).$$
 (3.8)

(d) R Formula: Royer derived an analytical formula (Royer, 2000) for alpha decay half-life within the liquid-drop model including proximity effects where the  $\alpha$ -decay half-life depends on  $Q_{\alpha}$ , A and Z of the parent nucleus as

$$\log_{10} T_{1/2}^{R} = \frac{aZ}{\sqrt{O_{\alpha}}} + bA^{\frac{1}{6}}\sqrt{Z} + c, \tag{3.9}$$

where a = 1.5864, b = -1.1629 and c = -25.31 are adjustable parameters and depend on the parity of the parent nucleus combination Z, N.

(e) Wang Formula: The Wang formula is given as (Y. Wang et al., 2015) uniquely captures the shell effect S and hindrance term due to parity changes  $d^{1-(-1)^l}$ . However, l=0 since all nuclei under study are considered to be in the ground state.

$$\log_{10} T_{1/2}^{wang} = a + bA^{\frac{1}{6}} \sqrt{z} + \frac{cZ}{\sqrt{Q_{\alpha}}} + \frac{d^{1-(-1)^{l}} l(l+1)}{\sqrt{(A-4)(Z-2)A^{-2/3}}} + S.$$
 (3.10)

where a = -25.432, b = -1.146, c = 1.577, d = 0 (even-even nuclei) and S = 0.5 are the constant parameters.

(f) MYQZR formula: The YQZR formula (Akrawy et al., 2018) has been modified by adding the two asymmetry dependent I and  $I^2$  terms that are linearly related to the logarithm of  $\alpha$ -decay half-lives; the MYQZR is,

$$\log_{10} T_{1/2}^{MYQZR} = a\sqrt{\mu} Z_d Z_\alpha Q_\alpha^{-1/2} + b\sqrt{\mu} (Z_d Z_\alpha)^{1/2} + c\frac{l(l+1)}{\mu^{\sqrt{Z_d Z_\alpha A_d^{1/6}}}} + d + eI + fI^2,$$
(3.11)

where a = 0.41107, b = -1.44914, c = 0, d = 14.87085, e = 13.38618 and f = -61.47107 are the fitting parameters. Using the above-mentioned six formulae, the decay half-lives are predicted for the Decay energy  $(Q_{\alpha})$  for both rotational and non-rotational cases within DRHBc for the PC-PK1 parameter set whose values are given in Table 3.1.

## 3.3 Microscopic Approaches

The Self-Consistent Mean Field (SCMF) framework provides a comprehensive understanding of nuclear and collective properties across the spectrum of light, medium, heavy, and superheavy nuclei, extending from the valley to the drip line. Within the SCMF theory, each nucleon is characterized by one-body density matrices for either a single particle or a

quasi-particle state, effectively transforming many-body problems into one-body problems. Through an iterative process, the nucleon-nucleon interaction is derived, incorporating masses, charge radii, and pseudo data for nuclear matter properties. This approach, reminiscent of the Kohn-Sham density functional theory, successfully captures the intricacies of nuclear dynamics. The success of Dirac phenomenology has facilitated the development of relativistic descriptions of nuclear properties, notably through the Quantum Hadrodynamic (QHD) Walecka and Serot model. In this framework, nucleons interact with meson fields, with constraints of causality and relativistic propagator naturally incorporated. The Relativistic Mean-Field (RMF) model approximates the self-consistent Hartree approximation of the QHD model, focusing on Lagrangian densities and classical meson fields. Notably, in the RMF approach, the  $\sigma$  meson represents the mid and long-range attractive part, while the  $\omega$  and  $\rho$  mesons account for isospin dependence of nucleon interaction. The Coulomb interaction is handled by the photon field  $A_{\mu}$ . By introducing non-linear self-coupling terms in various meson fields, the RMF theory effectively explains nuclear properties and nucleon interactions in both finite nuclei and infinite nuclear matter, thus providing a comprehensive framework for understanding nuclear dynamics.

#### **3.3.1** Deformed Relativistic-Hartree- Bogoliubov theory in continuum (DRHBc)

The DRHBc theory stems from the meson-exchange density functional that delineates the interactions within the many-body system of nucleons and mesons which are expressed via the point-coupling Lagrangian density (Meng, 2016; Nikšić et al., 2008; K. Zhang et

Table 3.1: The point coupling constant and the pairing strengths of PC-PK1 parameter set.

Coupling constants	Values
$\alpha_S$	$-3.96291 \times 10^{-4} MeV^{-2}$
$eta_S$	$8.6653 \times 10^{-11} MeV^{-5}$
$\gamma_S$	$-3.80724 \times 10^{-17} MeV^{-8}$
$\delta_S$	$-1.09108 \times 10^{-10} MeV^{-4}$
$\alpha_V$	$-2.6904 \times 10^{-4} MeV^{-2}$
$\gamma_V$	$-3.64219 \times 10^{-18} MeV^{-8}$
$\delta_V$	$-4.32619 \times 10^{-10} MeV^{-4}$
$  \alpha_{TV}  $	$2.95018 \times 10^{-5} MeV^{-2}$
$\delta_{TV}$	$-4.11112 \times 10^{-10} MeV^{-4}$
$V_n$	$-349.5 MeV fm^3$
$V_p$	$-330.0 MeV fm^3$

al., 2020),

$$L = \overline{\psi}(i\gamma_{\mu}\partial_{\mu} - M)\psi - \frac{1}{2}\alpha_{S}(\overline{\psi}\psi)(\overline{\psi}\psi) - \frac{1}{2}\alpha_{V}(\overline{\psi}\gamma_{\mu}\psi)(\overline{\psi}\gamma^{\mu}\psi)$$

$$- \frac{1}{2}\alpha_{TV}(\overline{\psi}\vec{\tau}\gamma_{\mu}\psi)(\overline{\psi}\vec{\tau}\gamma^{\mu}\psi) - \frac{1}{2}\alpha_{TS}(\overline{\psi}\vec{\tau}\psi)(\overline{\psi}\vec{\tau}\psi) - \frac{1}{3}\beta_{S}(\overline{\psi}\psi)^{3} - \frac{1}{4}\gamma_{S}(\overline{\psi}\psi)^{4}$$

$$- \frac{1}{4}\gamma_{V}[(\overline{\psi}\gamma_{\mu}\psi)(\overline{\psi}\gamma^{\mu}\psi)]^{2} - \frac{1}{2}\delta_{S}\partial_{\nu}(\overline{\psi}\psi)\partial^{\nu}(\overline{\psi}\psi) - \frac{1}{2}\delta_{TV}\partial_{\nu}(\overline{\psi}\vec{\tau}\gamma_{\mu}\psi)\partial^{\nu}(\overline{\psi}\vec{\tau}\gamma^{\mu}\psi)$$

$$- \frac{1}{2}\delta_{S}\partial_{\nu}(\overline{\psi}\gamma_{\mu}\psi)\partial^{\nu}(\overline{\psi}\gamma^{\mu}\psi) - \frac{1}{2}\delta_{TV}\partial_{\nu}(\overline{\psi}\vec{\tau}\psi)\partial^{\nu}(\overline{\psi}\vec{\tau}\psi)$$

$$- \frac{1}{4}F^{\mu\nu}F_{\mu\nu} - e\overline{\psi}_{i}\gamma^{\mu}(\frac{1-\tau_{3}}{2})A_{\mu}\psi. \tag{3.12}$$

Here M and e are the nucleon mass and the proton charge, respectively. S, V and T denote the scalar, vector and isovector terms. The coupling constants are  $\alpha_S$ ,  $\alpha_V$ ,  $\alpha_{TS}$  and  $\alpha_{TV}$  whose higher order terms accounts for the medium effects include  $\beta_S$ ,  $\gamma_S$  and  $\gamma_V$  and the gradient terms include  $\delta_S$ ,  $\delta_V$ ,  $\delta_{TS}$  and  $\delta_{TV}$ .  $A_\mu$  and  $F_{\mu\nu}$  are the four-vector potentials and field strength tensor of the photon field, respectively. The equations of motion are deduced under the mean-field approximation.

To calculate the  $Q_{\alpha}$  values, the binding energies are calculated from the DRHBc theory for the PC-PK1 parameter set, which is consistent with those of the recent mass table (K. Zhang et al., 2022). The pairing correlations and mean field are treated in a

self-consistent manner and the RHB equation takes the form,

$$\begin{pmatrix} h_D - \lambda_\tau & \Delta \\ -\Delta^* & -h_D^* + \lambda_\tau \end{pmatrix} \begin{pmatrix} U_k \\ V_k \end{pmatrix} = E_k \begin{pmatrix} U_k \\ V_k \end{pmatrix}. \tag{3.13}$$

The quantities  $E_k$ ,  $\lambda_{\tau}$ , and  $h_D$  stand for the quasiparticle energy, Fermi energy / chemical potential and the Dirac Hamiltonian,

$$h_D(r) = \alpha . p + V(r) + \beta [M + S(r)],$$
 (3.14)

respectively. Here, S(r) and V(r) denote the scalar and vector potentials, respectively. The pairing potential is of the form

$$\Delta(r_1, r_2) = V^{PP}(r_1, r_2).k(r_1, r_2), \tag{3.15}$$

where

$$V^{PP}(r_1, r_2) = V_0 \frac{1}{2} (1 - P^{\sigma}) \delta(r_1 - r_2) \left( 1 - \frac{\rho(r_1)}{\rho_{sat}} \right), \tag{3.16}$$

with the pairing strength  $V_0 = -325$  MeV fm<sup>3</sup>, saturation density  $\rho_{sat} = 0.152$  fm<sup>3</sup> and k is the pairing tensor. As discussed in the preceding section, it is necessary to consider corrections to the binding energies calculated in DRHBc due to the restoration of rotational symmetry for deformed nuclei, under the mean-field approximation (K. Zhang et al., 2020; P.-W. Zhao et al., 2010). The cranking approximation (Girod & Grammaticos, 1979) is employed here to obtain the rotational energy as

$$\varepsilon_{rot} = -\frac{1}{2I} < \hat{J}^2 >, \tag{3.17}$$

where I denotes the moment of inertia estimated by the Inglis-Belyaev formula (Ring & Schuck, 1980) and  $J = \sum_{i}^{A} \hat{J}i$  is the total angular momentum where A is the mass number. A full description of the connection between the RHB Lagrangian density, rotational correction energies, and centre-of-mass can be found in Ref. (P.-W. Zhao et al., 2010). Using this formalism, the calculated binding energies are used to estimate the Q-value which is a crucial input for calculating the decay half-lives.

## 3.3.2 Relativistic-Hartree-Bogoliubov (RHB) Formalism

The relativistic mean-field approach has been very successful and widely applied to describe the structural properties of finite and infinite nuclear matter. As an advantage, its meson-nucleon interaction automatically accounts for the spin-orbit strength and the corresponding nuclear shell structure (S. K. Singh et al., 2014). In the RMF formalism (whose theoretical foundation is clearly given in the Appendix A.1), the local nucleonic interactions in Eq. (3.12) are replaced with the meson-exchange terms. The theory considers the nucleons as Dirac spinors  $\psi$  interacting via the exchange of mesons through the Lagrangian (Boguta & Bodmer, 1977; Joshua et al., 2022; Majekodunmi, Bhuyan, et al., 2022; Majekodunmi, Rana, et al., 2022; Ring, 1996; Serot & Walecka, 1986),

$$L = \overline{\psi} \{ i \gamma^{\mu} \partial_{\mu} - M \} \psi + \frac{1}{2} \partial^{\mu} \sigma \partial_{\mu} \sigma - \frac{1}{2} m_{\sigma}^{2} \sigma^{2} - \frac{1}{3} g_{2} \sigma^{3} - \frac{1}{4} g_{3} \sigma^{4}$$

$$- g_{\sigma} \overline{\psi} \psi \sigma - \frac{1}{4} \Omega^{\mu \nu} \Omega_{\mu \nu} + \frac{1}{2} m_{\omega}^{2} \omega^{\mu} \omega_{\mu} - g_{\omega} \overline{\psi} \gamma^{\mu} \psi \omega_{\mu} - \frac{1}{4} \vec{B}^{\mu \nu} . \vec{B}_{\mu \nu}$$

$$+ \frac{1}{2} m_{\rho}^{2} \vec{\rho}^{\mu} . \vec{\rho}_{\mu} - g_{\rho} \overline{\psi} \gamma^{\mu} \vec{\tau} \psi \cdot \vec{\rho}^{\mu} - \frac{1}{4} F^{\mu \nu} F_{\mu \nu} - e \overline{\psi} \gamma^{\mu} \frac{(1 - \tau_{3})}{2} \psi A_{\mu}. \tag{3.18}$$

The parameters  $g_{\sigma}$ ,  $g_{\omega}$  and  $g_{\rho}$  denotes the respective coupling constants of the participating mesons namely; isoscalar scalar  $\sigma$ , isoscalar vector  $\omega$  and isovector vector  $\rho$  mesons whose corresponding masses are  $m_{\sigma}$ ,  $m_{\omega}$  and  $m_{\rho}$ . M is the mass of the nucleons. The third component of the isospin is  $\tau_{3i}$ .

Table 3.2: Density Dependent meson-nucleon exchange coupling DD-ME2 parameter set. All masses are given in MeV

$\sigma$	ω	ρ
$m_{\sigma} = 550.1238$	$m_{\omega} = 783.0000$	$m_{\rho} = 763.0000$
$g_{\sigma}(\rho_{sat}) = 10.5396$	$g_{\omega}(\rho_{sat}) = 13.0189$	$g_{\rho}(\rho_{sat}) = 3.6836$
$a_{\sigma} = 1.3881$	$a_{\omega} = 1.3892$	$a_{\rho} = 0.5647$
$b_{\sigma} = 1.0943$	$b_{\omega} = 0.9240$	
$c_{\sigma} = 1.7057$	$c_{\omega} = 1.4620$	
$d_{\sigma} = 0.4421$	$d_{\omega} = 0.4775$	

The field tensors for  $\omega^{\mu}$ ,  $\vec{\rho}_{\mu}$  and  $A_{\mu}$  fields are given as

$$\Omega_{\mu\nu} = \partial_{\mu}\omega_{\nu} - \partial_{\nu}\omega_{\mu}, \tag{3.19}$$

$$\vec{B}^{\mu\nu} = \partial_{\mu}\vec{\rho}_{\nu} - \partial_{\nu}\vec{\rho}_{\mu}, \tag{3.20}$$

$$F^{\mu\nu} = \partial_{\mu}A_{\nu} - \partial_{\nu}A_{\mu}. \tag{3.21}$$

By taking these field tensors as classical fields, the Dirac equation is obtained for the nucleons. Similarly, the Klein-Gordon equations provide the field equation for the participating mesons under the mean-field approximation as (Lalazissis et al., 2005)

$$(-\nabla^{2} + m_{\sigma}^{2})\sigma(r) = -g_{\sigma}\rho_{s}(r) - g_{2}\sigma^{2}(r) - g_{3}\sigma^{3}(r),$$

$$(-\nabla^{2} + m_{\omega}^{2})V(r) = g_{\omega}\rho(r),$$

$$(-\nabla^{2} + m_{\rho}^{2})\rho(r) = g_{\rho}\rho_{3}(r).$$
(3.22)

#### **3.3.2.1** Medium-dependent Relativistic *NN* potential

It is worth mentioning that the relativistic R3Y NN potential obtained for linear and non-linear RMF parameter sets is well known for its successful exploration of several nuclear phenomena (Bhuyan & Kumar, 2018; Bhuyan et al., 2020; Joshua et al., 2022; Kumar et al., 2022; Majekodunmi, Bhuyan, et al., 2022; Majekodunmi, Rana, et al., 2022; Rana et al., 2022; B. Singh et al., 2012). In the aforementioned studies, the comparison between

Reid M3Y and R3Y NN potentials using different sets of non-linear RMF parameters reveals that the R3Y NN potential is more consistent with the experimentally measured data. However, the introduction of explicit density dependence in the M3Y NN potential (which accounts for the in-medium effects) was found to give a more comprehensive description of the properties of infinite nuclear matter (Anantaraman et al., 1983; Bertsch et al., 1977). This is the motivation to introduce the medium dependence in the relativistic R3Y NN potential. Unlike the M3Y potential in which the medium effect is introduced by multiplying with a weighted density function, the non-linear meson self-interaction terms in the R3Y NN potential obtained for non-linear RMF parameter sets effectively include the medium effects (Boguta & Bodmer, 1977). An alternative method to consider the medium effects in the relativistic NN potential (R3Y) is to introduce density-dependent parameterization in the relativistic-Hartree-Bogoliubov (RHB) approach (Fuchs et al., 1995; F. Hofmann et al., 2001; Lalazissis et al., 2005; Nikšić et al., 2002; Typel & Wolter, 1999).

$$g_i(\boldsymbol{\rho}) = g_i(\boldsymbol{\rho}_{sat}) f_i(\boldsymbol{x})|_{i=\sigma,\omega}, \tag{3.23}$$

where

$$f_i(x) = a_i \frac{1 + b_i(x + d_i)^2}{1 + c_i(x + d_i)^2}$$
(3.24)

and

$$g_{\rho}(\boldsymbol{\rho}) = g_{\rho}(\boldsymbol{\rho}_{sat}) exp[-a_{\rho}(x-1)]. \tag{3.25}$$

Here the nucleon-meson couplings are medium dependent with  $x = \rho/\rho_{sat}$ , and  $\rho_{sat}$  is the baryon density of symmetric nuclear matter at saturation. The properties of nuclear matter at saturation calculated with DD-ME2 include density  $\rho_{sat} = 0.152 \text{ fm}^{-3}$ , binding energy per particle E / A = -16.14 MeV, and incompressibility K = 250.97 MeV (Lalazissis et al., 2005). The five constraints  $f_i(1) = 1$ ,  $f_i''(0) = 0$ , and  $f_{\sigma}''(1) = f_{\omega}''(1)$  reduce the number of independent parameters in Eq. (3.24) from eight to three (Lalazissis et al., 2005). The independent parameters (the meson mass and coupling parameters) of the RHB formalism are obtained to fit the ground state properties of finite nuclei as well as the properties of symmetric and asymmetric nuclear matter. This study adopts a widely known DD-ME2 parameter set (Lalazissis et al., 2005) whose values are given in Table 3.2, to study the clustering of  $\alpha$  particles of neutron-deficient  $^{207,208}$ Th isotopes. The density-dependent R3Y (DD-R3Y) NN potential ( $V_{eff}^{R3Y}(r, \rho_{\alpha}, \rho_{d})$ ) is presented in terms of density-dependent meson-nucleon coupling constants such as (Bhuyan et al., 2022),

$$V_{eff}^{R3Y}(r, \boldsymbol{\rho}_{\alpha}, \boldsymbol{\rho}_{d}) = \sum_{i=\omega,\rho} \frac{g_{i}(\boldsymbol{\rho}_{\alpha})g_{i}(\boldsymbol{\rho}_{d})}{4\pi} \frac{e^{-m_{i}r}}{r} - \frac{g_{\sigma}(\boldsymbol{\rho}_{\alpha})g_{\sigma}(\boldsymbol{\rho}_{d})}{4\pi} \frac{e^{-m_{\sigma}r}}{r} + J_{00}\delta(r).$$
(3.26)

Here,  $m_{\sigma}$ ,  $m_{\omega}$  and  $m_{\rho}$  represent the masses of the corresponding  $\sigma$ ,  $\omega$  and  $\rho$  mesons, which intermediate the interaction between the nucleons.  $g_{\sigma}$ ,  $g_{\omega}$  and  $g_{\rho}$  are the nucleon-meson coupling constants and  $J_{00}(E)\delta(r)$  is the long-range one-pion exchange potential (OPEP). The expression for DD-R3Y in Eq. (3.26) is identical in form to that of the R3Y NN potential used in previous studies of Refs. (Bhuyan & Kumar, 2018; Bhuyan et al., 2020; Joshua et al., 2022; Kumar et al., 2022; Majekodunmi, Bhuyan, et al., 2022; Majekodunmi, Rana, et al., 2022; Rana et al., 2022; Sahu et al., 2014; B. Singh et al., 2012). In DD-R3Y, the nucleon-meson coupling constants are density-dependent, while they are constant in the

case of the R3Y NN potential. In other words, in the DD-R3Y NN potential, the coupling constants in the bare R3Y NN potential are replaced with their density-dependent terms. By implication, Eq. (3.26) now depends on the densities of the emitted  $\alpha$ -particle and the daughter nucleus. This is because the DD-R3Y NN potential is obtained microscopically within the relativistic (RHB) approach and the terms  $[|g_i(\rho_\alpha)g_i(\rho_d)|_{i=\sigma,\omega,\rho}]$  account for the meson exchange between the nucleons of the  $\alpha$ -particle and the daughter nuclei. Thus, the relativistic DD-R3Y NN potential is obtained for DD-ME2 within the relativistic-Hartree-Bogoliubov approach. Elaborate details on the relativistic parameterizations employed in the present analysis can be found in Refs. (Lalazissis et al., 2009, 2005; Nikšić et al., 2002).

## 3.4 The Double Folding Technique

The RHB (DD-ME2) density are integrated over Eq.(3.26) using the double folding technique (Satchler & Love, 1979) to calculate the nuclear interaction potential  $V_n(R)$  that takes the expression

$$V_n(R) = \int dr_{\alpha} \int dr_{d} \rho_{\alpha}(\vec{r}_{\alpha}) \rho_{d}(\vec{r}_{d}) V_{eff}^{R3Y}(\vec{r}_{\alpha d} = \vec{R} + \vec{r}_{d} - \vec{r}_{\alpha}). \tag{3.27}$$

Here, $\rho_{\alpha}$  and  $\rho_{d}$  are the nuclear densities of the  $\alpha$ -particle and daughter nuclei respectively. An alternative method in the literature that introduces the density-dependence for a composite system includes the Migdal approach (Migdal, n.d.) in which effective NN force incorporates the internal and external components. However, it has been lately shown that this phenomenological density-dependent nucleus-nucleus potential tends to underestimate the height of the Coulomb barrier (Antonenko et al., 2022). The relaxed density approximation (RDA) (Denisov, 2013, 2015) is another convenient approach by which the density dependence can be incorporated into the decay of the cluster (and  $\alpha$ –),

which is a deep sub-barrier process. Thus, the RDA assumes the clustering of  $\alpha$ -particles to be a very slow process, leading to the relaxation of the proton and neutron densities. Nonetheless, in an application to fusion studies, two of us and collaborators (Bhuyan et al., 2022) have recently demonstrated that the RDA adapts well with Eq. (3.26) but dwindles at small nuclear separation distance (r). Hence, Eq. (3.26) is used in the present study. The short-range nuclear interaction  $V_n(R)$  given in Eq. (3.27) is combined with the Coulomb potential  $V_C(R) = \frac{Z_\alpha Z_d}{R} e^2$  to produce the total interaction potential.

$$V_T(R) = V_n(R) + V_C(R),$$
 (3.28)

which is used to estimate the WKB penetration probability of the emitted  $\alpha$ -particle and hence the  $\alpha$ -decay half-lives using the preformed cluster-decay model (PCM) (Kumar, 2012).

## 3.5 The WKB Penetration Probability

The penetration probability of the  $\alpha$ -particle through the tunneling barrier is given as

$$P = P_a P_b \tag{3.29}$$

which involves a three-step process (Majekodunmi, Bhuyan, et al., 2022). Here,  $P_a$  and  $P_b$  are the integrals in the WKB approximation given as

$$P_a = \exp\left(-\frac{2}{\hbar} \int_{R_a}^{R_i} \{2\mu[V(R) - V(R_i)]\}^{1/2} dR\right), \tag{3.30}$$

and

$$P_b = \exp\left(-\frac{2}{\hbar} \int_{R_i}^{R_b} \{2\mu [V(R_i) - Q]\}^{1/2} dR\right). \tag{3.31}$$

The mechanism around Eq. (3.29-3.31) will be comprehensively analyzed in Section (4.3.2).

## 3.6 The Preformed Cluster-Decay Model

In the Preformed Cluster Model (PCM), the Decay half-life  $(T_{1/2})$  is given as

$$T_{1/2} = \frac{\ln 2}{\lambda},\tag{3.32}$$

where the radioactive decay constant  $(\lambda)$  is usually expressed in terms of Penetration probability (P) and Preformation Probability  $(P_{\alpha})$  as

$$\lambda = \nu_0 P_\alpha P. \tag{3.33}$$

The impact Assault frequency ( $\nu_0$ ) has a nearly constant value of  $10^{21}~{\rm s}^{-1}$  and can be estimated as

$$v_0 = \frac{\text{velocity}}{R_0} = \frac{\sqrt{2E_c/\mu}}{R_0}.$$
 (3.34)

Here,  $R_0$  symbolizes the radius of the parent nucleus and  $E_c$  is the kinetic energy of the emitted  $\alpha$ -particle. The Q-values are calculated from the experimental binding energies data (Uusitalo et al., 2005; Yang et al., 2022) using the expression

$$Q_{\alpha} = BE(A, Z) - BE(A - 4, Z - 2) - BE(4, 2), \tag{3.35}$$

where BE(A, Z), BE(A-4, Z-2) and BE(4, 2) are the binding energies of the parent, daughter nuclei and the emitted  $\alpha$ -particle respectively.

#### 3.6.1 A New Preformation Probability

Instead of the well-known one-parameter-based scaling factor of Blendowske and Walliser (Blendowske & Walliser, 1988), close attention is given to studying the relationships among various theoretically established properties/factors that influence Preformation Probability ( $P_{\alpha}$ ). Here, to obtain the  $\alpha$ -preformation probability, the newly derived formula (Majek et al., 2023) is employed, based on theoretically established characteristics governing the  $\alpha$  particle and/or cluster formation that includes the mass  $A_c$  (B. Singh et al., 2011), mass and charge asymmetries ( $\eta_A$  and  $\eta_Z$ ) defined such as  $\eta_A = (A_d - A_c)/(A_d + A_c)$  and  $\eta_Z = (Z_d - Z_c)/(Z_d + Z_c)$  (since emission of the same cluster from different parent nuclei and different clusters from the same parent nucleus is an experimentally observed fact (Bonetti & Guglielmetti, 1999, 2007; Gupta & Greiner, 1994)) and ( $r_B$ ) is the relative separation between the centers of fragments  $r_B = 1.2(A_c^{1/3} + A_d^{1/3})$  (Delion, 2009; Qian & Ren, 2011). Therefore, a new  $P_{\alpha}$  formula is proposed (Majek et al., 2023)

$$\log P_{\alpha} = -\frac{aA_c\eta_A}{r_B} - Z_c\eta_Z. \tag{3.36}$$

To evaluate the accuracy of the formula, the expression for  $\chi^2$  is,

$$\chi^2 = \sum_{i=1}^n \frac{\left[ \log_{10}^{Expt.} T_{1/2} - \log_{10}^{cal} T_{1/2} \right]^2}{\log_{10}^{cal} T_{1/2}}$$

for  $5 \, even-even$  nuclei and  $5 \, Odd-A$  nuclei, the constants  $a_{e-e}=-0.19$  and  $a_{e-o}=0.031$ . The newly derived  $P_{\alpha}$  formula in Eq. (3.36) has been successfully applied to the emission of clusters from various spherical heavy nuclei within the mass range 114 < A < 252 (Majek et al., 2023; Majekodunmi et al., 2023). Here, the experimentally measured systems (following the discovery of  $^{207}$ Th and the remeasured  $^{208}$ Th isotopes (Yang et al., 2022))

within the  $\alpha$ -decay chains are exclusively considered.

## 3.7 Pairing Correlation

Pairing energy serves as a potent tool for quantitatively analyzing nuclear properties. The pairing interaction is fundamental in elucidating nuclear structure phenomena in both open-shell and deformed nuclei. Various methods, including the BCS approach, the Bogoliubov transformation, and the particle number conservation approach, have been employed to tackle pairing correlations (Bhuyan & Kumar, 2018; Hao et al., 2012; Z.-H. Zhang et al., 2011). Among these, the Bogoliubov transformation emerges as the predominant method for incorporating pairing correlations, especially concerning nuclei near the drip-line region (Lalazissis, Vretenar, & Ring, 1999; Lalazissis, Vretenar, Ring, Stoitsov, & Robledo, 1999). However, for nuclei situated relatively close to the  $\beta$ -stability line, employing the constant gap BCS pairing approach provides a reasonably accurate estimation of pairing effects (Das et al., 2022, 2023; Dobaczewski et al., 1984). Consequently, this analysis adopts the constant gap BCS approach, with the pairing gaps for protons and neutrons obtained from the investigations conducted by Madland and Nix (Madland & Nix, 1988). The number of oscillator bases used is  $N_F = N_B = 20$  for both fermions and bosons fields.

In the BCS method, the pairing energy is given by  $E_{pair} = G[\Sigma_{i>0}u_iv_i]^2$ , where G represents the pairing force constant, and the occupation probabilities are  $u_i$  and  $v_i$  respectively. The densities included in the occupation number are  $n_i = v_i^2 = \frac{1}{2}$  [1- $\frac{\epsilon_i - \lambda}{\sqrt{(\epsilon_i - \lambda)^2 + \Delta^2}}$ ]. In this study, a constant gap for both protons and neutrons is adopted, as specified in Ref. (Madland & Nix, 1988), to account for pairing effects:  $\Delta_p = RB_s e^{-SI - tI^2/Z^{1/3}}$  and  $\Delta_n = RB_s e^{-SI - tI^2/A^{1/3}}$ . Here, the relative neutron excess is  $I = \frac{N-Z}{N+Z}$  and the other values are R = 5.72, s = 0.118, t = 8.12,  $B_s = 1$ , and s = 0.118 respectively. In solving the RMF equations, the pairing force constant G is not explicitly determined;

instead, the occupation probability is directly determined using the aforementioned gap parameter. The number of protons and neutrons in an atom determines the chemical potentials  $\lambda_n$  and  $\lambda_p$ . The final formula for the pairing energy is  $E_{pair} = -\Delta \Sigma_{i>1} u_i v_i$ . The pairing energy  $E_{pair}$  diverges when extended to an infinite configuration space given a constant pairing parameter and the force constant G. Indeed, for high momenta near the Fermi surface,  $\Delta$  decreases with the state (spherical or deformed) in all realistic calculations with finite-range forces (Bhuyan, Patra, Arumugam, & Gupta, 2011).

#### **CHAPTER 4: RESULTS AND DISCUSSION**

#### 4.1 Introduction

This chapter delves into the results and ensuing discussions stemming from the examination of nuclear rotation corrections on  $\alpha$ -decay half-lives of superheavy nuclei (SHN). Within this investigation, the chapter initially explores the bulk properties of SHN within the range of  $98 \le Z \le 120$ , followed by an analysis of the half-lives of the alpha decay of these nuclei utilizing various semi-empirical formulae. Furthermore, it scrutinizes the  $\alpha$ -particle clustering observed in the recently discovered  $^{207,208}$  Th decay chains within the Relativistic-Hartree-Bogoliubov (RHB) approach. This section examines both the structural and decay properties of the  $^{207,208}$ Th isotopic chains, contributing to a comprehensive understanding of these intriguing phenomena.

## 4.2 Nuclear Rotation Corrections on $\alpha$ -decay Half-lives of SHN

By employing the various semi-empirical formulae discussed in the preceding chapter, the  $\alpha$ -decay half-lives of superheavy nuclei whose atomic number ranges from Z=98-120 is estimated and analyzed. It is reiterated that, until now, only SHN with  $Z \leq 118$  has been successfully synthesized by a cold or hot fusion reaction in terrestrial laboratories (S. Hofmann & Münzenberg, 2000a; Münzenberg & Morita, 2015; Y. T. Oganessian et al., 2006, 2004, 1999; Ts et al., 2000). Thus, the present study is aimed at obtaining a correct estimate of the experimentally synthesized nuclei as a reliable basis upon which one can make a meaningful extension to an unknown nuclear regime. Preferential consideration has been given to the effect of nuclear rotation in the  $Q_{\alpha}$ -value calculated from the binding energies of the participating nuclei using the deformed relativistic Hartree-Bogoliubov theory in the continuum (DRHBc) with the PC-PK1 parameter set.

## **4.2.1** Bulk Properties of SHN within $98 \le Z \le 120$

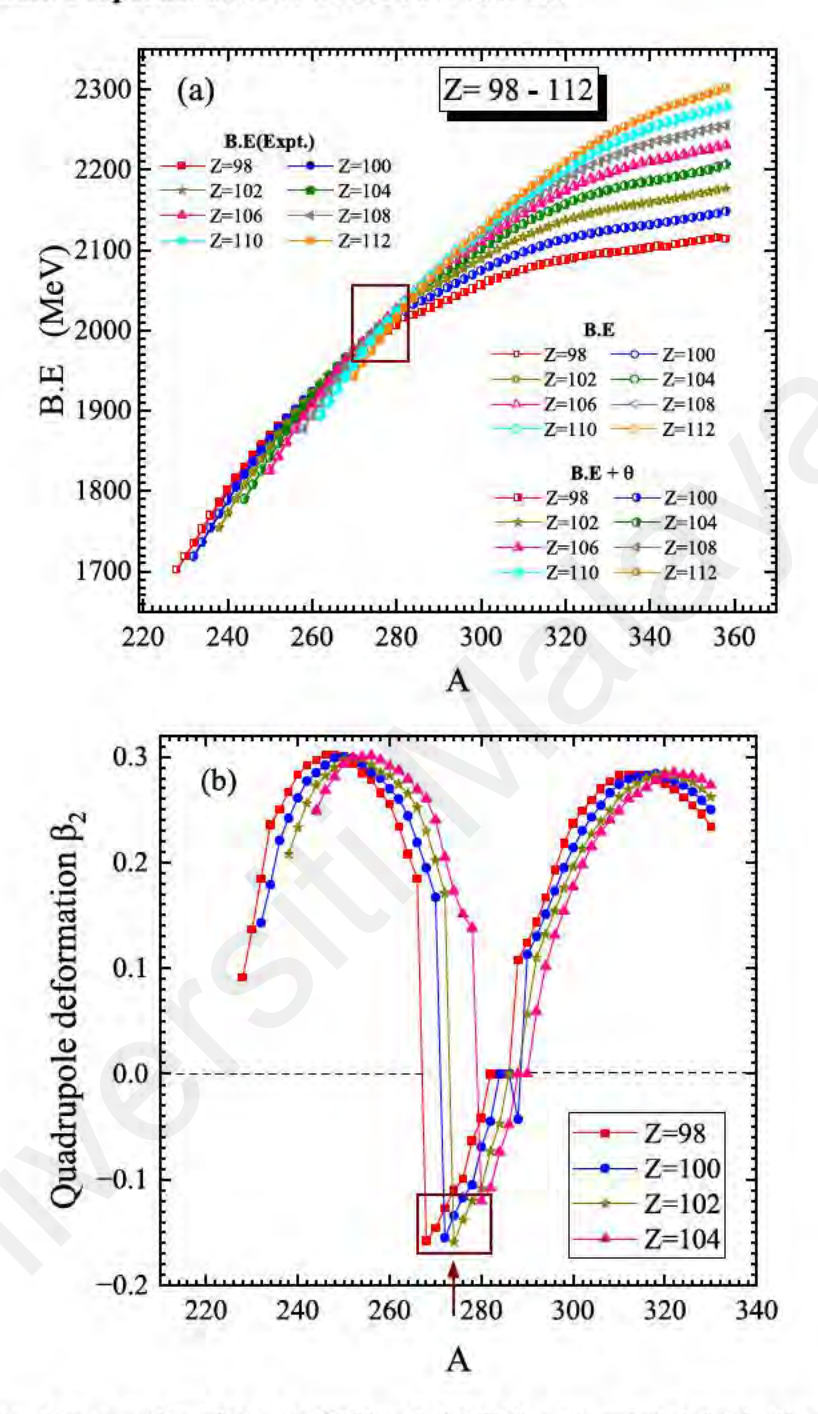


Figure 4.1: The profile of the DRHBc (PC-PK1) estimated (a) binding energies without (open shape) and with rotation correction (half-open shape) for an illustrative case of Z=98-112 isotopic chains. The results are compared with the available experimental data (solid shape) (Kondev et al., 2021). (b) Quadrupole deformation  $\beta_2$  of Z=98-104. A similar profile is observed for all the considered systems (with slightly different magnitudes), but only a few are shown here for the sake of clarity.

Fig. 4.1a displays the profile of the binding energies (B.E) with and without the inclusion

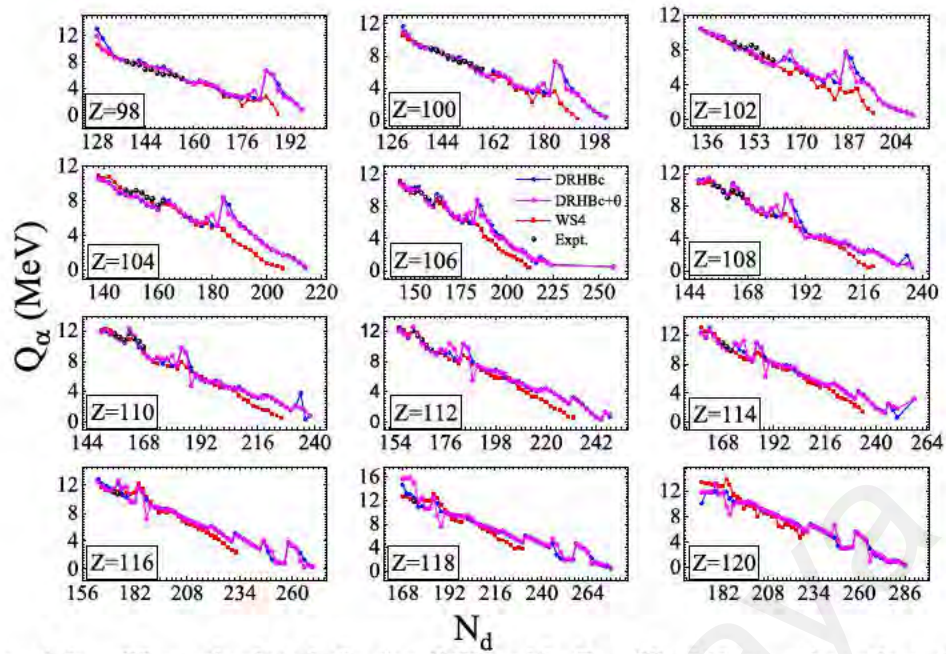


Figure 4.2: The calculated  $Q_{\alpha}$  for SHN with Z=98-120 as a function of the neutron number of the daughter nuclei  $(N_d)$  for DRHBc (solid line with blue circle) and DRHBc+ $\theta$  (solid line with magenta star) using the PC-PK1 parameter set in comparison with those calculated from the WS4 (N. Wang et al., 2014) (solid line with red rectangles) and the experimental data (Kondev et al., 2021) (solid black sphere), wherever available.

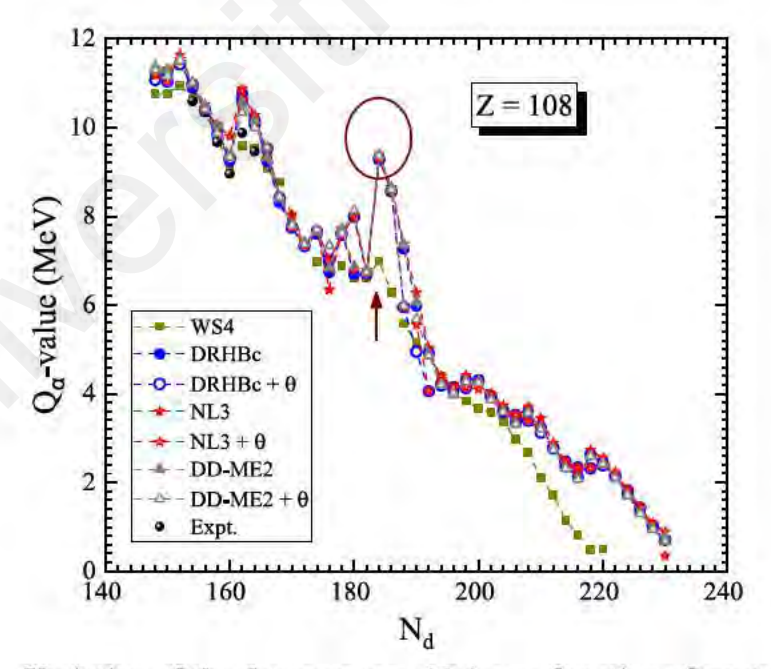


Figure 4.3: Variation of the decay energy  $(Q_{\alpha})$  as a function of neutron number of the daughter nuclei  $(N_d)$  using DRHBc (PC-PK1) and the relativistic mean-field based (NL3 and DD-ME2) parameters sets for a representative case of Z=108. The results are compared with the  $Q_{\alpha}$  values estimated from the WS4 and the available experimental data (Kondev et al., 2021).

of the rotational effect  $(\theta)$  as a function of the mass number of the participating nuclei using the DRHBc formalism. In case a similar pattern is noticed with slightly different magnitudes. However, for the sake of clarity, only the B.E of 98 - 112 isotopic chain is graphically shown. From the figure, it is apparent that the binding energies increase with their mass number A. However, a careful inspection of Table A.1 (in the appendix) reveals that the quantitative estimate of  $(B.E + \theta)$  agrees more closely with the experimental binding energies (Kondev et al., 2021) as also shown in the figure. Thus, the effect of nuclear rotation cannot be undermined. Additionally, the dark-red rectangle marked portion, highlighted with an upward arrow around A = 270 - 282 in Fig. 4.1a indicates an interesting phenomenon in each of the isotopic chains which can be easily unravelled from the profile of their respective quadrupole deformation ( $\beta_2$ ) in Fig. 4.1b. Here, only the variation in  $\beta_2$  for Z = 98 - 104 is shown to keep clarity. The figure clearly shows that most of the examined isotopes are prolate ( $\beta_2 > 0$ ). Nonetheless, all nuclei in the valley (below the black dash lines) marked with the dark-red square around A = 270 - 282in Fig. 4.1b are found to be oblate  $(\beta_2)$  in shape. The abrupt change in shape in this valley is informed by the interplay between deformation and shell effects (Nesterenko et al., 2023). The presence of magic numbers, which correspond to filled energy levels, can be affected by quadrupole deformation (Sheline, 1976). In some cases, the magic numbers can be preserved even in deformed nuclei, while in others, they can be modified or disappear (Sheline, 1976). The behavior of magic numbers in deformed nuclei is an active area of research and can have significant implications for the stability and properties of these nuclei. Conventionally, an abrupt drop or increase in the nuclear binding energy is usually associated with the appearance of a shell and/or sub-shell closure (especially at the traditional magic numbers 2, 8, 20, 28, 50, 82, and 126). Various theoretical studies in the superheavy region have also predicted Z = 120 (Afanasjev et al., 2003; Bender et al.,

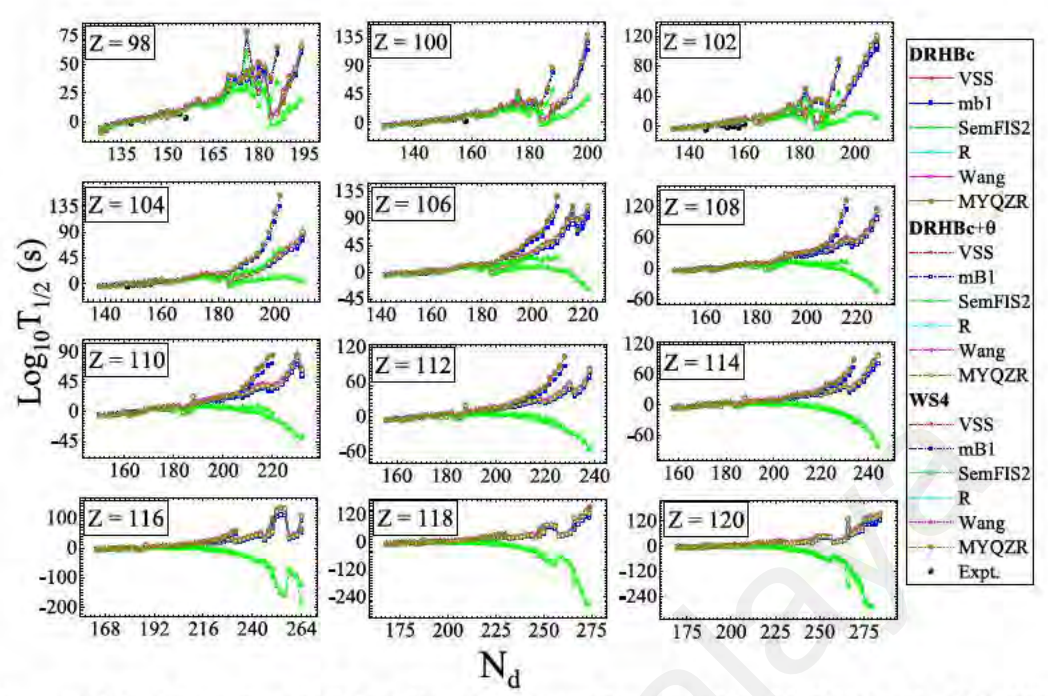


Figure 4.4: The estimated half-lives (in logarithmic scale) of SHN for Z=98 - 120 using DRHBc (solid line and shape) and DRHBc+ $\theta$  (dashed line and open shape) for PC-PK1 parameter set as a function of neutron number of the daughter nuclei (N<sub>d</sub>) for six semi-empirical formulae. The results are compared with experimental results(Kondev et al., 2021) (solid black sphere) and the WS4 (N. Wang et al., 2014) (dotted line and half-open shape).

1999; Lalazissis et al., 1996; Prassa et al., 2012) and N = 172, 184 (Dzuba et al., 2017; Gupta et al., 1997; Pattnaik et al., 2021; Sil et al., 2004; Taninah et al., 2020) as possible shell closures. These binding energies are used as inputs to calculate the  $Q_{\alpha}$ -values which can provide valuable information on the stability of the decay fragments.

Fig. 4.2 illustrates the variation of the theoretically calculated  $Q_{\alpha}$ -values from the DRHBc binding energies (with rotation (solid line with blue circle) and without rotation (solid line with magenta star)) in comparison with those of the macroscopic-microscopic (mac-mic) WS4 (solid line with red rectangles) (N. Wang et al., 2014) and the available experimental data (in black spheres) (Kondev et al., 2021). In other words, the DRHBc binding energies and those from the mentioned mass tables for the parent B.E(N, Z) and daughter nuclei B.E(N-2, Z-2) as well as  $\alpha$ -particle  $B.E_{\alpha}$  are calculated using the expression  $Q_{\alpha} = B.E(N, Z) - B.E(N-2, Z-2) - B.E_{\alpha}$ . The quantitative estimates of

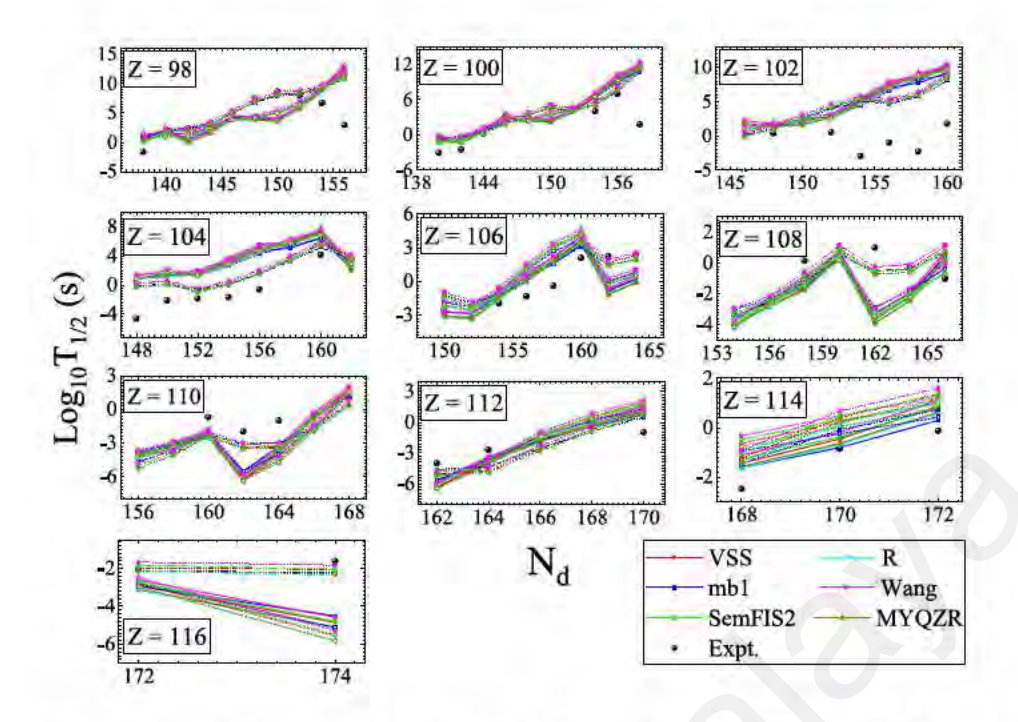


Figure 4.5: The estimated half-lives (in logarithmic scale) of SHN for Z=98 - 116 for DRHBc (solid line and shape) and DRHBc+ $\theta$  (dashed line and open shape) using the PC-PK1 parameter set for the nuclei with experimental data (Kondev et al., 2021) (solid black sphere) along with the WS4 (N. Wang et al., 2014) (dotted line and half-open shape) for six different empirical formula

the theoretical and experimental  $Q_{\alpha}$ -values are further shown in columns 3 and 4 of Table A.1 for the considered isotopic chains. The deviation (un-evenness) or abrupt surge at  $N_d = 184$  supports the allusion to previous theoretical findings that  $N_d = 184$  could be a probable shell closure (Dzuba et al., 2017; Gupta et al., 1997; Sil et al., 2004; Taninah et al., 2020). It is salient to note that the shell closure properties manifest in a strong enhancement of the binding energy and the binding energy per particle. The estimated binding energies of the considered isotopes can further reveal a rich collective phenomenology to obtain the two-neutron separation energies  $S_{2n}(N,Z) = B.E(N,Z) - B.E(N-2,Z)$ . The  $S_{2n}$  is usually used to explore structural properties such as the shell and subshell closures. In other words,  $S_{2n}$  gradually decreases with increasing neutron number, and noticeable kinks are usually clear indicators of nuclear magicity. The kink obtained within the isotopic chains (not shown here to avoid unnecessary repetition) further asserts  $N_d = 184$  as a

possible magic number. Besides, based on calculations of pairing gap,  $S_{2n}$ , and shell correction energy, the next proton magic number beyond Z = 82 has been suggested to be Z = 120 and N = 172, 182/184, 208 and 258 as the next neutron magic numbers (Bhuyan & Patra, 2012).

## 4.2.2 Alpha Decay Half-lives of Superheavy Nuclei within $98 \le Z \le 120$ using different Semi-Empirical Formulae

To estimate the effect of the rotational energy correction in the estimation of  $\alpha$ -decay half-lives, the  $Q_{\alpha}$  values calculated from the DRHBc binding energies are compared with those obtained from the relativistic mean-field (RMF) based on the NL3 and DD-ME2 parameter sets (with and without the effect of the rotational energy correction) and the macroscopic-microscopic based WS4 in Fig. 4.3 as a function of Neutron number of the daughter nucleus  $(N_d)$ . All the adopted functional and parameter sets are found to be in good agreement with the available experimental data (N. Wang et al., 2014). In each case, a similar profile is maintained with slightly different magnitudes. However, a careful inspection of the figure reveals that the DRHBc +  $\theta$ , NL3 +  $\theta$  chapter and DD-ME2 +  $\theta$ are relatively more in line with WS4 and those obtained from the experimental mass table. It is important to note that the closeness of the WS4 mass model can be attributed to the fact that it was originally phenomenologically fitted to 2353 measured masses (Joshua et al., 2022; B. Zhao & Zhang, 2019). The dark-red circle and the upward arrow beneath it reveal the presence of uniform notable peaks in the predictions of all the employed models, asserting the consideration of  $N_d = 184$  as a neutron shell closure in the superheavy region. The difference in magnitude and other noticeable fluctuations arise because the Q-value is a model-dependent parameter.

To perform a close examination of the DRHBc estimates with and without rotation for PC-PK1 parameter sets for the nuclei (only for the nuclei having experimental values)

Table 4.1: The calculated standard deviation  $(\sigma)$  of the logarithmic half-lives (with and without nuclear rotation effect) of  $98 \le Z \le 118$  using VSS, mB1, SemFIS2, R, Wang and MYQZR formulae.

Z	SEF	$\sigma$		Z	Z SEF		$\sigma$		
		$-T_{1/2}$	$T_{1/2}$ + $\theta$	•		$T_{1/2}$	$T_{1/2}$ + $\theta$		
98	VSS	3.973	3.575	110	VSS	1.985	2.222		
	mB1	3.725	3.375		mB1	1.682	1.907		
	SemFIS2	3.807	3.390		SemFIS2	1.868	2.113		
	R	3.956	3.552		R	2.081	2.335		
	Wang	3.951	3.590		Wang	1.806	2.029		
	MYQZR	3.931	3.522		MYQZR	2.073	2.332		
100	VSS	3.590	3.600	112	VSS	1.559	1.860		
	mB1	3.330	3.343		mB1	1.170	1.409		
	SemFIS2	3.330	3.343		SemFIS2	1.417	1.736		
	R	3.549	3.556		R	1.539	1.800		
	Wang	3.756	3.773		Wang	1.507	1.855		
	MYQZR	3.522	3.527		MYQZR	1.525	1.797		
102	VSS	6.925	6.727	114	VSS	0.864	1.400		
	mB1	6.506	6.325		mB1	0.552	1.000		
	SemFIS2	6.851	6.651		SemFIS2	0.929	1.484		
	R	6.837	6.636		R	0.648	1.180		
	Wang	7.212	7.016		Wang	1.123	1.665		
	MYQZR	6.833	6.630		MYQZR	0.698	1.241		
104	VSS	4.010	3.825	116	VSS	2.355	2.829		
	mB1	3.768	3.600		mB1	2.135	2.521		
	SemFIS2	4.095	3.899		SemFIS2	2.287	2.751		
	R	3.954	3.762		R	2.577	3.043		
	Wang	4.351	4.178		Wang	2.123	2.605		
	MYQZR	4.007	3.813		MYQZR	2.566	3.039		
106	VSS	1.841	2.008	118	VSS	1.426	6.129		
	mB1	1.694	1.850		mB1	1.199	5.048		
	SemFIS2	1.946	2.123		SemFIS2	1.203	5.716		
	R	1.880	1.994		R	1.640	6.335		
	Wang	1.879	2.178		Wang	1.103	5.770		
	MYQZR	1.914	2.037		MYQZR	1.586	6.337		
108	VSS	2.117	1.854						
	mB1	1.920	1.693						
	SemFIS2	2.051	1.801						
	R	2.212	1.965						
	Wang	1.945	1.663						
	MYQZR	2.209	1.961					_	

Z=98 - 116 are shown in Fig. 4.5 along with the experimental values and the WS4 predictions (N. Wang et al., 2014) (dotted line and half-open shape) for six different empirical formula. Although the graphs in Fig. 4.2 give the impression that both values are nearly overlapping, the estimated values in both cases in Fig. 4.5 and Table A.1 reveal that the consideration of the correction of the nuclear rotation ( $\theta$ ) brings the results closer to the available experimental data, especially for  $98 \le Z \le 104$ . The standard deviation ( $\sigma$ ) for predicted logarithmic half-lives of each of the semi-empirical formulae shown in Table 4.1 is mathematically expressed as

$$\sigma = \sqrt{\frac{1}{n} \sum_{i=1}^{n} \left[ \log_{10} T_{1/2}^{Expt.} - \log_{10} T_{1/2}^{Theo.} \right]^2}.$$
 (4.1)

From Table 4.1, it is quite apparent that incorporation of the rotational correction yields a larger deviation, especially for Z = 106 and 110 < Z < 118. In other words, the table gives the impression that considerable deviations could occur at large values of  $N_d$ , although this region lacks sufficient experimental data to draw an accurate inference or conclusion.

The decay half-lives are calculated using different semi-empirical formulae (namely, the Viola-Seaborg formula, modified Brown formula, semi-empirical formula based on fission theory, Royer Formula, Wang Formula, and Modified Yibin *et al.*), with and without the nuclear rotation effect. As shown in the previous section, each of these formulae is composed of certain influential ingredients on  $\alpha$ -radioactivity that distinguishes them from one another. All the employed formulae produce similar half-life predictions at lower values of  $N_d$ . However, as  $N_d$  increases across the isotopic chain, large deviations are noticed for SemFIS2. Such deviations are traceable to their respective formulations, which involve several ad-hoc parameters whose physical meaning/implications are not known in the  $\alpha$ -decay process. On the other hand, the predicted half-lives from VSS, mB1,

R, and Wang appear to be more consistent with the available experimentally measured half-lives. Fig. 4.4 shows the variation of the logarithmic half-lives ( $\log_{10} T_{1/2}$ ) for SHN with Z = 98 - 120 as a function of the neutron number of their respective daughter nuclei using the aforementioned semi-empirical formulae with different Q-values (WS4, DRHBc (with and without nuclear rotation correction)) as input. It is quite obvious that  $\log_{10} T_{1/2}$  produces a similar behaviour for each of the examined isotopic chains. It is worth noting that the most dominant decay mode of SHN is  $\alpha$ -emission, or in rare circumstances, spontaneous fission (Nagaraja et al., 2021).

A downward kink at  $N_d = 184$  in the half-life is observed in each of the isotopic chains considered, confirming its shell closure property and thus its likelihood to be the next magic number after the canonical magic numbers (2, 8, 20, 28, 50, 82, and 126). Thus, the stability of the  $\alpha$ -emitters is traceable to the shell closure effect. As seen in the figure (and in Table A.1), the effect of nuclear rotation correction (DRHBc  $+\theta$ ) brings the results closer to those of the WS4 and the available experimental results. While the  $\alpha$ -decay half-lives most of the isotopes await experimental measurement, it is apparent that the effect of nuclear rotation should be appraised and that the probability undergoing spontaneous fission for nuclei with  $N_d > 184$  is not feasible from the theoretical point of view. This is because the SemFIS2 model (green colour) deviates from the systematic trend beyond this point (and descends lower than the predicted shell closure- which is unphysical). Further, the decay properties of these nuclei over the isotopic chain  $N_d = 184$  confirms the shell and/or sub-shell closure of the previous theoretical findings (Dzuba et al., 2017; Gupta et al., 1997; Sil et al., 2004; Taninah et al., 2020). The implication of this predicted shell closure on the single-particle energy levels and its variation with different parameter sets have been elaborately discussed in Ref.(Bhuyan & Patra, 2012).

## **4.2.3** Systematic Study of Rotational effect on even-even <sup>254,256</sup>Rf isotopes

Here, close attention is given to calculating the  $\alpha$ -decay half-lives of the even-even <sup>254,256</sup>Rf isotopic chains using the deformed relativistic Hartree-Bogoliubov theory in the continuum (DRHBc) formalism with the PC-PK1 parameter set (P.-W. Zhao et al., 2010) along with and without rotational effect for deformed ground state nuclei. The  $Q_{\alpha}$  is calculated using the binding energies (BE) of the parent BE(N, Z) and daughter nuclei BE(N-2, Z-2), and <sup>4</sup>He nuclei by using the relation,  $Q_{\alpha} = BE(N, Z) - BE(N-2, Z-2) -$ BE (<sup>4</sup>He). As mentioned in the preceding section, the binding energies for the parents and daughters are obtained from the DRHBc approach for the PC-PK1 parameter set. Elaborate details about this approach can be found in Refs. (Dutra & Loureno, 2014; K. Zhang et al., 2022) and references therein. The  $\alpha$ -decay energy  $Q_{\alpha}$  is the key ingredient for obtaining the half-lives  $T_{1/2}$  and exploring the related phenomena. The ground state  $Q_{\alpha}$ -values for two decay chains (a)  $^{254}\text{Rf} \rightarrow ^{250}\text{No} \rightarrow ^{246}\text{Fm} \rightarrow ^{242}\text{Cf} \rightarrow ^{238}\text{Cm}$  and (b)  $^{256}\text{Rf} \rightarrow ^{252}\text{No}$  $\rightarrow$  <sup>248</sup>Fm  $\rightarrow$  <sup>244</sup>Cf  $\rightarrow$  <sup>240</sup>Cm are shown in Fig. 4.7. The  $Q_{\alpha}$ -values is calculated for each subsequent decay by using the binding energies obtained with (DRHBc) and without (DRHBc + rot) rotational effect as shown in Fig. 4.7 and also listed in Table 4.2. The corresponding experimental data (Kondev et al., 2021) are also given for comparison, wherever available. In Fig. 4.7 and Table 4.2, one can notice the variation of the decay energy with each parent nuclei along the <sup>254,256</sup>Rf decay chains for DRHBc formalism with the PC-PK1 parameter set. In both chains, the nuclear rotations seem to impose a lowering effect on the decay energy except in a few cases. Furthermore, the rotational effect is found to bring the  $Q_{\alpha}$ -values closer to the experimental data (Kondev et al., 2021). Hence, it can be concluded that the inclusion of nuclear rotation compensates for the weakness of the bare DRHBc approach. Besides, a detailed inspection of the values in the Table shows that the DRHBc (with or without rotation) gives a more precise  $Q_{\alpha}$  value at

Table 4.2: Comparison of the logarithm of half-lives of the even-even chains (a)  $^{254}$ Rf  $\rightarrow$   $^{250}$ No  $\rightarrow$   $^{246}$ Fm  $\rightarrow$   $^{242}$ Cf  $\rightarrow$   $^{238}$ Cm and (b)  $^{256}$ Rf  $\rightarrow$   $^{252}$ No  $\rightarrow$   $^{248}$ Fm  $\rightarrow$   $^{244}$ Cf  $\rightarrow$   $^{240}$ Cm using six different semi-empirical formulae. The predictive accuracy of each of these formulae is evaluated by comparing them to the experimental data (Kondev et al., 2021). The  $\alpha$ -decay energies ( $Q_{\alpha}$ ) for the above decay chains are calculated from the DRHBc formalism. See details in the text.

Parent	Daughter	Parameter	$Q_{\alpha}$ (I	MeV)	$\log_{10} T_{1/2}(\mathbf{s})$						
Nuclei	Nuclei		Theo.	Expt.	VSS	mB1	SemFIS2	R	Wang	MYQZR	Expt.
Chain (a)											
$^{254}_{104}$ Rf	$^{250}_{102}$ No	DRHBc	8.656	9.260	0.902	0.921	0.959	0.923	1.402	1.024	-4.635
		DRHBc+rot	8.706		0.742	0.781	0.799	0.762	1.242	0.861	
$^{250}_{102}$ No	$^{246}_{100}$ Fm	DRHBc	8.186	8.917	1.726	1.790	1.783	1.768	2.239	1.861	-5.301
		DRHBc+rot	8.456		0.820	0.991	0.875	0.857	1.334	0.943	
$^{246}_{100}$ Fm	<sup>242</sup> Cf	DRHBc	8.336	8.378	0.471	0.829	0.526	0.526	1.002	0.594	0.188
		DRHBc+rot	8.266		0.702	1.035	0.756	0.759	1.233	0.828	
<sup>242</sup> Cf	$_{96}^{238}$ Cm	DRHBc	8.266	7.518	-0.050	0.515	0.009	0.026	0.501	0.074	2.321
		DRHBc+rot	7.976		0.917	1.387	0.974	1.000	1.470	1.055	
$^{238}_{96}$ Cm	$_{94}^{234}$ Pu	DRHBc	6.296	6.670	6.858	6.971	6.982	7.020	7.451	7.095	3.899
50	74	DRHBc+rot	6.416		6.292	6.455	6.406	6.450	6.884	6.521	
Chain (b)											
$^{256}_{104}$ Rf	$^{252}_{102}$ No	DRHBc	8.556	8.928	1.228	1.205	1.348	1.211	1.689	1.295	-2.176
		DRHBc+rot	8.436		1.626	1.554	1.749	1.610	2.086	1.698	
$^{252}_{102}$ No	$^{248}_{100}$ Fm	DRHBc	8.296	8.548	1.352	1.460	1.462	1.352	1.826	1.420	0.389
102	100	DRHBc+rot	8.286		1.385	1.490	1.496	1.386	1.860	1.454	
$_{100}^{248}$ Fm	<sup>244</sup> Cf	DRHBc	7.626	7.996	2.956	3.046	3.073	2.988	3.449	3.049	1.538
		DRHBc+rot	7.856		2.114	2.295	2.222	2.141	2.607	2.196	
<sup>244</sup> Cf	$_{96}^{240}$ Cm	DRHBc	7.806	7.329	1.509	1.920	1.606	1.557	2.024	1.587	3.066
		DRHBc+rot	7.596		2.268	2.604	2.370	2.321	2.783	2.357	
$_{96}^{240}$ Cm	<sup>236</sup> Pu	DRHBc	6.386	6.398	6.432	6.583	6.594	6.552	6.985	6.592	6.368
	21	DRHBc+rot	5.296		12.294	11.926	12.622	12.463	12.862	12.542	

lower masses ( $^{246,248}$ Fm  $\rightarrow$   $^{242,244}$ Cf  $\rightarrow$   $^{238,240}$ Cm) beyond which a little deviation may set in. Such deviations in the relativistic mean-field (RMF) approach have been elaborately discussed in Ref. (Joshua et al., 2022). These  $Q_{\alpha}$  values are used as inputs into each of the considered semi-empirical formulae to compute the decay half-lives.

The  $\alpha$ -decay half-lives for the chosen decay chains are estimated for six empirical formulae, namely, the VSS formula, mB1 formula, SemFIS2 formula, R formula, Wang formula, and MYQZR. The calculated results for  $\alpha$ -decay half-lives using the two different (with and without rotation)  $Q_{\alpha}$ -values for DRHBc (PC-PK1) parameter set are given in Table 4.2 and also shown in Fig. 4.7 along with the experimental data (Kondev et al., 2021). Fig. 4.7 (a) and (b) reveals that most of the formulae are consistent with the experimental data. A more careful inspection of the figure shows that the difference in the predictions of the formulae can be largely attributed to their respective ingredients and formulations. However, the inclusion of rotation appears to be more compatible with the experimental

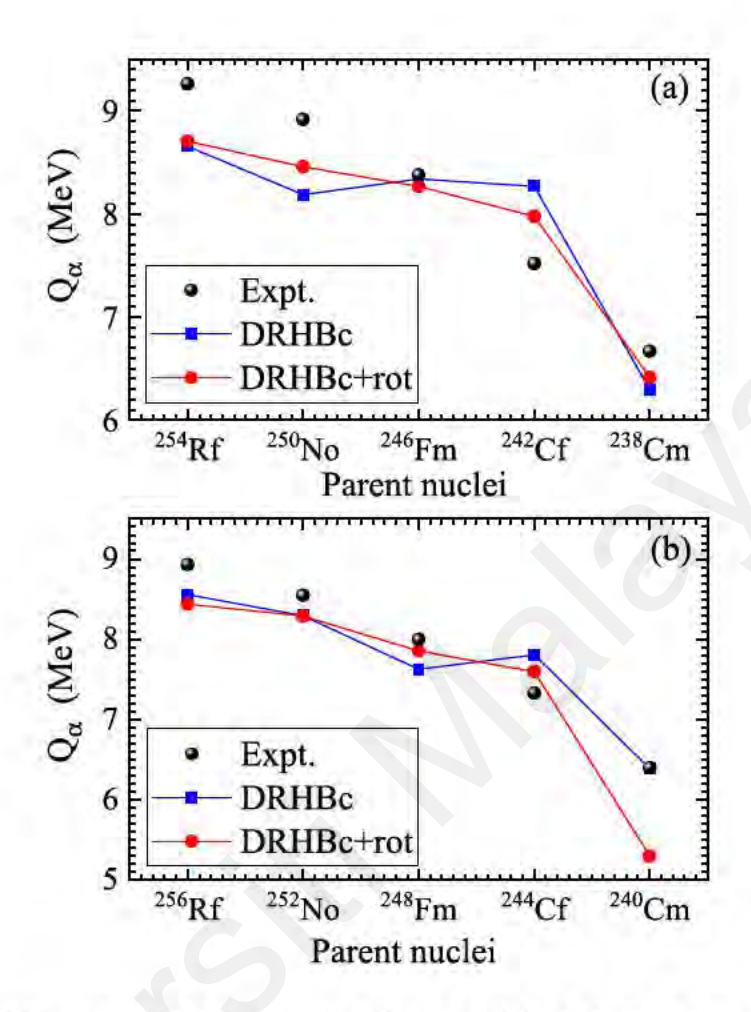


Figure 4.6: The calculated decay energy ( $Q_{\alpha}$ -values) for the decay chains (a)  $^{254}$ Rf  $\rightarrow$   $^{250}$ No  $\rightarrow$   $^{246}$ Fm  $\rightarrow$   $^{242}$ Cf  $\rightarrow$   $^{238}$ Cm and (b)  $^{256}$ Rf  $\rightarrow$   $^{252}$ No  $\rightarrow$   $^{248}$ Fm  $\rightarrow$   $^{244}$ Cf  $\rightarrow$   $^{240}$ Cm for DRHBc and DRHBc+rot using the PC-PK1 parameter set in comparison with the experimental data (Kondev et al., 2021).

data. As a consequence of the aforementioned deviation in the DRHBc binding energies (and Q-values) for certain nuclei with large mass like <sup>254,256</sup>Rf and <sup>250</sup>No, the half-life predictions from most of the semi-empirical formulae are relatively large as compared to the experimental data. It is salient to reiterate that the observed deviating points in Fig. 4.7 are directly traceable to the DRHBc estimate of the Q-values in the previous figures. This suggests the need for certain improvements in the DRHBc prediction and description of trans-fermium elements. This is because the trans-fermium region may

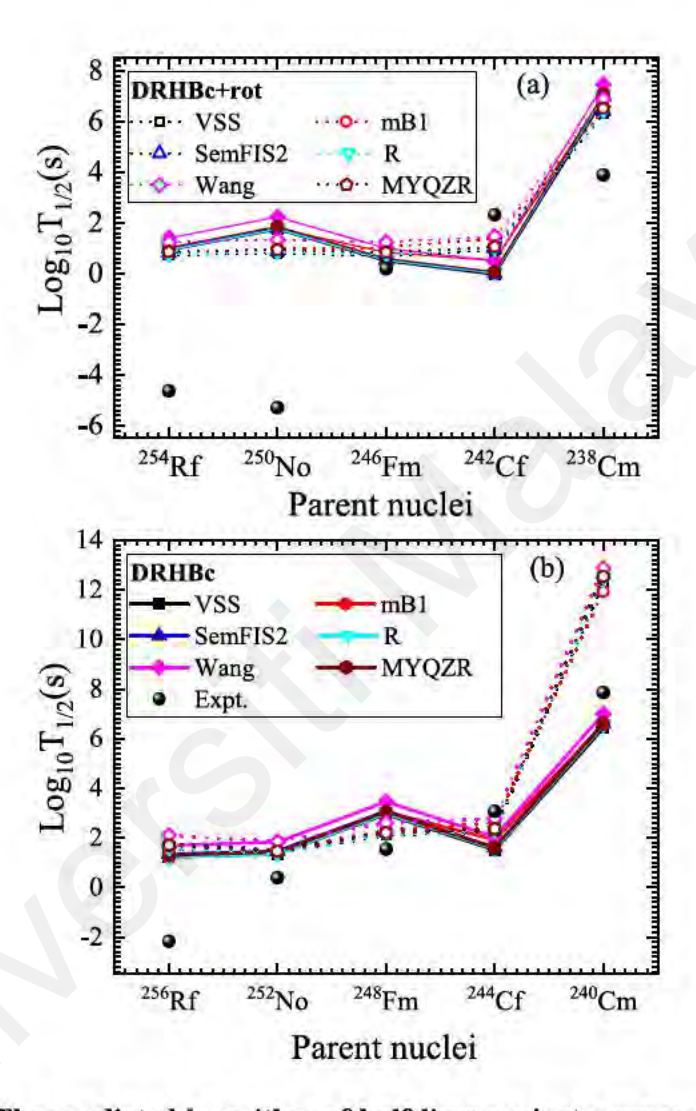


Figure 4.7: The predicted logarithm of half-lives against mass number by the six models compared with experimental results (Kondev et al., 2021) for(a)  $^{254}Rf \rightarrow ^{250}No \rightarrow ^{246}Fm \rightarrow ^{242}Cf \rightarrow ^{238}Cm$  and (b)  $^{256}Rf \rightarrow ^{252}No \rightarrow ^{248}Fm \rightarrow ^{244}Cf \rightarrow ^{240}Cm$  for DRHBc and DRHBc+rot. using the PC-PK1 parameter set in comparison with the experimental data (Kondev et al., 2021). The legends are split into both figures for the sake of visibility.

require special treatment due to their peculiar nuclear stability where the fission barriers tend to decrease to zero (Flerov et al., 1970). From all the figures (Fig. 4.7(a) - Fig. 4.7(b)), a recurring interesting phenomenon is observed in <sup>246,248</sup>Fm isotopes i.e. both points appear as a middle ground after which an upward trend is reversed (to a lower trend). This phenomenon is characteristic of nuclei with stabilized shells and thus, congruent with the recent findings of Das *et al.* (Das et al., 2022). The repeated discrepancy for Curium (Cm) isotopes could be due to the other dominant factors such as sub-shell/shell correction, occupancies, and a higher degree of deformation etc (Swain et al., 2019). which will be incorporated in future works.

# 4.3 $\alpha$ -particle clustering of the newly discovered $^{207,208}$ Th decay chains within RHB Approach

The theoretical formalism that is chronicled in the previous section is now used to investigate the decay and structural properties of the decay chains of  $\alpha$ -emitting  $^{207,208}$ Th decay chains. It is reiterated that the densities of the decay chains  $1^{st}$  ( $^{207}$ Th $\rightarrow$  $^{203}$ Ra  $\rightarrow$  $^{199}$ Rn  $\rightarrow$  $^{195}$ Po  $\rightarrow$  $^{191}$ Pb) and  $2^{nd}$  ( $^{208}$ Th $\rightarrow$  $^{204}$ Ra  $\rightarrow$  $^{200}$ Rn  $\rightarrow$  $^{196}$ Po  $\rightarrow$  $^{192}$ Pb) decay chains are obtained from the RHB (DD-ME2) parameter set, while the density of the  $\alpha$ -particle ( $^{4}$ He) is deduced from experimental data (De Vries et al., 1987).

## **4.3.1** Structural Properties of <sup>207,208</sup>Th Isotopic Chains

Fig. 4.8 depicts the profile of the radial distribution of the total density ( $\rho_T$ ) (which is expressed as the sum of the proton densities  $\rho_P$  and the neutron densities  $\rho_N$ ) for each of the participating nuclei. From the graph, it is apparent that the density profile of the  $\alpha$ -particle (green dash-dotted lines) is separate from those of the Thorium isotopes due to the difference in their respective mass compositions. On the contrary, the  $^{207,208}$ Th isotopes are characterized by lower density values. A similar trend is noticed for both isotopes and their strongly overlapping densities can be largely attributed to their nearly

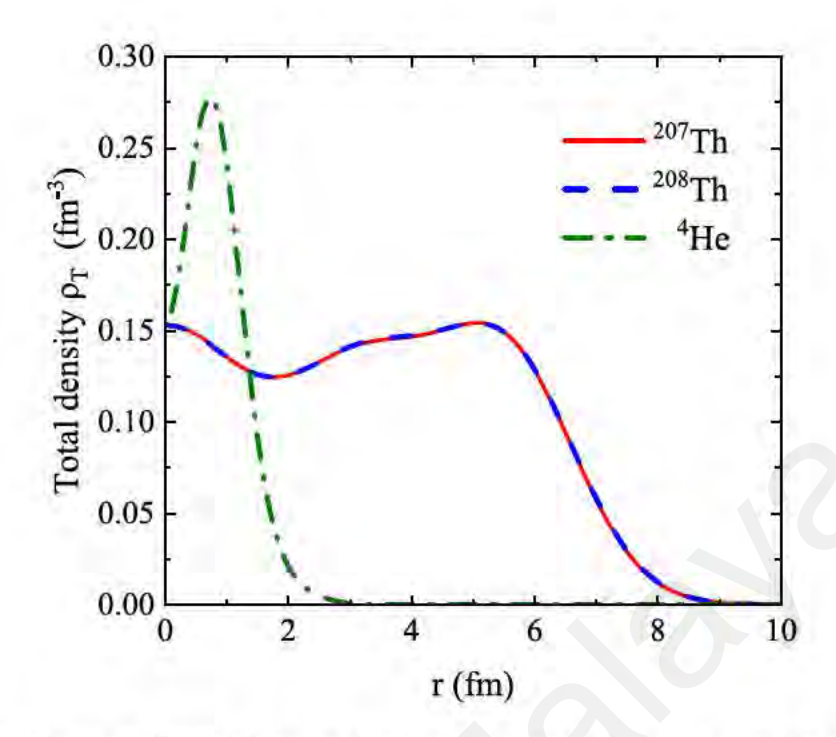


Figure 4.8: The radial distribution of the total density ( $\rho_T = \rho_P + \rho_N$ ) obtained from the RHB (DD-ME2) parameter set for  $^{207}$ Th (solid red line) and  $^{208}$ Th (blue dashes) decay chains. The density of the  $\alpha$ -particle ( $^4$ He) in green dash-dotted lines is deduced from experimental data (De Vries et al., 1987).

equal masses and constituents. In both cases, the profiles are governed by a low-density value in the central region, an increase in magnitude towards the nuclear surface, and a sharp decline in the tail region, which is a hallmark of heavy nuclei (Bhuyan et al., 2010). The contribution of the surface region to the nucleus-nucleus interaction is highly significant in nuclear clustering (Antonenko et al., 2022). While the nuclear density is saturated in the internal region, the nuclear surface region encapsulates the information about the nuclear structure (Horiuchi & Inakura, 2020, 2021). Here, the results are found to be consistent with the recent findings in refs. (Horiuchi & Itagaki, 2022; Ishizuka et al., 2022) where the authors outlined the mechanism that governs the emergence of  $\alpha$ -cluster around the nuclear surface for medium-mass nuclei.

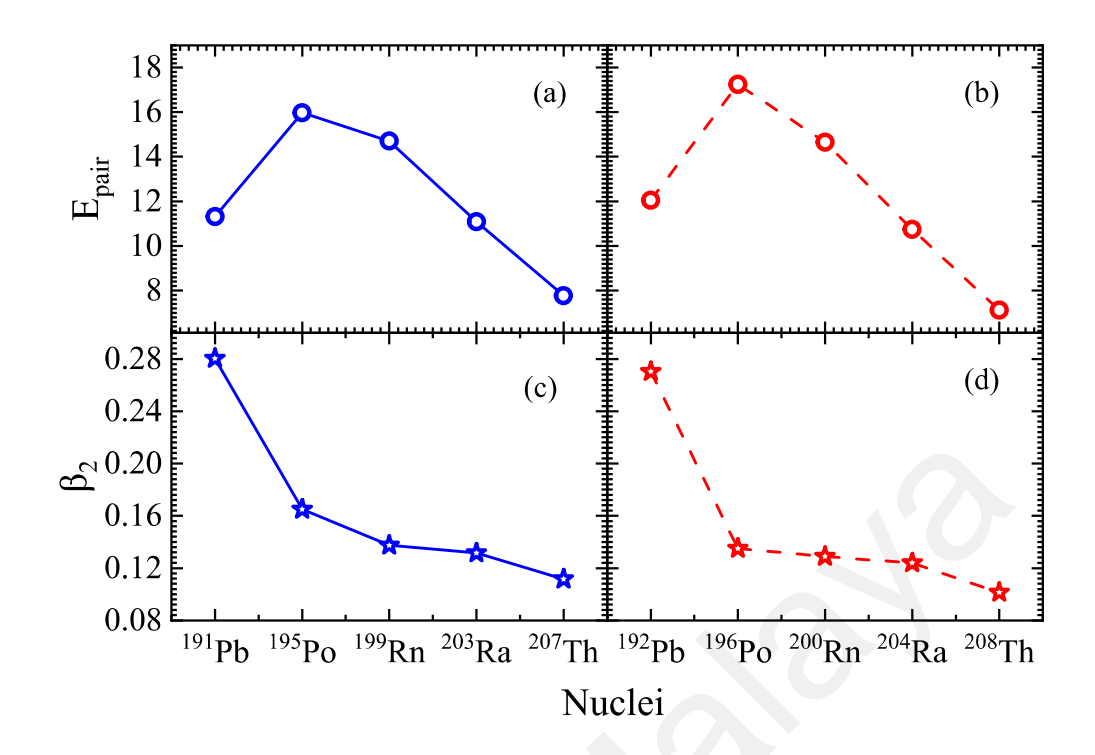


Figure 4.9: A profile of the pairing energies (upper panels a and b) and the quadrupole deformation parameter  $\beta_2$  (lower panel c and d) along the  $^{207,208}$ Th decay chains.

Table 4.3: The predicted DD-ME2 values for pairing energy  $(E_{pair})$ , center of mass energy  $E_{cm}$ ), binding energy (B.E), binding energy per nucleon (B.E/A), charge radii  $(r_c)$ , proton radii  $(r_p)$  and neutron radii  $(r_n)$ , root-mean-square radii  $(r_{rms})$  and the quadrupole deformation  $(\beta_2)$ . The energies are expressed in MeV and radii in fm.

$E_{pair}$	$E_{cm}$	B.E	B.E/A	$r_c$	$r_n$	$r_p$	$r_{rms}$	$\beta_2$
11.32	-5.34	1499.85	7.85	5.52	5.60	5.47	5.54	0.28
12.05	-5.33	1508.07	7.86	5.53	5.61	5.47	5.55	0.27
15.97	-5.30	1522.19	7.81	5.51	5.59	5.45	5.53	0.17
17.24	-5.29	1531.24	7.81	5.50	5.59	5.44	5.53	0.14
14.70	-5.27	1545.17	7.77	5.54	5.61	5.48	5.55	0.14
14.66	-5.26	1554.40	7.77	5.54	5.62	5.48	5.56	0.13
11.09	-5.23	1567.44	7.72	5.58	5.64	5.52	5.59	0.13
10.75	-5.22	1576.88	7.73	5.58	5.65	5.52	5.60	0.12
7.77	-5.20	1588.82	7.68	5.61	5.68	5.56	5.62	0.11
7.12	-5.19	1598.50	7.69	5.62	5.69	5.56	5.63	0.10
	11.32 12.05 15.97 17.24 14.70 14.66 11.09 10.75 7.77	11.32 -5.34 12.05 -5.33 15.97 -5.30 17.24 -5.29 14.70 -5.27 14.66 -5.26 11.09 -5.23 10.75 -5.22 7.77 -5.20	11.32 -5.34 1499.85 12.05 -5.33 1508.07 15.97 -5.30 1522.19 17.24 -5.29 1531.24 14.70 -5.27 1545.17 14.66 -5.26 1554.40 11.09 -5.23 1567.44 10.75 -5.22 1576.88 7.77 -5.20 1588.82	11.32 -5.34 1499.85 7.85 12.05 -5.33 1508.07 7.86 15.97 -5.30 1522.19 7.81 17.24 -5.29 1531.24 7.81 14.70 -5.27 1545.17 7.77 14.66 -5.26 1554.40 7.77 11.09 -5.23 1567.44 7.72 10.75 -5.22 1576.88 7.73 7.77 -5.20 1588.82 7.68	11.32       -5.34       1499.85       7.85       5.52         12.05       -5.33       1508.07       7.86       5.53         15.97       -5.30       1522.19       7.81       5.51         17.24       -5.29       1531.24       7.81       5.50         14.70       -5.27       1545.17       7.77       5.54         14.66       -5.26       1554.40       7.77       5.54         11.09       -5.23       1567.44       7.72       5.58         10.75       -5.22       1576.88       7.73       5.58         7.77       -5.20       1588.82       7.68       5.61	11.32         -5.34         1499.85         7.85         5.52         5.60           12.05         -5.33         1508.07         7.86         5.53         5.61           15.97         -5.30         1522.19         7.81         5.51         5.59           17.24         -5.29         1531.24         7.81         5.50         5.59           14.70         -5.27         1545.17         7.77         5.54         5.61           14.66         -5.26         1554.40         7.77         5.54         5.62           11.09         -5.23         1567.44         7.72         5.58         5.64           10.75         -5.22         1576.88         7.73         5.58         5.65           7.77         -5.20         1588.82         7.68         5.61         5.68	11.32         -5.34         1499.85         7.85         5.52         5.60         5.47           12.05         -5.33         1508.07         7.86         5.53         5.61         5.47           15.97         -5.30         1522.19         7.81         5.51         5.59         5.45           17.24         -5.29         1531.24         7.81         5.50         5.59         5.44           14.70         -5.27         1545.17         7.77         5.54         5.61         5.48           14.66         -5.26         1554.40         7.77         5.54         5.62         5.48           11.09         -5.23         1567.44         7.72         5.58         5.64         5.52           10.75         -5.22         1576.88         7.73         5.58         5.65         5.52           7.77         -5.20         1588.82         7.68         5.61         5.68         5.56	11.32         -5.34         1499.85         7.85         5.52         5.60         5.47         5.54           12.05         -5.33         1508.07         7.86         5.53         5.61         5.47         5.55           15.97         -5.30         1522.19         7.81         5.51         5.59         5.45         5.53           17.24         -5.29         1531.24         7.81         5.50         5.59         5.44         5.53           14.70         -5.27         1545.17         7.77         5.54         5.61         5.48         5.55           14.66         -5.26         1554.40         7.77         5.54         5.62         5.48         5.56           11.09         -5.23         1567.44         7.72         5.58         5.64         5.52         5.59           10.75         -5.22         1576.88         7.73         5.58         5.65         5.52         5.60           7.77         -5.20         1588.82         7.68         5.61         5.68         5.56         5.62

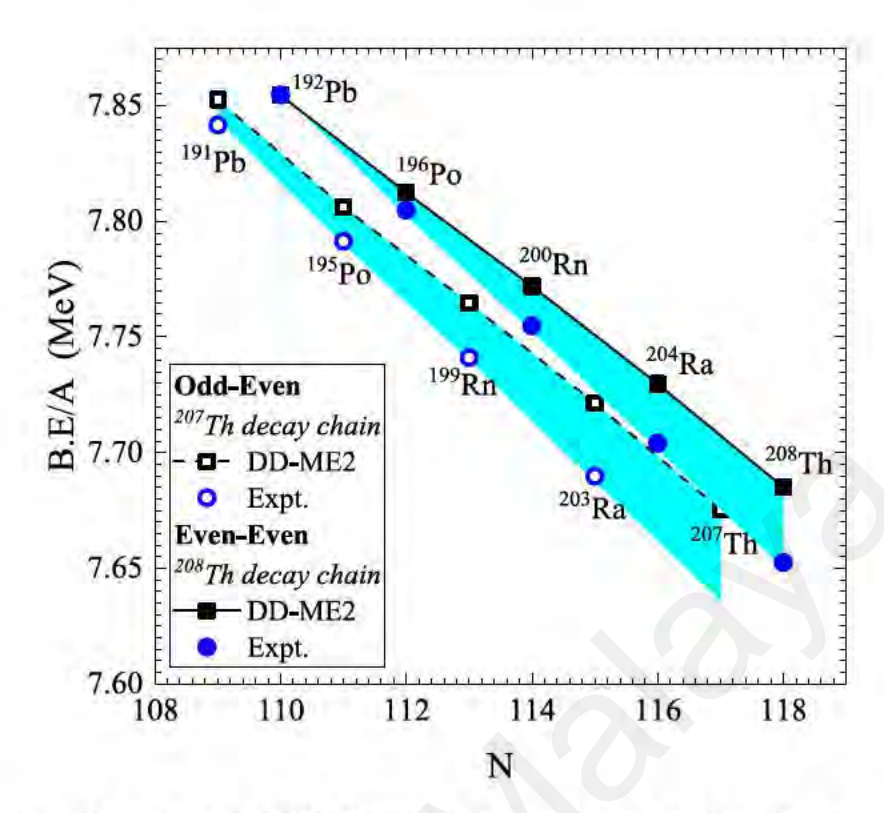


Figure 4.10: The estimated DD-ME2 binding energy per nucleon for each participating nuclei within the <sup>207,208</sup>Th decay chains. The open black- and closed black-squares denotes the <sup>207</sup>Th and <sup>208</sup>Th decay chain respectively. For comparison, the experimental binding energies (blue circles) are taken from ref. (M. Wang et al., 2021).

The mean-field equations are solved in a self-consistent manner using different values of the initial deformation  $\beta_0$ . To achieve convergence of the ground state solution in the mass region under study, the present calculations are carried out on an axially deformed harmonic oscillator basis where the number of major shells for fermions and bosons is  $N_F = N_B = 18$ . The number of the mesh points for Gauss-Hermite and Gauss-Laguree integration are 20 and 24 respectively. To examine the ground state properties of the considered isotopic chains, bulk properties such as the pairing energy  $(E_{pair})$ , center of mass energy  $(E_{cm})$ , binding energy (B.E), the binding energy per nucleon (B.E/A), charge radii  $(r_c)$ , proton radii  $(r_p)$  and neutron radii  $(r_n)$ , root-mean-square radii  $(r_{rms})$  and quadrupole deformation  $(\beta_2)$  calculated from the DD-ME2 parameter set are given in Table A.1. The second column of the table represents the pairing energies (measured in MeV)

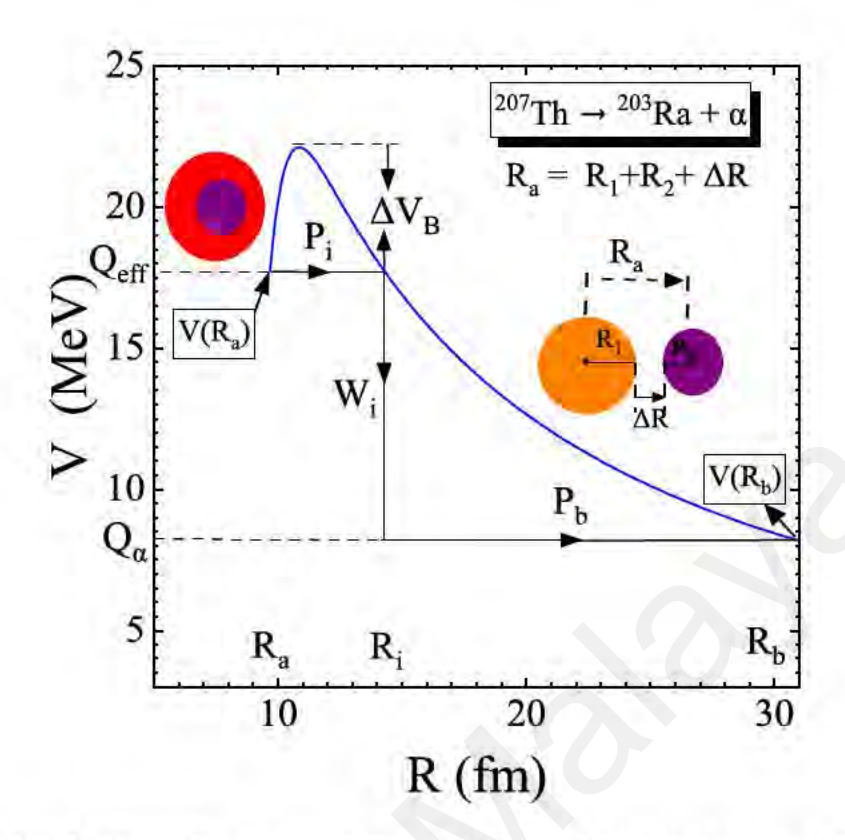


Figure 4.11: A schematic representation of the total interaction potential of  $^{207}$ Th  $\rightarrow$   $^{203}$ Ra +  $\alpha$  as a function of the mass-center distance between the decaying fragments (R). Prior to the decay process,  $\alpha$ -particle (purple circle) is assumed to pre-exist within the  $^{207}$ Th -parent nuclei (red circle). The orange circle represents the daughter nucleus ( $^{203}$ Ra).

for the participating nuclei within the mentioned decay chains. It is worth mentioning that these pairing correlations are evaluated using the Bardeen–Cooper–Schrieffer (BCS) approach. The profile of the pairing energies for each of the decay chains is shown in Fig. 4.9. It is evident that in both cases, the  $^{195,196}$  Po isotopes assume the highest magnitude. This behavior can be ascribed to the proximity of Polonium (Z = 84) to the closure of the magic proton shell (Z = 82). Thus, the pairing energy can be said to be maximum at conventional magic numbers or their nearest neighbours. Interestingly,  $E_{pair}$  is marginally related to the quadrupole deformation parameter  $\beta_2$  (Ahmad et al., 2012; Joshua et al., 2022). In other words, the variation of  $\beta_2$  yields a small change in  $E_{pair}$ . However, a careful examination of columns 2 and 10 of Table A.1, as well as Fig. 4.9 c-d, reveals that

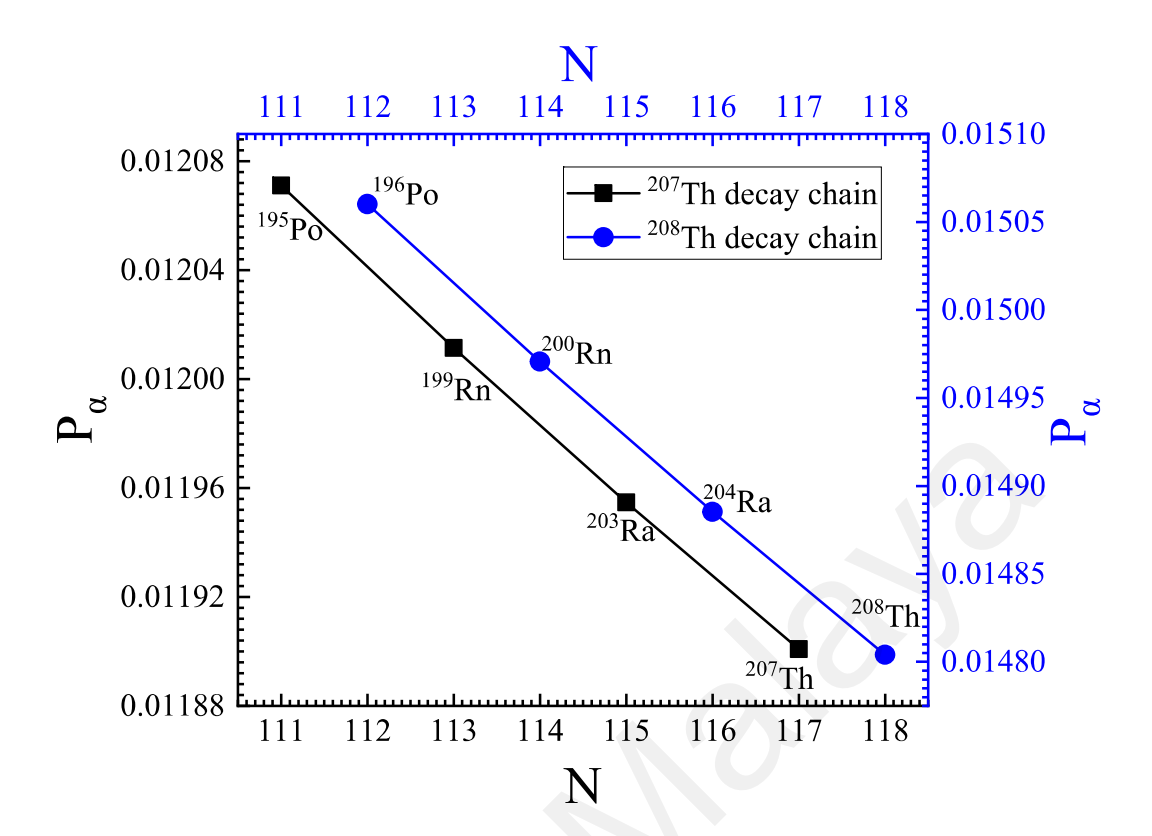


Figure 4.12: The estimated  $\alpha$ -preformation probabilities  $(P_{\alpha})$  versus the parent nuclei for the  $^{207,208}$ Th decay chains.

having a fixed value of  $\beta_2$  for two different nuclei yields different pairing energies. Thus, it is presumed that the pairing energy could be influenced by several other factors within the inherent features of a nucleus.

The last column of Table A.1 succinctly expresses the shape of all the considered nuclei as prolate. Although the result does not give the possibility of a change in shape, it is obvious that  $\beta_2$  decreases in magnitude with increasing nuclear mass and, most probably,  $\beta_2$  will be approximately zero at neutron shell closures due to their stability. However, a close inspection of the  $2^{nd}$  and  $10^{th}$  columns reveals that even though the value of  $\beta_2$  can be the same for two different nuclei, each of them have a unique pairing energy. The recent findings of Geldhof *et al.* (Geldhof et al., 2022) reveal that the influence of strong pairing correlation on the nuclear mean field is more apparent at the surface and also enhances the charge radius. The authors also reported that such couplings are also found to increase

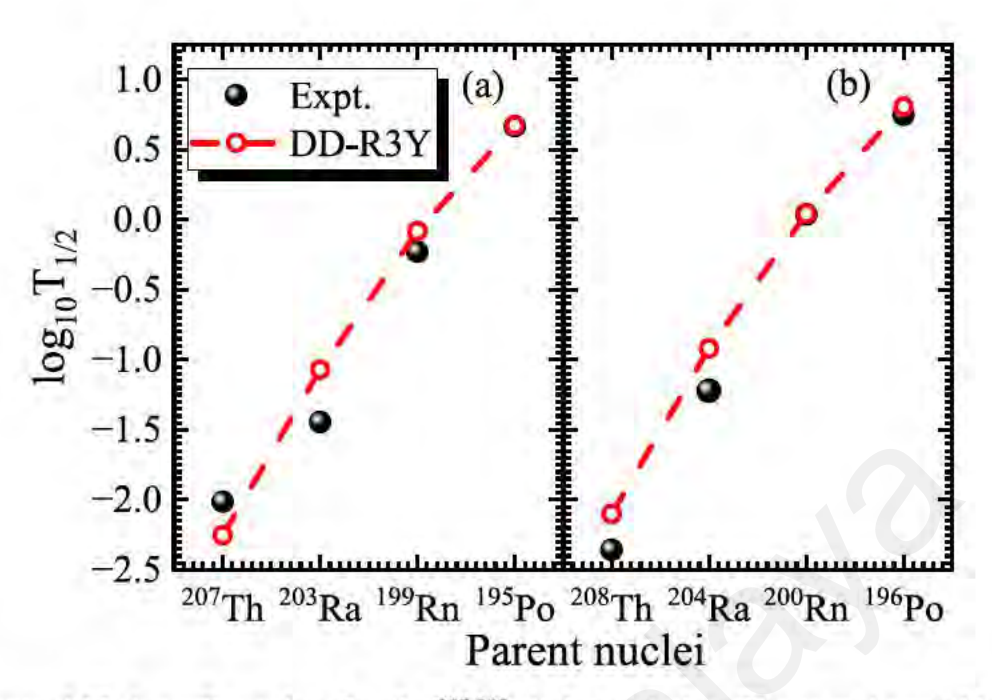


Figure 4.13:  $\log_{10} T_{1/2}$  values for the  $^{207,208}$ Th decay chains. The experimental half-lives are obtained from ref. (Kondev et al., 2021; Yang et al., 2022) and given in Table 4.4.

the odd-even staggering of the charge radius, particularly in isotopes with odd neutron numbers, where the blocking of the odd particle induces a reduction in the strength of the pairing correlations and eventuates a smaller radius. Evaluation of the root-mean-square radii  $(r_{rms})$  and charge radii  $(r_c)$  further gives insight into the nuclear structure. In both quantities, it is quite apparent that there is a departure from the systematic trend at the end of the decay chain, leading to an abrupt increase in their respective magnitude as one crosses from Polonium Po to lead Pb. The binding energy (B.E) and binding energy per particle (B.E/A) decrease in magnitude as the number of neutrons increases and provide a good benchmark for evaluating the stability of nuclei. Besides, Fig 4.10 depicts the variation of B.E/A along the  $^{207,208}$ Th isotopic chain using the set of parameters DD-ME2. In each case, the results are compared with the deduced experimental binding energy per particle taken from Ref. (M. Wang et al., 2021). Relatively, it is obvious that the DD-ME2 values are in closer agreement with the experimental measurements (open and closed blue circles) for nuclei with lower masses. The shaded portion (in cyan colour) highlights the

Table 4.4: The calculated  $\alpha$ -preformation probabilities  $(P_{\alpha})$  and the half-lives of  $^{207,208}$ Th decay chains. The experimental half-lives are deduced from the latest evaluated nuclear properties table (Kondev et al., 2021) and the recent experimental measurements (Yang et al., 2022). The experimental decay energies  $(Q_{\alpha}^{exp})$  in MeV are taken from refs. (Uusitalo et al., 2005; Yang et al., 2022).

$\alpha$ -transition	$Q_{\alpha}^{exp}$	$P_{\alpha}$	$\log_{10} T_{1/2}^{exp}$	$\log_{10} T_{1/2}^{cal}$
Chain 1				
$^{207}\text{Th} \rightarrow ^{203}\text{Ra}$	8.167	0.0119	-2.01	-2.25
$^{203}$ Ra $\rightarrow$ $^{199}$ Rn	7.589	0.0120	-1.44	-1.07
$^{199}$ Rn $\rightarrow$ $^{195}$ Po	6.989	0.0120	-0.23	-0.08
$^{195}\text{Po}{\rightarrow}^{191}\text{Pb}$	6.617	0.0121	0.67	0.67
Chain 2				
$^{208}\text{Th} \rightarrow ^{204}\text{Ra}$	8.053	0.0148	-2.36	-2.10
$^{204}$ Ra $\rightarrow$ $^{200}$ Rn	7.486	0.0149	-1.22	-0.92
$^{200}$ Rn $\rightarrow$ $^{196}$ Po	6.903	0.0150	0.04	0.04
$\underline{\hspace{1.5cm}^{196}\text{Po} \rightarrow^{192}\text{Pb}}$	6.533	0.0151	0.75	0.81

difference of about (0.01-0.03)MeV between the DD-ME2 predictions and the experimental data for each of the considered isotopic chains. Furthermore, the relatively lower B.E/A values in the  $^{207}$ Th decay chain are traceable to the unfilled valence neutron, leading to an odd or even staggering effect. This phenomenon will be discussed later. Both quantities (B.E and B.E/A) are highly dependent on the model and the parameterization, and there is the possibility of large variations with experimental measurements. Thus, to ensure accuracy, the half-lives are calculated using the experimentally measured decay energies  $(Q_{\alpha}^{exp})$  (Uusitalo et al., 2005; Yang et al., 2022). Details of the transitions from the ground state to the ground state of the decay chain of the  $\alpha$ -emitting  $^{207,208}$ Th isotopes are given in Table 4.4. To avoid undue repetition, readers are referred to (Fig. 2 of Ref. (Yang et al., 2022) and its corresponding text) for the step-wise pattern of the  $Q_{\alpha}$  value.

## **4.3.2** Decay Properties of <sup>207,208</sup>Th Isotopic Chains

Fig. 4.11 shows the schematic sketch of the three-step process in which the  $\alpha$  particle penetrates the interaction barrier. The figure gives an illustrative case of the total interaction potential of  $^{207}$ Th  $\rightarrow$   $^{203}$ Ra +  $\alpha$  as a function of the centre-of-mass distance between the

decaying fragments (R). It shows a picture of the  $\alpha$ -particle (purple sphere) conceived within a decaying nucleus  $^{207}$ Th (red sphere) before the penetration process, which begins at the point  $R_a$  corresponding to a potential  $V(R_a)$  (otherwise called the effective Q-value,  $Q_{eff}$  which is usually higher than  $Q_{\alpha}$ ). The de-excitation commences at point  $R_i$  with a probability  $W_i$  computed to be unity (i.e.  $W_i = 1$ ) according to the Greiner and Scheid de-excitation ansatz (M. Greiner & Scheid, 1986). The penetration process continues until it terminates at the point  $R_b$  with a potential  $V(R_b) = Q_{\alpha}$  that corresponds to the scission point, that is, where the decay fragments (the daughter nuclei (orange sphere) and the  $\alpha$ -particle) dissociate.

In the PCM framework, one of the most important inputs in obtaining decay half-lives is the  $\alpha$ -preformation probability  $(P_{\alpha})$ . From the  $3^{rd}$  column of Table 4.4 and Fig. 4.12,  $P_{\alpha}$ increases with decreasing mass of the parent nuclei. When comparing the isotopes of each parent nucleus in Fig. 4.12, it is clear that larger magnitudes of  $(P_{\alpha})$  are needed as the neutron number increases and the magnitudes of the odd-A nuclei are generally lower than those of the even-even nuclei. This behaviour can be largely attributed to the Pauli blocking effect, as also observed in ref. (Wan & Fan, 2021). This suggests that pairing plays a significant role in  $\alpha$ -clustering. Moreover, the  $P_{\alpha}$  values are generally found to decrease with increasing neutron numbers. This is due to the fact that the valence neutron increases as one moves far away from the neutron magic shell closure N=82 which will result in a stronger Pauli blocking effect on the  $\alpha$ -clustering and a smaller preformation factor. One notable inference here is that there is a close correlation between the  $\alpha$ -preformation probability and structural properties of nuclei such as the nuclear pairing gaps. Since all the considered systems are in the open-shell region, the  $P_{\alpha}$  values tend to vary smoothly with the increasing mass of the parent nuclei which is consistent with earlier experimental findings (Hodgson & Běták, 2003). Similarly, Fig. 4.13 displays the variation of the

calculated logarithmic half-lives  $\log_{10} T_{1/2}$  for the  $\alpha$ -transitions along the  $^{207,208}$ Th decay chains. Peaks at  $^{195,196}$  Po  $\rightarrow \alpha + ^{191,192}$  Pb indicate the presence of a proton shell closure Z=82 in their respective daughter nuclei. Additionally, a similar trend is observed in both cases where  $\log_{10} T_{1/2}$  increases as the mass of the parent nuclei decreases and the DD-R3Y predictions are found to agree closely with the experimental measurement. This supports the allusion that the microscopic DD-R3Y NN potential produces reliable results in this region of study.

## **CHAPTER 5: SUMMARY AND CONCLUSION**

This thesis seeks to investigate or explore certain phenomena that presumably constitute the complexity of the superheavy region using the simple semi-empirical formulae and the well-established microscopic approaches. It is salient to note that in the superheavy region, nuclei have extremely high atomic numbers, which is beyond the reach of current experimental capabilities. Thus, there are limited experimental data available for these nuclei. Semi-empirical formulas provide a way to extrapolate and predict alpha decay properties for these superheavy nuclei based on known trends and principles derived from experimental data in lighter nuclei. Moreover, they are often derived from theoretical frameworks that combine fundamental principles of nuclear physics with empirical parameters fitted to experimental data. While fully theoretical models may be too computationally expensive or complex to apply in the superheavy region, semi-empirical formulas offer a balance between accuracy and computational feasibility.

On the other hand, the consideration of relativistic effects is highly important in this region. The RHB formalism accounts for relativistic effects which play a significant role in determining the structure and stability of superheavy nuclei. This ensures a more accurate description of the nuclear dynamics involved in alpha decay. Similarly, the interplay between the nuclear forces and shell effects can be adequately captured using the axially deformed DRHBc theory. This theory also incorporates the continuum effects (arising from the emission of alpha particles from unbound states) that are not adequately described by traditional bound-state models. Thus, The RHB and DRHBc theories incorporate nucleon-nucleon correlations within a self-consistent framework, accounting for the rearrangement of nucleons in the nuclear medium. These correlations are crucial for accurately describing the ground-state properties and dynamics of superheavy nuclei,

including their alpha decay characteristics. By treating correlations consistently, these theories provide a more reliable prediction of alpha decay properties in the superheavy region.

The novel contribution of this study to the body of knowledge is the incorporation of the nuclear rotation effects on the decay half-lives of superheavy nuclei within the range  $98 \le Z \le 120$  which is investigated using the axially deformed relativistic Hartree-Bogoliubov theory in the continuum (DRHBc) with the PC-PK1 parameter set. The deduced DRHBc decay energies (with and without the rotation effect) are compared with those calculated from the macroscopic-microscopic WS4 and the available experimental binding energies. Six semi-empirical formulae, such as the Viola-Seaborg formula (VSS), the modified Brown formula (mB1), the semi-empirical relationship based on fission theory (SemFIS2), the Royer formula (R), the Wang formula (Wang) and the modified YQZR formula (MYQZR) are employed to estimate the half-lives of  $\alpha$  decay. Among these formulae, the half-live predictions of SemFIS2 are found to gradually deviate from the systematic trend beyond  $N_d = 184$ , showing that the probability of undergoing spontaneous fission is less feasible beyond this point. A minimum is observed at  $N_d = 184$ , reflecting its neutron shell closure for the mass region considered on the nuclear chart. The results further indicate that, for  $98 \le Z \le 104$ , the predictions of all semi-empirical formulae are more closely matched to the available experimental data when the rotation effect is taken into account. However, it has been demonstrated that the effect of nuclear rotation gradually reduces as the atomic nucleus becomes heavier.

This study also examined the structural and decay properties of the ground state of recently discovered neutron-deficient <sup>207</sup>Th and remeasured <sup>208</sup>Th isotopes by Yang *et. al.* (Yang et al., 2022) using the Relativistic-Hartree-Bogoliubov (RHB) formalism using the DD-ME2 parameter set within the preformed cluster-decay model (PCM). The relativistic

medium-dependant R3Y so-called DD-R3Y NN potentials are for the first time used to obtain the nucleus-nucleus potential as input into the PCM. The penetration probability is calculated using the WKB approximation, and the preformation probability  $(P_{\alpha})$  is estimated using the newly derived formula, which is based on parameters well known to influence the  $\alpha$ -particle radioactivity. A close correlation is observed between the  $\alpha$ -preformation factor and the crucial role of the pairing correlation in the  $\alpha$ -decay process. Furthermore, the  $P_{\alpha}$  values for the even-even nuclei are generally found to be of higher magnitude than those for the odd-A nuclei. The results further affirm that the odd-even staggering effect on the  $Q_{\alpha}$  values and its accompanying effects on other observables such as the charge radii and the decay half-lives can be largely attributed to the pairing correlation and Pauli blocking of the unpaired valence nucleons.

Overall, this research contributes valuable insights into the complex dynamics of superheavy nuclei, enhancing our theoretical understanding, and could serve as a guide for future experimental investigations. However, it is important to note that there may be other features such as nuclear shape degrees of freedom and the role of quasiparticle structure in alpha decay of superheavy nuclei that were not considered in the present study, being the first attempt. Incorporating such effects in future works could further deepen our understanding of the superheavy region and refine predictive models for nuclear decay processes.

## **REFERENCES**

- Adamian, G., Malov, L., Antonenko, N., Lenske, H., Wang, K., & Zhou, S.-G. (2018). Incorporating self-consistent single-particle potentials into the microscopic-macroscopic method. *The European Physical Journal A*, *54*, 1–12.
- Afanasjev, A., Khoo, T., Frauendorf, S., Lalazissis, G., & Ahmad, I. (2003). Cranked relativistic hartree-bogoliubov theory: Probing the gateway to superheavy nuclei. *Physical Review C*, 67(2), 024309.
- Ahmad, S., Bhuyan, M., & Patra, S. (2012). Properties of z= 120 nuclei and the  $\alpha$ -decay chains of the 292, 304120 isotopes using relativistic and nonrelativistic formalisms. *International Journal of Modern Physics E*, 21(11), 1250092.
- Ahmed, S. M. S., Yahaya, R., Radiman, S., Yasir, M. S., Kassim, H. A., & Khandaker, M. U. (2015). Analytic view at alpha clustering in even-even heavy nuclei near magic numbers 82 and 126. *The European Physical Journal A*, 51, 1–12.
- Akrawy, D. T., Hassanabadi, H., Hosseini, S., & Santhosh, K. (2018). Systematic study of  $\alpha$ -decay half-lives using royer and related formula. *Nuclear Physics A*, 971, 130–137.
- Akrawy, D. T., Poenaru, D. N., Ahmed, A. H., & Sihver, L. (2022).  $\alpha$ -decay half-lives new semi-empirical relationship including asymmetry, angular momentum and shell effects. *Nuclear Physics A*, 1021, 122419.
- Anantaraman, N., Toki, H., & Bertsch, G. (1983). An effective interaction for inelastic scattering derived from the paris potential. *Nuclear Physics A*, 398(2), 269–278.
- Andreyev, A., Huyse, M., Van Duppen, P., Weissman, L., Ackermann, D., Gerl, J., ... others (2000). A triplet of differently shaped spin-zero states in the atomic nucleus 186pb. *Nature*, 405(6785), 430–433.
- Andreyev, A., et al. (1819). Hindered alpha decay and shape staggering in 191po. *Physical Review Letters*, 82, 1999.
- Angeli, I., Gangrsky Yu, P., Marinova, K., Boboshin, I., Komarov, S. Y., Ishkhanov, B., ... others (2009). Alberico wm: see czerski p 025008 aleksejevs a, barkanova s and blunden pg: Computational model for electron–nucleon scattering and weak

- Antonenko, N., Adamian, G., Sargsyan, V., & Lenske, H. (2022). Double-folding nucleus—nucleus interaction potential based on the self-consistent calculations. *The European Physical Journal A*, 58(11), 211.
- Armbruster, P. (2000). On the production of superheavy elements. *Annual Review of Nuclear and Particle Science*, *50*(1), 411–479.
- Bender, M., Nazarewicz, W., & Reinhard, P.-G. (2001). Shell stabilization of super-and hyperheavy nuclei without magic gaps. *Physics Letters B*, 515(1-2), 42–48.
- Bender, M., Rutz, K., Reinhard, P.-G., Maruhn, J. A., & Greiner, W. (1999). Shell structure of superheavy nuclei in self-consistent mean-field models. *Physical Review C*, 60(3), 034304.
- Bertsch, G., Borysowicz, J., McManus, H., & Love, W. (1977). Interactions for inelastic scattering derived from realistic potentials. *Nuclear Physics A*, 284(3), 399–419.
- Bethe, H., & Bacher, R. (1936). Welcome to the new version of caltechauthors. login is currently restricted to library staff. if you notice any issues, please email coda@ library. caltech. edu. *Rev Mod Phys*, 8, 82.
- Bhagwat, A., Vinas, X., Centelles, M., Schuck, P., & Wyss, R. (2012). Microscopic-macroscopic approach for binding energies with the wigner-kirkwood method. ii. deformed nuclei. *Physical Review C*, 86(4), 044316.
- Bhuyan, M. (2015). Structural evolution in transitional nuclei of mass 82 a 132. *Physical Review C*, 92(3), 034323.
- Bhuyan, M., & Kumar, R. (2018). Fusion cross section for ni-based reactions within the relativistic mean-field formalism. *Physical Review C*, 98(5), 054610.
- Bhuyan, M., Kumar, R., Rana, S., Jain, D., Patra, S. K., & Carlson, B. V. (2020, Apr). Effect of density and nucleon-nucleon potential on the fusion cross section within the relativistic mean field formalism. *Phys. Rev. C*, *101*, 044603. Retrieved from https://link.aps.org/doi/10.1103/PhysRevC.101.044603 doi: 10.1103/PhysRevC.101.044603

- Bhuyan, M., Panda, R., Routray, T., & Patra, S. (2010). Application of relativistic mean field and effective field theory densities to scattering observables for ca isotopes. *Physical Review C*, 82(6), 064602.
- Bhuyan, M., & Patra, S. (2012). Magic nuclei in superheavy valley. *Modern Physics Letters A*, 27(30), 1250173.
- Bhuyan, M., Patra, S., Arumugam, P., & Gupta, R. K. (2011). Nuclear sub-structure in 112–122 ba nuclei within relativistic mean field theory. *International Journal of Modern Physics E*, 20(05), 1227–1241.
- Bhuyan, M., Patra, S., & Gupta, R. K. (2011). Relativistic mean-field study of the properties of z= 117 nuclei and the decay chains of the 293, 294 117 isotopes. *Physical Review C*, 84(1), 014317.
- Bhuyan, M., Rana, S., Jain, N., Kumar, R., Patra, S. K., & Carlson, B. (2022). Medium-dependent relativistic nn potential: Application to fusion dynamics. *Physical Review C*, 106(4), 044602.
- Blendowske, R., & Walliser, H. (1988). Systematics of cluster-radioactivity-decay constants as suggested by microscopic calculations. *Physical review letters*, 61(17), 1930.
- Boguta, J., & Bodmer, A. (1977). Relativistic calculation of nuclear matter and the nuclear surface. *Nuclear Physics A*, 292(3), 413–428.
- Bonetti, R., & Guglielmetti, A. (1999). Measurements on cluster radioactivity present experimental status.. Retrieved from https://api.semanticscholar.org/CorpusID:100215924
- Bonetti, R., & Guglielmetti, A. (2007). Cluster radioactivity: an overview after twenty years. *Romanian reports in Physics*, 59(2), 301.
- Budaca, A., & Silisteanu, I. (2011). Alpha-decay as sensitive tool to derive nuclear shell structure of superheavy nuclei. *Rom. Rep. Phys.*, *63*, 1147.
- Cai, B., Chen, G., Xu, J., Yuan, C., Qi, C., & Yao, Y. (2020). α decay half-life estimation and uncertainty analysis. *Physical Review C*, 101(5), 054304.

- Chadwick, J. (1932). Possible existence of a neutron. *Nature*, 129(3252), 312–312.
- Clark, R. M., & Rudolph, D. (2023). Role of quasiparticle structure in  $\alpha$  decay of superheavy nuclei. *Physical Review C*, 107(3), 034321.
- Ćwiok, S., Heenen, P.-H., & Nazarewicz, W. (2005). Shape coexistence and triaxiality in the superheavy nuclei. *Nature*, 433(7027), 705–709.
- Das, M., Bhuyan, M., Majekodunmi, J. T., Biswal, N., & Panda, R. (2022). Structure and decay chain of fermium isotopes using relativistic mean-field approach. *Modern Physics Letters A*, *37*(21), 2250133.
- Das, M., Majekodunmi, J., Biswal, N., Panda, R., & Bhuyan, M. (2023). Correlation between the nuclear structure and reaction dynamics of ar-isotopes as projectile using the relativistic mean-field approach. *Nuclear Physics A*, 122703.
- De Groote, R., Billowes, J., Binnersley, C. L., Bissell, M. L., Cocolios, T. E., Day Goodacre, T., . . . others (2020). Measurement and microscopic description of odd—even staggering of charge radii of exotic copper isotopes. *Nature Physics*, *16*(6), 620–624.
- Delion, D. (2009). Universal decay rule for reduced widths. *Physical Review C*, 80(2), 024310.
- Deng, J.-G., & Zhang, H.-F. (2021). Correlation between  $\alpha$ -particle preformation factor and  $\alpha$  decay energy. *Physics Letters B*, 816, 136247.
- Denisov, V. Y. (2013). Multidimensional model of cluster radioactivity. *Physical Review C*, 88(4), 044608.
- Denisov, V. Y. (2015). Nucleus-nucleus potential with shell-correction contribution. *Physical Review C*, 91(2), 024603.
- De Vries, H., De Jager, C., & De Vries, C. (1987). Nuclear charge-density-distribution parameters from elastic electron scattering. *Atomic data and nuclear data tables*, 36(3), 495–536.
- Dobaczewski, J., Flocard, H., & Treiner, J. (1984). Hartree-fock-bogolyubov description

- of nuclei near the neutron-drip line. *Nuclear Physics A*, 422(1), 103–139.
- Dong, J., Zuo, W., & Scheid, W. (2011). Correlation between  $\alpha$ -decay energies of superheavy nuclei involving the effects of symmetry energy. *Physical Review Letters*, 107(1), 012501.
- Dong, T., & Ren, Z. (2010).  $\alpha$ -decay energy formula for superheavy nuclei based on the liquid-drop model. *Physical Review C*, 82(3), 034320.
- Dutra, M., & Loureno, O. (2014). S. s¿ avancini, by carlson, a. delfino, dp menezes, c. providencia, s. typel and jr stone. *Phys. Rev. C*, 90, 055203.
- Dzuba, V., Flambaum, V., & Webb, J. (2017). Isotope shift and search for metastable superheavy elements in astrophysical data. *Physical Review A*, 95(6), 062515.
- Eichler, R., Aksenov, N., Belozerov, A., Bozhikov, G., Chepigin, V., Dressler, R., ... others (2007). Confirmation of the decay of 283112 and first indication for hg-like behavior of element 112. *Nuclear Physics A*, 787(1-4), 373–380.
- Einstein, A. (1905). Üon a heuristic point of view concerning the production and transformation of light. *Annals of physics*, 4.
- Fink, H., Maruhn, J., Scheid, W., & Greiner, W. (1974). Theory of fragmentation dynamics in nucleus-nucleus collisions. *Zeitschrift für Physik*, 268(3), 321–331.
- Fiset, E., & Nix, J. (1972). Calculation of half-lives for superheavy nuclei. *Nuclear Physics A*, 193(2), 647–671.
- Flerov, G. N., Druin, V. A., & Pleve, A. (1970). The stability of heavy nuclei and the limit of the periodic system of elements. *Soviet Physics Uspekhi*, 13(1), 24.
- Fu, G., Cheng, Y., Jiang, H., Zhao, Y., & Arima, A. (2016). Odd-even staggering of binding energy for nuclei in the s d shell. *Physical Review C*, 94(2), 024312.
- Fuchs, C., Lenske, H., & Wolter, H. (1995). Density dependent hadron field theory. *Physical Review C*, 52(6), 3043.

- Gallagher Jr, C. J., & Rasmussen, J. O. (1957). Alpha-decay hindrance-factor calculations. *Journal of Inorganic and Nuclear Chemistry*, *3*(6), 333–344.
- Geldhof, S., Kortelainen, M., Beliuskina, O., Campbell, P., Caceres, L., Cañete, L., ... others (2022). Impact of nuclear deformation and pairing on the charge radii of palladium isotopes. *Physical Review Letters*, 128(15), 152501.
- Ghodsi, O., & Amiri, M. (2021). Exploring  $\alpha$  decay properties in the superheavy region through the double-folding formalism and skyrme interactions. *Physical Review C*, 104(4), 044618.
- Girod, M., & Grammaticos, B. (1979). The zero-point energy correction and its effect on nuclear dynamics. *Nuclear Physics A*, *330*(1), 40–52.
- Giuliani, S. A., Matheson, Z., Nazarewicz, W., Olsen, E., Reinhard, P.-G., Sadhukhan, J., ... Schwerdtfeger, P. (2019). Colloquium: Superheavy elements: Oganesson and beyond. *Reviews of Modern Physics*, 91(1), 011001.
- Greiner, M., & Scheid, W. (1986). Radioactive decay into excited states via heavy ion emission. *Journal of Physics G: Nuclear Physics*, 12(10), L229.
- Greiner, W. (2012). Heavy into stability. Physics, 5, 115.
- Gupta, R. K., & Greiner, W. (1994). Cluster radioactivity. *International Journal of Modern Physics E*, 3(supp01), 335–433.
- Gupta, R. K., Patra, S., & Greiner, W. (1997). Structure of 294, 302120 nuclei using the relativistic mean-field method. *Modern Physics Letters A*, 12(23), 1727–1736.
- Hao, T. N., Quentin, P., & Bonneau, L. (2012). Parity restoration in the highly truncated diagonalization approach: Application to the outer fission barrier of 240 pu. *Physical Review C*, 86(6), 064307.
- Hassanzad, M., & Ghodsi, O. (2021). Theoretical study on the favored alpha-decay half-lives of deformed nuclei. *Chinese Physics C*, 45(12), 124106.
- Heenen, P.-H., Skalski, J., Staszczak, A., & Vretenar, D. (2015). Shapes and  $\alpha$ -and  $\beta$ -decays of superheavy nuclei. *Nuclear Physics A*, 944, 415–441.

- Heisenberg, W. (1932). 4. Über den bau der atomkerne iii. In *Kernkräfte* (pp. 211–218). Berlin, Boston: De Gruyter. Retrieved 2024-02-29, from https://doi.org/10.1515/9783112596807-010 doi: doi:10.1515/9783112596807-010
- Hodgson, P. E., & Běták, E. (2003). Cluster emission, transfer and capture in nuclear reactions. *Physics reports*, *374*(1), 1–89.
- Hofmann, F., Keil, C., & Lenske, H. (2001). Density dependent hadron field theory for asymmetric nuclear matter and exotic nuclei. *Physical Review C*, 64(3), 034314.
- Hofmann, S. (2015). Super-heavy nuclei. *Journal of Physics G: Nuclear and Particle Physics*, 42(11), 114001.
- Hofmann, S., & Münzenberg, G. (2000a). The discovery of the heaviest elements. *Reviews of Modern Physics*, 72(3), 733.
- Hofmann, S., & Münzenberg, G. (2000b). The discovery of the heaviest elements. *Reviews of Modern Physics*, 72(3), 733.
- Horiuchi, W., & Inakura, T. (2020). Core swelling in spherical nuclei: An indication of the saturation of nuclear density. *Physical Review C*, 101(6), 061301.
- Horiuchi, W., & Inakura, T. (2021, 07). Deformation effect on nuclear density profile and radius enhancement in light- and medium-mass neutron-rich nuclei. *Progress of Theoretical and Experimental Physics*, 2021(10), 103D02. Retrieved from https://doi.org/10.1093/ptep/ptab087 doi: 10.1093/ptep/ptab087
- Horiuchi, W., & Itagaki, N. (2022). Density profiles near the nuclear surface of ti 44, 52: An indication of  $\alpha$  clustering. *Physical Review C*, 106(4), 044330.
- Ishizuka, C., Takemoto, H., Chiba, Y., Ono, A., & Itagaki, N. (2022). Role of tensor interaction as salvation of cluster structure in ti 44. *Physical Review C*, 105(6), 064314.
- Ismail, M., Ellithi, A., Adel, A., & Abbas, M. (2022). Improved empirical formulas for  $\alpha$ -decay half-lives of heavy and superheavy nuclei. *Physica Scripta*, 97(7), 075303.

- Jachimowicz, P., Kowal, M., & Skalski, J. (2018). Hindered  $\alpha$  decays of heaviest high-k isomers. *Physical Review C*, 98(1), 014320.
- Jain, N., Kumar, R., & Bhuyan, M. (2022). Exploring the ground state bulk and decay properties of the nuclei in superheavy island. *Nuclear Physics A*, *1019*, 122379.
- Jia, J., Qian, Y., & Ren, Z. (2021). Systematics of  $\alpha$ -decay energies in the valence correlation scheme. *Physical Review C*, 103(2), 024314.
- Jiang, H., Fu, G., Bao, M., He, Z., Zhao, Y., & Arima, A. (2012). Nucleon separation energies in the valence correlation scheme. *Physical Review C*, 86(1), 014327.
- Joshua, T. M., Jain, N., Kumar, R., Anwar, K., Abdullah, N., & Bhuyan, M. (2022). Divergence in the relativistic mean field formalism: A case study of the ground state properties of the decay chain of 214,216,218 u isotopes. *Foundations*, 2(1), 85–104.
- Kondev, F., Wang, M., Huang, W., Naimi, S., & Audi, G. (2021). The nubase2020 evaluation of nuclear physics properties. *Chinese Physics C*, 45(3), 030001.
- Koyuncu, F., & Soylu, A. (2020). The alpha-decay chains and decay mode predictions of the nuclei z= 1 1 8, 119 and 120. *International Journal of Modern Physics E*, 29(07), 2050053.
- Kruppa, A. T., Bender, M., Nazarewicz, W., Reinhard, P.-G., Vertse, T., & Ćwiok, S. (2000). Shell corrections of superheavy nuclei in self-consistent calculations. *Physical Review C*, 61(3), 034313.
- Kumar, R. (2012). Cluster radioactivity using various versions of nuclear proximity potentials. *Physical Review C*, 86(4), 044612.
- Kumar, R., Rana, S., Bhuyan, M., & Mohr, P. (2022). Fusion cross section of  $\alpha$ -induced reactions for heavy target nuclei. *Physical Review C*, 105(4), 044606.
- Lalazissis, G., Karatzikos, S., Fossion, R., Arteaga, D. P., Afanasjev, A., & Ring, P. (2009). The effective force nl3 revisited. *Physics Letters B*, 671(1), 36–41.
- Lalazissis, G., Nikšić, T., Vretenar, D., & Ring, P. (2005). New relativistic mean-field

- interaction with density-dependent meson-nucleon couplings. *Physical Review C*, 71(2), 024312.
- Lalazissis, G., Sharma, M., Ring, P., & Gambhir, Y. (1996). Superheavy nuclei in the relativistic mean-field theory. *Nuclear Physics A*, 608(2), 202–226.
- Lalazissis, G., Vretenar, D., & Ring, P. (1999). Ground-state properties of deformed proton emitters in the relativistic hartree-bogoliubov model. *Nuclear Physics A*, 650(2), 133–156.
- Lalazissis, G., Vretenar, D., Ring, P., Stoitsov, M., & Robledo, L. (1999). Relativistic hartree+ bogoliubov description of the deformed n= 28 region. *Physical Review C*, 60(1), 014310.
- Li, L., Meng, J., Ring, P., Zhao, E.-G., Zhou, S.-G., et al. (2012). Deformed relativistic hartree-bogoliubov theory in continuum. *Physical Review C*, 85(2), 024312.
- Liu, H.-M., Xu, J.-Y., Deng, J.-G., He, B., & Li, X.-H. (2019). Predictions of  $\alpha$  decay half-lives for even—even superheavy nuclei with 1 0 4 z 1 2 8 based on two-potential approach within cluster-formation model. *International Journal of Modern Physics E*, 28(10), 1950089.
- Liu, J.-H., Guo, S.-Q., Bao, X.-J., & Zhang, H.-F. (2017). Predictions of decay modes for the superheavy nuclei most suitable for synthesis. *Chinese Physics C*, 41(7), 074106.
- Lopez-Martens, A., Hauschild, K., & Collaboration, G. (2022). Spectroscopy of super heavy elements with gabriela. *The European Physical Journal A*, 58(7), 134.
- Madland, D. G., & Nix, J. R. (1988). New model of the average neutron and proton pairing gaps. *Nuclear Physics A*, 476(1), 1–38.
- Majek, J., Bhuyan, M., Anwar, K., Abdullah, N., & Kumar, R. (2023). Preformation probability and kinematics of clusters emission yielding pb-daughters. *Chinese Physics C*.
- Majekodunmi, J. T., Bhuyan, M., Jain, D., Anwar, K., Abdullah, N., & Kumar, R. (2022). Cluster decay half-lives of ba 112–122 isotopes from the ground state and intrinsic excited state using the relativistic mean-field formalism within the

- preformed-cluster-decay model. Physical Review C, 105(4), 044617.
- Majekodunmi, J. T., Kumar, R., & Bhuyan, M. (2023). Quest for a universal cluster preformation formula: A new paradigm for estimating the cluster formation energy. arXiv preprint arXiv:2305.05613.
- Majekodunmi, J. T., Rana, S., Jain, N., Anwar, K., Abdullah, N., Kumar, R., & Bhuyan, M. (2022). Relativistic r3y nucleon–nucleon potential: Decay characteristics of 124 ba isotope within the preformed cluster decay approach. In *Intelligent systems: Proceedings of icmib 2021* (pp. 135–142). Springer.
- Malov, L., Adamian, G., Antonenko, N., & Lenske, H. (2021). Landscape of the island of stability with self-consistent mean-field potentials. *Physical Review C*, 104(6), 064303.
- Manjunatha, H. (2016). Alpha decay properties of superheavy nuclei z= 126. *Nuclear Physics A*, 945, 42–57.
- Manjunatha, H., Sowmya, N., & Gupta, P. D. (2021). Competition between different decay modes in the isotopes of actinide nuclei. *Iranian Journal of Science and Technology, Transactions A: Science*, 45(6), 2201–2217.
- Marinov, A., Rodushkin, I., Kashiv, Y., Halicz, L., Segal, I., Pape, A., . . . Brandt, R. (2007). Existence of long-lived isomeric states in naturally-occurring neutron-deficient th isotopes. *Physical Review C*, 76(2), 021303.
- Marinov, A., Rodushkin, I., Pape, A., Kashiv, Y., Kolb, D., Brandt, R., ... Segal, I. (2009). Existence of long-lived isotopes of a superheavy element in natural au. *International Journal of Modern Physics E*, 18(03), 621–629.
- Marsh, B. A., Day Goodacre, T., Sels, S., Tsunoda, Y., Andel, B., Andreyev, A. N., ... others (2018). Characterization of the shape-staggering effect in mercury nuclei. *Nature Physics*, 14(12), 1163–1167.
- Maruhn, J., & Greiner, W. (1974). Theory of fission-mass distributions demonstrated for ra 226, u 236, fm 258. *Physical Review Letters*, 32(10), 548.
- Mayer, M. G., & Jensen, J. H. D. (1961). Nuclear shell structure. *Modern Physics for the Engineer*, 40.

- Meng, J. (2016). Relativistic density functional for nuclear structure (Vol. 10). World Scientific.
- Migdal, A. (n.d.). Theory of finite fermi systems, and applications to atomic nuclei.
- Mirea, M., Sandulescu, A., & Delion, D. S. (2011). Predictions for 232u cluster-decays within the macroscopic-microscopic approximation. *Nuclear Physics A*, 870, 23–41.
- Morita, K., Morimoto, K., Kaji, D., Goto, S., Haba, H., Ideguchi, E., . . . others (2004). Status of heavy element research using garis at riken. *Nuclear Physics A*, 734, 101–108.
- Münzenberg, G., & Morita, K. (2015). Synthesis of the heaviest nuclei in cold fusion reactions. *Nuclear Physics A*, 944, 3–4.
- Nagaraja, A., Manjunatha, H., Sowmya, N., Seenappa, L., Gupta, P. D., Manjunatha, N., & Raj, S. A. C. (2021). Heavy particle radioactivity of superheavy element z= 126. Nuclear Physics A, 1015, 122306.
- Nesterenko, V., Mardyban, M., Reinhard, P.-G., Repko, A., & Kvasil, J. (2023). Anomalous deformation dependence of moments of inertia in light deformed nuclei. *arXiv* preprint arXiv:2304.10873.
- Nikšić, T., Vretenar, D., Finelli, P., & Ring, P. (2002). Relativistic hartree-bogoliubov model with density-dependent meson-nucleon couplings. *Physical Review C*, 66(2), 024306.
- Nikšić, T., Vretenar, D., & Ring, P. (2008). Relativistic nuclear energy density functionals: Adjusting parameters to binding energies. *Physical Review C*, 78(3), 034318.
- Nilsson, S. G., Tsang, C. F., Sobiczewski, A., Szymański, Z., Wycech, S., Gustafson, C., ... Nilsson, B. (1969). On the nuclear structure and stability of heavy and superheavy elements. *Nuclear Physics A*, 131(1), 1–66.
- Oganessian, Y. (2007). Heaviest nuclei from 48ca-induced reactions. *Journal of Physics G: Nuclear and Particle Physics*, 34(4), R165.

- Oganessian, Y. T. (1988). Problems of the synthesis of heavy nuclei. *Nuclear Physics A*, 488, 65–82.
- Oganessian, Y. T., Abdullin, F. S., Alexander, C., Binder, J., Boll, R. A., Dmitriev, S., ... others (2012). Production and decay of the heaviest nuclei 1 293, 294 17 and 1 294 18. *Physical review letters*, 109(16), 162501.
- Oganessian, Y. T., Abdullin, F. S., Bailey, P., Benker, D., Bennett, M., Dmitriev, S., ... others (2011). Eleven new heaviest isotopes of elements z= 105 to z= 117 identified among the products of bk 249+ ca 48 reactions. *Physical Review C*, 83(5), 054315.
- Oganessian, Y. T., Sobiczewski, A., & Ter-Akopian, G. (2017). Superheavy nuclei: from predictions to discovery. *Physica Scripta*, 92(2), 023003.
- Oganessian, Y. T., Utyonkov, V., Kovrizhnykh, N., Abdullin, F. S., Dmitriev, S., Ibadullayev, D., . . . others (2022). First experiment at the super heavy element factory: High cross section of mc 288 in the am 243+ ca 48 reaction and identification of the new isotope lr 264. *Physical Review C*, 106(3), L031301.
- Oganessian, Y. T., Utyonkov, V., Lobanov, Y. V., Abdullin, F. S., Polyakov, A., Sagaidak, R., . . . others (2006). Synthesis of the isotopes of elements 118 and 116 in the cf 249 and cm 245+ ca 48 fusion reactions. *Physical Review C*, 74(4), 044602.
- Oganessian, Y. T., Utyonkov, V., Lobanov, Y. V., Abdullin, F. S., Polyakov, A., Shirokovsky, I., . . . others (2004). Publisher's note: Experiments on the synthesis of element 115 in the reaction am 243 (ca 48, x n) 115 291- x [phys. rev. c 69, 021601 (r)(2004)]. *Physical Review C*, 69(2), 029902.
- Oganessian, Y. T., Yeremin, A., Popeko, A., Bogomolov, S., Buklanov, G., Chelnokov, M., . . . others (1999). Synthesis of nuclei of the superheavy element 114 in reactions induced by 48ca. *Nature*, 400(6741), 242–245.
- Okunev, V. (2018). About islands of stability and limiting mass of the atomic nuclei. In *Iop conference series: Materials science and engineering* (Vol. 468, p. 012012).
- Patra, S., Bhuyan, M., Mehta, M., & Gupta, R. K. (2009). Superdeformed and hyperdeformed states in z= 122 isotopes. *Physical Review C*, 80(3), 034312.
- Patra, S., Gupta, R. K., Sharma, B., Stevenson, P., & Greiner, W. (2007). Exotic clustering

- in heavy and superheavy nuclei within the relativistic and non-relativistic mean field formalisms. *Journal of Physics G: Nuclear and Particle Physics*, *34*(9), 2073.
- Pattnaik, J. A., Bhuyan, M., Panda, R., & Patra, S. (2021). Isotopic shift in magic nuclei within relativistic mean-field formalism. *Physica Scripta*, *96*(12), 125319.
- Pei, J., Xu, F., Lin, Z., & Zhao, E. (2007).  $\alpha$ -decay calculations of heavy and superheavy nuclei using effective mean-field potentials. *Physical Review C*, 76(4), 044326.
- Poenaru, D., & Ivascu, M. (1984). *The island of alpha activity close to the double magic nucleus 100 sn* (Tech. Rep.). Institutul Central de Fizica.
- Poenaru, D., Ivascu, M., & Mazilu, D. (1980). A new semiempirical formula for the alpha decay half-lives. *Journal de Physique Lettres*, 41(24), 589–590.
- Poenaru, D. N., Plonski, I.-H., & Greiner, W. (2006).  $\alpha$ -decay half-lives of superheavy nuclei. *Physical Review C*, 74(1), 014312.
- Prassa, V., Nikšić, T., Lalazissis, G., & Vretenar, D. (2012). Relativistic energy density functional description of shape transitions in superheavy nuclei. *Physical Review C*, 86(2), 024317.
- Prathapan, K., Deneshan, P., Rajan, M. P., & Biju, R. (2023). A systematic study of alpha decay half-lives of isotones in superheavy region. *Indian Journal of Physics*, 1–12.
- Qian, Y., & Ren, Z. (2011). Unified description of  $\alpha$ -decay and cluster radioactivity in the trans-tin region. *Journal of Physics G: Nuclear and Particle Physics*, 39(1), 015103.
- Rana, S., Bhuyan, M., & Kumar, R. (2022). Systematic study of fusion barrier characteristics within the relativistic mean-field formalism. *Physical Review C*, 105(5), 054613.
- Reinhard, P.-G., Bender, M., & Maruhn, J. A. (2000). Mean-field models and superheavy elements. *arXiv* preprint nucl-th/0012095.
- Ren, Z., Zhao, P., Meng, J., et al. (2022). Dynamics of rotation in chiral nuclei. *Physical Review C*, 105(1), L011301.

- Ring, P. (1996). Relativistic mean field theory in finite nuclei. *Progress in Particle and Nuclear Physics*, *37*, 193–263.
- Ring, P., & Schuck, P. (1980). *The nuclear many-body problem*. New York: Springer-Verlag.
- Royer, G. (2000). Alpha emission and spontaneous fission through quasi-molecular shapes. *Journal of Physics G: Nuclear and Particle Physics*, 26(8), 1149.
- Rutherford, E., & Geiger, H. (1908). An electrical method of counting the number of  $\alpha$ -particles from radio-active substances. *Proceedings of the Royal Society of London. Series A, Containing Papers of a Mathematical and Physical Character*, 81(546), 141-161.
- Rydin, R. A. (2011). A new approach to finding magic numbers for heavy and superheavy elements. *Annals of Nuclear Energy*, 38(2-3), 238–242.
- Sahu, B., Singh, S., Bhuyan, M., Biswal, S., & Patra, S. (2014). Importance of nonlinearity in the n n potential. *Physical Review C*, 89(3), 034614.
- Satchler, G. R., & Love, W. G. (1979). Folding model potentials from realistic interactions for heavy-ion scattering. *Physics Reports*, 55(3), 183–254.
- Seif, W. (2015). Nucleon pairing correlations and the  $\alpha$  cluster preformation probability inside heavy and superheavy nuclei. *Physical Review C*, 91(1), 014322.
- Serot, B., & Walecka, J. (1986). Advances in nuclear physics, edited by jw negele and e. vogt. Plenum, New York.
- Seyyedi, S. (2021). Systematic study of alpha-decay of super-heavy isotopes with z= 120–126. *Modern Physics Letters A*, 36(06), 2150033.
- Sheline, R. K. (1976). Spectroscopy of nuclei far from stability.
- Sil, T., Patra, S., Sharma, B., Centelles, M., & Vinas, X. (2004). Superheavy nuclei in a relativistic effective lagrangian model. *Physical Review C*, 69(4), 044315.

- Singh, B., Bhuyan, M., Patra, S., & Gupta, R. K. (2012). Optical potential obtained from relativistic-mean-field theory-based microscopic nucleon–nucleon interaction: applied to cluster radioactive decays. *Journal of Physics G: Nuclear and Particle Physics*, 39(2), 025101.
- Singh, B., Patra, S., & Gupta, R. K. (2011). Importance of preformation probability in cluster radioactive-decays using relativistic mean field theory within the preformed cluster model. *International Journal of Modern Physics E*, 20(04), 1003–1007.
- Singh, S. K., Biswal, S., Bhuyan, M., & Patra, S. (2014). Effects of  $\delta$  mesons in relativistic mean field theory. *Physical Review C*, 89(4), 044001.
- Smits, O. R., Düllmann, C. E., Indelicato, P., Nazarewicz, W., & Schwerdtfeger, P. (2024). The quest for superheavy elements and the limit of the periodic table. *Nature Reviews Physics*, 6(2), 86–98.
- Smits, O. R., Indelicato, P., Nazarewicz, W., Piibeleht, M., & Schwerdtfege, P. (2023). Pushing the limits of the periodic table—a review on atomic relativistic electronic structure theory and calculations for the superheavy elements. *Physics Reports*, 1035, 1-57.
- Smolańczuk, R. (1997). Properties of the hypothetical spherical superheavy nuclei. *Physical Review C*, 56(2), 812.
- Sobiczewski, A., Patyk, Z., & Ćwiok, S. (1989). Deformed superheavy nuclei. *Physics letters B*, 224(1-2), 1–4.
- Sridhar, K., Manjunatha, H., & Ramalingam, H. (2019). A study on the synthesis of superheavy element z= 125. *Brazilian Journal of Physics*, 49, 232–248.
- Sridhara, G., Manjunatha, H., Sowmya, N., & Gupta, P. D. (2021). A study of alpha-decay using effective liquid drop model. *International Journal of Modern Physics E*, 30(12), 2150094.
- Staszczak, A., Baran, A., & Nazarewicz, W. (2013). Spontaneous fission modes and lifetimes of superheavy elements in the nuclear density functional theory. *Physical Review C*, 87(2), 024320.
- Stone, J., Morita, K., Guichon, P., & Thomas, A. (2019). Physics of even-even superheavy

- nuclei with 96< z< 110 in the quark-meson-coupling model. *Physical Review C*, 100(4), 044302.
- Sun, X.-D., Duan, C., Deng, J.-G., Guo, P., & Li, X.-H. (2017). Systematic study of α decay for odd-a nuclei within a two-potential approach. *Physical Review C*, 95(1), 014319.
- Swain, R., Sahu, B., Moharana, P., & Patra, S. (2019). Nuclear structure and  $\alpha$ -decay study of og isotopes. *International Journal of Modern Physics E*, 28(06), 1950041.
- Taninah, A., Agbemava, S., & Afanasjev, A. (2020). Covariant density functional theory input for r-process simulations in actinides and superheavy nuclei: The ground state and fission properties. *Physical Review C*, 102(5), 054330.
- Thomson, J. J. (1897). Discovery of the electron. *Philosophical Magazine*, 44, 93.
- Ts, O. Y. (2001). The synthesis and decay properties of the heaviest element. *Nucl Phys A*, 685, 17c.
- Ts, O. Y., Utyonkov, V., Lobanov Yu, V., et al. (2000). Synthesis of superheavy nuclei in the 48ca+ 244 pu reaction: 288 114. *Phys Rev C*, 62, 041604.
- Typel, S., & Brown, B. (2003). Skyrme hartree-fock calculations for the  $\alpha$ -decay q values of superheavy nuclei. *Physical Review C*, 67(3), 034313.
- Typel, S., & Wolter, H. (1999). Relativistic mean field calculations with density-dependent meson-nucleon coupling. *Nuclear Physics A*, 656(3-4), 331–364.
- Uusitalo, J., Leino, M., Enqvist, T., Eskola, K., Grahn, T., Greenlees, P., . . . others (2005).  $\alpha$  decay studies of very neutron-deficient francium and radium isotopes. *Physical Review C*, 71(2), 024306.
- Velasquez, J. P., Caballero, O., & Kelkar, N. (2023). Corrigendum: Alpha decay of thermally excited nuclei (2023 j. phys. g: Nucl. part. phys. 50 015203). *Journal of Physics G: Nuclear and Particle Physics*, 50(9), 099501.
- Viola Jr, V., & Seaborg, G. (1966). Nuclear systematics of the heavy elements—ii lifetimes for alpha, beta and spontaneous fission decay. *Journal of Inorganic and Nuclear*

- Wan, N., & Fan, J. (2021). Systematical calculations on  $\alpha$ -cluster preformation factors and decay half-lives of light nuclei near the recently observed  $\alpha$  emitters xe 108 and te 104. *Physical Review C*, 104(6), 064320.
- Wang, M., Huang, W., Kondev, F. G., Audi, G., & Naimi, S. (2021). The ame 2020 atomic mass evaluation (ii). tables, graphs and references. *Chinese Physics C*, 45(3), 030003.
- Wang, N., Liu, M., Wu, X., & Meng, J. (2014). Surface diffuseness correction in global mass formula. *Physics Letters B*, 734, 215–219.
- Wang, Y., Wang, S., Hou, Z., Gu, J., et al. (2015). Systematic study of  $\alpha$ -decay energies and half-lives of superheavy nuclei. *Physical Review C*, 92(6), 064301.
- Ward, D., Carlsson, B., & Åberg, S. (2013).  $\alpha$ -decay calculations of heavy nuclei using an effective skyrme interaction. *Physical Review C*, 88(6), 064316.
- Ward, D., Carlsson, B., & Åberg, S. (2015).  $\alpha$ -decay spectra of odd nuclei using the effective skyrme interaction. *Physical Review C*, 92(1), 014314.
- Weizsäcker, C. v. (1935). Zur theorie der kernmassen. Zeitschrift für Physik, 96(7-8), 431–458.
- Xu, C., & Ren, Z. (2005). Favored  $\alpha$ -decays of medium mass nuclei in density-dependent cluster model. *Nuclear Physics A*, 760(3-4), 303–316.
- Yadav, A., Shukla, A., & Kumar, V. (2023). Study of alpha-decay chain for even—even isotopes of z= 120 superheavy nuclei. *Pramana*, 97(1), 48.
- Yahya, W., & Falaye, B. (2021). Alpha decay study of thorium isotopes using double folding model with nn interactions derived from relativistic mean field theory. *Nuclear Physics A*, *1015*, 122311.
- Yahya, W., Oluwadare, O., & Falaye, B. (2024). Alpha decay half-lives of heavy and superheavy nuclei within a deformed double folding model. *International Journal of Theoretical Physics*, 63(2), 1–15.

- Yang, H., Gan, Z., Zhang, Z., Huang, M., Ma, L., Zhang, M., . . . others (2022). New isotope th 207 and odd-even staggering in  $\alpha$ -decay energies for nuclei with z> 82 and n< 126. *Physical Review C*, 105(5), L051302.
- Yukawa, H. (1935). On the interaction of elementary particles. i. *Proceedings of the Physico-Mathematical Society of Japan. 3rd Series*, 17, 48–57.
- Zhang, K., Cheoun, M.-K., Choi, Y.-B., Chong, P. S., Dong, J., Dong, Z., . . . others (2022). Nuclear mass table in deformed relativistic hartree–bogoliubov theory in continuum, i: Even–even nuclei. *Atomic Data and Nuclear Data Tables*, 144, 101488.
- Zhang, K., Cheoun, M.-K., Choi, Y.-B., Chong, P. S., Dong, J., Geng, L., . . . others (2020). Deformed relativistic hartree-bogoliubov theory in continuum with a point-coupling functional: Examples of even-even nd isotopes. *Physical Review C*, 102(2), 024314.
- Zhang, W., Meng, J., Zhang, S., Geng, L., & Toki, H. (2005). Magic numbers for superheavy nuclei in relativistic continuum hartree–bogoliubov theory. *Nuclear Physics A*, 753(1-2), 106–135.
- Zhang, Z., Yang, H., Huang, M., Gan, Z., Yuan, C., Qi, C., ... others (2021). New  $\alpha$ -emitting isotope u 214 and abnormal enhancement of  $\alpha$ -particle clustering in lightest uranium isotopes. *Physical Review Letters*, 126(15), 152502.
- Zhang, Z.-H., Zeng, J.-Y., Zhao, E.-G., Zhou, S.-G., et al. (2011). Particle-number conserving analysis of rotational bands in 247, 249 cm and 249 cf. *Physical Review C*, 83(1), 011304.
- Zhao, B., & Zhang, S. Q. (2019, mar). The r-process with the newly developed high-precision mass model ws4. *The Astrophysical Journal*, 874(1), 5. Retrieved from https://dx.doi.org/10.3847/1538-4357/ab0702 doi: 10.3847/1538-4357/ab0702
- Zhao, P.-W., Li, Z.-P., Yao, J.-M., Meng, J., et al. (2010). New parametrization for the nuclear covariant energy density functional with a point-coupling interaction. *Physical Review C*, 82(5), 054319.
- Zhou, S.-G., Meng, J., Ring, P., Zhao, E.-G., et al. (2010). Neutron halo in deformed nuclei. *Physical Review C*, 82(1), 011301.